DEVELOPMENT OF A NOVEL DRUG DELIVERY SYSTEM BASED ON POLYMERIC, THERMORESPONSIVE, HYDROGEL NANOPARTICLES

PAR

Dimitrios MISIRLIS

diplôme d'ingénieur chimique, Université de Patras, Grèce
de nationalité hellénique et canadienne

Lausanne, EPFL
2005

Table of Contents

Summary

Carrier-mediated drug delivery has emerged as a powerful methodology for the treatment of various pathologies. The therapeutic index of traditional and novel drugs is enhanced via the increase of specificity due to targeting of drugs to a particular tissue, cell or intracellular compartment, the control over release kinetics, the protection of the active agent or a combination of the above. Nanoparticles (NPs) were proposed as drug carriers over 30 years ago and have received growing attention since, mainly due to their stability, enhanced loading capabilities and control over physicochemical properties. The unique pathophysiology of solid tumors allows passive accumulation of NPs at these sites upon intravenous injection. Furthermore, stealth NPs with long circulation times are more efficient in reaching tumor tissue.

In addition to systemic administration, localized drug release may be achieved using macroscopic drug depots close to the target site. Among various systems considered for this approach, *in situ*-forming biomaterials in response to environmental stimuli have gained considerable attention, due to the non-invasive character, reduction of side effects associated with systemic administration and better control over biodistribution.

This thesis focuses on the design, preparation and *in vitro* characterization of polymeric, hydrogel nanoparticles with thermoresponsive properties. Inverse emulsion polymerization was selected for their fabrication via cross-linking of acrylate derivatives of poly(ethylene glycol) (PEG) and poly(ethylene glycol)-*bl*-poly(propylene glycol)-*bl*-poly(ethylene glycol) (PEG-PPG-PEG) copolymers, also known as Pluronics®. This polymerization technique allows for control over size, is versatile in respect to initiation and composition, and proceeds to full double-bond conversion in relatively short times. Incorporation of functional comonomers in the polymeric network additionally offers the possibility of further modifications, as is demonstrated by fluorescent labeling of the colloids. Moreover, hydrogel NPs of 100-500 nm are stable against aggregation as aqueous dispersions and as freeze-dried solid powders.

The particles we discuss here, may be visualized as nanoscale, three-dimensional, polymeric networks consisting of PPG-rich, hydrophobic domains surrounded by a hydrophilic, PEG-rich matrix. The permanence of domains similar in hydrophobicity to Pluronic micellar cores, but insensitive to dilution under the critical micellar concentration, allows the accomodation of poorly water-soluble drugs through hydrophobic interactions, as

was experimentally shown using the anticancer agent doxorubicin. A fast and efficient solvent evaporation technique was developed in order to physically encapsulate the drug. Doxorubicin is thus partially protected from degradation and diffuses out of the NPs without a burst, over one week under sink conditions *in vitro*.

Thermosensitivity of nanoparticles is manifested as a size reduction of non-interacting colloids in dilute dispersions and as a macroscopic, fluid-to-solid, physical transition of concentrated samples. The driving force of these phenomena is an entropically-driven deswelling of the hydrogel NPs with increasing temperature, which leads to their hardening. At concentrations above which there is physical contact of neighboring particles, this intra-particulate event results in the dynamic arrest of particles within a 'cage' formed by their neighbors. This mild and reversible transition occurs at a clinically-relevant temperature range (25-30°C), with no syneresis or by-product formation, and is compatible with living cells. Upon dissolution in body fluids, the colloidal macroscopic drug depot will give rise to a colloidal dispersion; however, it is notable that the processes of encapsulated drug release and dissolution are independent and may be tailored on a case-to-case basis.

In vitro cell culture studies revealed that nanoparticle cytotoxicity was negligible even at high concentrations. Interactions with macrophage-like cells, intended to model cells of the mononuclear phagocyte system, showed limited colloidal uptake which is not influenced by the presence of serum, but is energy dependent to a considerable extent (approx. 30%). We believe this low association stems from the hydrophilic, protein-repellent nature of the materials employed and suggests a stealth character.

In conclusion, the nanoparticles presented here are well suited for certain drug delivery applications, including cancer therapy and in the prevention of post-operative adhesions, both in the form of injectable dilute dispersions or as *in situ* gelling thermoresponsive biomaterials.

Sommario

Il trasporto mediato di farmaci è risultato una metodologia molto valida nel trattamento di varie patologie. L'indice terapeutico di farmaci tradizionali e moderni è migliorato grazie all' incremento di specificità dovuto al raggiungimento preciso di un particolare tessuto, cellula o compartimento intracellulare, al controllo della cinetica di rilascio, alla protezione del principio attivo o alla combinazione di queste. Le nanoparticelle (NP) sono state proposte come trasportatori di farmaci da ormai 30 anni e ricevono sempre più attenzione dal mondo scientifico, principalmente dovuto alla loro stabilità, a un efficiente inglobamento del farmaco e al controllo delle proprietà psico-chimiche. Unicamente la patologia fisica di tumori solidi permette l'accumulazione passiva delle NP per mezzo di un iniezione intravenosa. Inoltre alcune NP che possiedono lunghi tempi di circolazione sono più efficienti nel raggiungere il tessuto tumorale.

Oltre alla somministrazione sistemica, il rilascio localizzato del farmaco potrebbe essere conseguito depositando il farmaco nelle vicinanze del sito target. Tra i vari sistemi considerati in tale contesto, i biomateriali originati in sito, in risposta a stimoli ambientali sono i più accreditati, in quanto la somministrazione non è invasiva, gli effetti secondari associati alla somministrazione sistemica, sono ridotti e c'è un maggiore controllo della biodistribuzione.

Tale progetto di tesi è focalizzato alla progettazione, alla preparazione e alla caratterizzazione in vitro nanoparticelle polimeriche (hydrogel), con proprietà termo-sensibili. Per la fabbricazione via cross-linking di derivati acrilati di poly(ethylene glicol) (PEG) e copolimeri a base di poly(ethylene glycol)-*bl*-poly(propylene glycol)-*bl*-poly(ethylene glycol) (PEG-PPG-PEG), conosciuto anche come Pluronics, è stata utilizzata la polimerizzazione in emulsione inversa. Tale tecnica permette il controllo delle dimensioni delle NP, è versatile rispetto alla composizione di tali e all'iniziazione della polimerizzazione, e raggiunge la conversione totale relativamente in breve tempo. Tra l' altro la possibilità di incorporare comonomeri funzionali nella rete polimerica offre la possibilità di ulteriori modifiche, come è dimostrato dalla marcatura fluorescente dei colloidi. In aggiunta le nanoparticelle di hydrogel, di 100-500 nm, come le sospensioni acquose e le polveri solide liofilizzate, sono stabili contro l'aggregazione.

Le particelle discusse fina ad ora possono essere considerate come reti polimeriche tridimensionali, costituite da domini idrofobici ricchi in PPG circondati da una matrice

idrofilia ricca in PEG. La permanenza dei domini, con idrofobicità simile al cuore pluronico della micella, ma insensibile alla diluizione al di sotto della CMC, permette la collocazione di farmaci poco idrosolubili via interazioni idrofobiche. Questo è stato sperimentalmente dimostrato con la Doxorubicina, l'agente antitumorale. Una tecnica di evaporazione del solvente veloce ed efficiente è stata sviluppata con lo scopo di incapsulare il farmaco. Doxoru... è quindi parzialmente protetta dalla degradazione e diffonde dalla NP in modo graduale e controllato per più di una settimana in vitro.

La termosensibilità delle NP è espressa come riduzione delle dimensioni dei colloidi non-interattivi in sospensioni diluite e come una transizione macroscopica liquida-solida in un mezzo concentrato. La forza motore di tali fenomeni è il rilascio di acqua dalle NP indotto dall'aumento dell'entropia associato all'aumento di temperatura, che porta alla loro solidificazione. Inoltre tale evento intra-particellare, in presenza di contatto fra le particelle adiacenti dovuto a concentrazioni abbastanza elevate, porta ad un dinamico arresto delle particelle in una "gabbia" formata dalle stesse particelle vicine. Questa transizione reversibile e non brusca avviene in un intervallo di temperatura (25-30°C) di applicabilità in campo clinico, senza degradazione del biomateriale e formazione di sottoprodotti, ed è compatibile con cellule viventi. Dopo la diluizione nei fluidi corporali, il deposito colloidale solido del farmaco si trasformerà in sospensione colloidale. Quindi è evidente che i processi di dissoluzione del farmaco incapsulato e di dissoluzione sono indipendenti e possono essere ingegnerizzati caso per caso.

Studi in vitro hanno rivelato che la citotossicità delle nanoparticelle è trascurabile anche ad alte concentrazioni. Le interazioni con cellule di tipo macrofago, intese come modello cellulare del sistema mononucleare fagocitico, mostrano limitata fagocitosi, la quale non viene influenzata dalla presenza del siero, ma risulta notevolmente dipendente dall'energia (appros. 30%). Noi crediamo che questa debole associazione sia dovuta alla natura idrofilica, protein-repellente del materiale utilizzato e suggerisce un carattere di auto-occultamento.

In conclusione, le nanoparticelle presentate in tale progetto sono un efficiente strumento nel campo del trasporto di farmaci, soprattutto nelle terapie tumorali e nella prevenzione delle adesioni post-operatorie, utilizzandole in forma di sospensione iniettabile diluita o di biomateriali creati in situ.

Chapter 1

General Introduction

1.1 Drug delivery

Humankind's efforts to confront disease dates back to early civilization. Substances taken from nature were tested and used to treat dysfunctions of physiological life processes, pain and discomfort. With the advancement of science, the active ingredients of these materials, the drugs, were identified, isolated and in many cases their mechanism of action elucidated. New drug candidates are tested even today in the quest to add increasingly effective tools against diseases.

Drug characteristics differ dramatically, even those aimed to treat the same symptoms; chemical composition, size, hydrophilicity and potency identify molecules whose function may be specific or highly complex. An increasing understanding of cellular biology at the molecular level, combined with the (decoding) of the human genome, and a technological breakthrough in the field of proteomics and DNA micro-arrays, has introduced even more applicants, like peptides and nucleic acids (gene delivery).

Drug activity is a result of molecular interaction(s) in certain cells; it is therefore easily deduced that it is necessary for the drug to reach somehow the site of action following administation (oral, intravenous, local, transdermal, etc.) at sufficient concentrations. The scientific field dealing with this issue is known as drug delivery and has essentially the following aim: *to deliver the drug at the right place, at the right concentration for the right period of time.* When this is impossible by simply selecting an appropriate administration route, or if such administration causes patient discomfort, strategies based on the association of the drug with a carrier (a drug delivery system – DDS) are an alternative[1, 2]. Additional motivations for such approaches include the reduction of required resources for therapy, accomplished by an increase of the drug's therapeutic index and the prevention of frequent, unpleasant or expensive treatments.

Drug delivery systems, ranging from implantable electronic devices to single polymer chains, are required to be compatible with processes in the body (biocompatibility) as well as with the drug to be delivered. DDS alter the biodistribution and pharmacokinetics of the assosciated drug: that is the time-dependent percentage of the administered dose in the different organs of the body. Furthermore, obstacles arising from low drug solubility, degradation (environmental or enzymatic), fast clearance rates, non-specific toxicity, inability to cross biological barriers, just to mention a few, may be addressed by DDS[2].

Overall, the challenge of increasing the therapeutic effect of drugs, with a concurrent minimization of side effects, can be tackled through proper design and engineering of the DDS, in a case-to-case manner[1, 3].

1.2 Long-circulating colloidal drug carriers

Nano-sized colloids are a major class of DDS[1, 4]. Administration (oral, intravascular) generally involves the residence and travel of the colloids in the bloodstream and their confrontation with the body's defense mechanisms. In order to allow a therapeutically relevant amount of carrier (and therefore drug) to reach its target and release its payload, long circulation times are crucial[5, 6]. The carrier leaves blood circulation by slow processes; long circulating vectors possess therefore a distinct advantage because of repeated passage through the target site.

Firstly, dimensions and structure of vessels establish size limitations on carrier design. Colloids larger than a few micrometers accumulate in the lung capillaries, while sufficiently small structures could escape from circulation through intercellular junctions of healthy endothelium (e.g. lymph nodes endothelium[7]), or may be removed by the sinus endothelium of the bone marrow[8]. A large amount of *in vivo* data have established an optimal size range of 20-200nm for prolonged blood residence[6].

Circumventing the mononuclear phagocyte system (MPS), consisting mainly of monocytes and macrophages (e.g. Kuppfer liver cells, Sleen red pulp macrophages), is an additional step towards succesful targeted delivery.

Recognition as foreign object and removal from circulation is mediated by surface interactions between cell and carrier. Blood proteins adsorb readily on colloids, in a pattern and kinetics which depend on its surface physicochemical properties (size, shape, charge density, hydrophobicity etc.)[9-11]. Opsonins are proteins that promote the activation of the complement system and/or assist in phagocytic uptake by macrophages. Prevention or delay of opsonin adsorption, by surface modification, has proven to be a succesful strategy for enhancement of circulation life times[5, 6]. Among the surface modifiers examined, poly(ethylene glycol) (PEG) is certainly the most famous[12-14]. Hydrated, non-ionic and highly flexible, PEG chains form a protein-repellent layer around the carrier. The density, homogeneity, thickness and method of attachment (covalent, adsorbed, entrapped) of the layer are key issues for efficient shielding of hydrophobic and/or charged domains[13, 15].

Dysopsonins on the other hand, are proteins that suppress recognition by macrophages; favoring their adsorption at the expense of opsonins is also a promising approach towards higher blood retention[5, 6].

Furthermore, some molecules have been identified as markers of self: for example, the integrin associated protein CD47 is essential for red blood cell longevity[16]. Display of this biomimetic marker on the surface emulsions reduced uptake by macrophages *in vitro*[17], although *in vivo* studies are still lacking.

As a final remark we would like to note that perhaps the most powerful strategy to prolong circulation life-times might be the appropriate choice of chemical and material properties of the carrier, rather that its coating.

1.3 Cancer as a target of DDS

Progress in fundamental cancer biology has not yet been met by a comparable advancement in its clinical treatment. Fundamental reason for this discrepancy is the inability to selectively reach and eliminate tumor tissue with marginal damage to healthy organs rather than the availability of potent chemotherapeutics[1, 18]. Cancer cell targeting by DDS aims at increasing selectivity and overcoming biological barriers, while transporting higher drug amounts[1].

Generally, targeting may be a result of (i) the unique tissue physiology of the target (passive targeting) (ii) a specific recognition of target cells by carrier-conjugated molecules (active targeting) (iii) a localized external energy activation or (iv) a synergistic combination of the above strategies. In tumor targeting all the above mentioned strategies are being investigated.

1.3.1 Enhanced Permeation and Retention (EPR) effect

Tumor angiogenesis is dysregulated as a consequence of rapid cancer growth and leads to a physiologically and structurally defective formation of vasculature[19]. The architectural anarchy, combined with an overproduction of permeability enhancers and impairement of lymphatic drainage, results in the preferential extravasation and retention of high molecular weight (MW) macromolecules and colloids in developing tumors, a feature which has been termed 'enhanced permeation and retention effect'[20]. Although a complete understanding of this phenomenon remains elusive (including a debate on whether

extravasation occurs via intracellular gaps[21] or the vesicular-vacuolar organelles[22]), the EPR effect is the most widely used targeting method, with clinical products based on it.
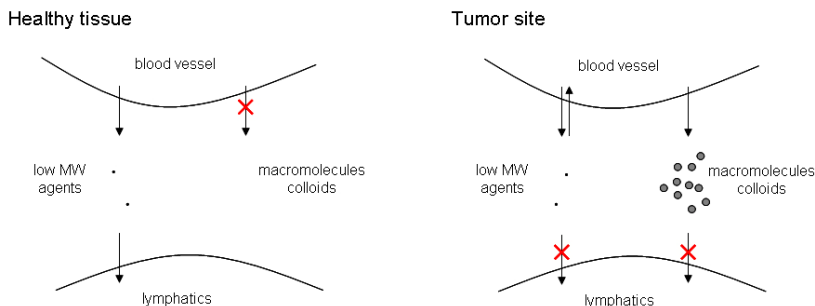

Figure 1.1 *A schematic representation of the EPR effect; healthy endothelium prevents extravasation of high MW molecules and colloids, whereas low MW agents are drained by the lymphatics (left). Dysfunctional lymphatics and highly permeable vascular endothelium allow the preferential accumulation and retention of macromolecules and colloids, in solid tumors (right).*

Accumulation is size dependent: low MW drugs also permeate into tumor interstitium, but rapidly diffuse out into the bloodstream. Moreover, a 'pore size' cut-off, which is dependent on tumor type, progression and site has been established in animal models[23]; qualitative correlation is assumed for human cancers.

It should be kept in mind that this unique microphysiology, which may be exploited for targeting, is a source of obstacles as well: high interstitial pressure and appearance of necrotic zones, distant from angiogenic areas introduce an additional challenge for delivery vectors[24]: their spatial intratumoral distribution.

1.3.2 Active targeting

Active targeting is accomplished by attachment of specific molecules on the carrier's surface, which enhance the binding and interactions with antigens or receptors expressed on specific cell populations[25]. Targeting ligands explored for cancer therapy include, but are not limited to, antibodies and antibody fragments[26], vitamins[27], peptides[28], folate[29] and transferrin[30]. The choice of appropriate ligand is based on its specificity, stability, availability and selective display of its corresponding pair on the target cells, as well as its cost. In addition to the above considerations, conjugation chemistry[31], density and accessibility of the ligand[32], need to be properly designed for efficient vector targeting.

Active targeting complements passive accumulation into tumors; selectivity and retention are improved as a result of specific interactions with target cells, at the expense of increased complexity, cost and risks (e.g. adverse biological reactions to ligand).

1.3.3 Intracellular trafficking

Once the drug delivery vehicle has reached the tumor tissue, subsequent drug release may occur in the extracellular space, or following internalization of the carrier. Drugs with intracellular action, incapable of crossing cell membranes, need to be assisted in reaching their target. Cellular uptake mechanisms vary according to cell type (e.g. phagocytic vs non-phagocytic cells), physicochemical properties of the internalized entity and mode of activation (e.g. receptor mediated endocytosis)[33].
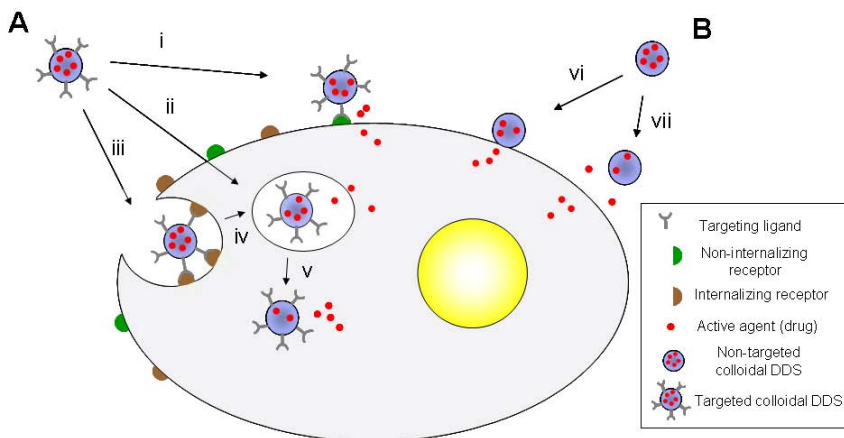

Figure 1.2 *Once the colloidal DDS reaches the extracellular space of the target cell, drug release may occur by different mechanisms (or their combination). Ligand-targeted colloids (A) bind to epitopes on the cell surface (i, iii). Endocytosis might occur non-specifically (ii) or following binding to receptors which promote internalization (iii). Upon internalization, the carrier either escapes into the cytoplasm (v) or releases the cargo in vesicular organelles in response to environmental stimuli (enzymes, pH, reductive conditions).*
Non-targeted colloids (B) which have reached their target through passive targeting, release the drug in the proximity of the cell (vii) or in contact with the cell membrane (vi).

Various strategies have been developed and succesfully applied to attain desirable sub-cellular localization: lysosome degradable linkers[34], nuclear localization signals[34, 35] and acid- or reduction-responsive carriers exploiting the endosomal maturation transformations[24, 36, 37], are some examples. Moreover, intracellular targeting is feasible through the use of ligands

that trigger receptor-mediated endocytosis. The last few years, the identification of cell-penetrating peptides, like the TAT protein transduction domain (PTD) derived from HIV-1 TAT protein, has added new tools for efficient carrier design[38, 39]; TAT-PTD has been used to deliver in the cytoplasm a wide, size-independent variety of cargo[32].

Active targeting still faces challenges, but it also holds immense potential; discrepancies are frequently observed between *in vitro* and *in vivo* situations. The use of diverse targeting moieties per carrier, the development of even more selective and efficient ligands (e.g. via phage display) and a better understaing of the complex trafficking pathways in the cell[40], may allow more precise control over the biological fate of colloidal drug delivery systems.

1.4 Anthracycline delivery in cancer

A major class of chemotherapeutics currently used in clinical practice, are the anthracycline molecules (Figure 1.3). Doxorubicin (also known as adriamycin) is probably the most known member of the anthracycline family. It was introduced in 1969 by Arcamone et al. who isolated it from *Streptomyces peucetius* var. *caesius*[41].
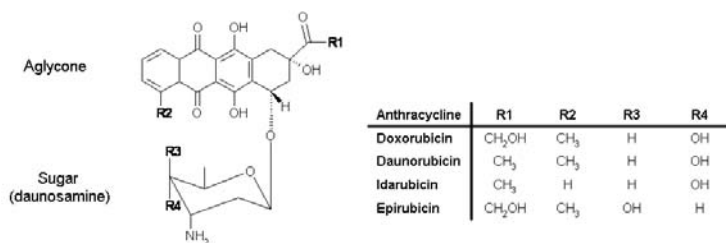

Anthracycline	R1	R2	R3	R4
Doxorubicin	CH₂OH	CH₃	H	OH
Daunorubicin	CH₃	CH₃	H	OH
Idarubicin	CH₃	H	H	OH
Epirubicin	CH₂OH	CH₃	OH	H

Figure 1.3 *The molecular structure of anthracyclines consists of a hydrophobic aglycone ring and a sugar containing a primary amine (pK_a= 7.2-8.4 for doxorubicin). The aglycone is responsible for the fluorescent properties of the molecule, whereas solubility is determined by pH.*

These potent anti-proliferative agents are a typical example of drugs whose efficacy is constrained by non-specific toxicities and would therefore benefit by targeted drug delivery approaches. Indeed, the most studied DDS in oncology are the anthracycline-based ones[42]. The aim of preserving (or enhancing) efficacy against tumors, while avoiding exposure to critical sites like the heart and bone marrow, linked with conventional administration, was

first addressed using liposomes. Liposomes are hollow structures, composed of a lipid bilayer (or multiple bilayers) and an internal aqueous pool; they are efficiently loaded with doxorubicin by ion-trapping methods. At present, a few liposomal formulations are available in the market for the treatment of AIDS related Kaposi's sarcoma, breast, ovarian and other tumor types[42]: Myocet® (Elan Pharmaceuticals) is provided in a dry powder form, whereas Doxil® and Caexyl® (Alza Pharmaceuticals), two pegylated liposomal formulations are supplied as dispersions for intravenous infusion[43]. These liposomes employ the EPR effect to reach tumors where they act as drug depots. Release in the interstitium occurs mainly via disruption of the liposomal bilayer and through macrophage uptake and subsequent drug release; uptake by tumor cells is minimal, a drawback which may be overcome by active liposome targeting.

It is noteworthy to mention that the existing carrier-mediated delivery approaches have not attained increased drug potency in the tumors; their success is rather a consequence of a decrease in undesired side toxicities[44]. The improvement and development of new carriers is an ongoing task, with anthracycline drugs in the front line.

1.5 Nanoparticles as colloidal drug carriers

Nanoparticles (NPs) occupy an increasingly prominent place in the armory of injectable, colloidal drug delivery systems[6, 45-48]. Alternative carriers including polymer-drug conjugates[49], dendrimers[50], micelles[51], lipid and polymeric vesicles[52], nanocapsules[53, 54], are also the subject of research and clinical evaluation.

Nanoparticles are solid colloidal drug carriers ranging from 10 to 1000nm in diameter, typically made of a single material, in which a drug is entrapped, encapsulated or adsorbed onto the surface[55]. NPs were introduced almost 3 decades ago[56]; since then poly(lactic acid) (PLA), poly(lactic-co-glycolic acid) (PLGA)[45] and poly(cyanoacrylate)[57] particles have been the 'pioneers'.

Whether of synthetic (polymers) or natural (sugar, protein, lipid) origin, nanoparticles are inherently stable structures, in contrast to self-assembled systems. This advantageous stability must however be coupled to a long-term degradation under physiological conditions, in order to prevent undesired body accumulation. Ideally, nanoparticles would deteriorate in products which are naturally excreted, or absorbed by the body.

Nanoparticle formation generally involves the use of organic solvents and/or some chemical reaction stabilizing the colloid structure. Stability and control over size from a single material are counterbalanced by the need of extensive purification.

The majority of microparticle preparation techniques have been tailored for the fabrication of nano-sized particles. Formation occurs either by polymerization of monomers (dispersion, emulsion polymerization) or by shaping/condensation of macromolecules (coacervation, spray drying, solvent evaporatrion). The former techniques require a size-dependent termination (e.g. polymer is insoluble in a solvent for monomer) or confined, isolated, nano-sized reactors (e.g. emulsion polymerization).

The selection of materials usually determines the choice of fabrication method. As this thesis deals with hydrophilic materials, the focus is placed on corresponding techniques and in particular, inverse emulsion polymerization.

1.6 Inverse emulsion polymerization

The term emulsion refers to a dispersion of one phase into another continuous phase (immiscible to the dispersed) with the help of an emulsifier (usually an amphipathic molecule). Emulsions are classified according to the nature of dispersed and continuous phase (oil-in-water or direct, water-in-oil or inverse, water-in-oil-in-water or double) and their size/stability (nanoemulsions[58], miniemulsions[59], microemulsions[60]). Control over structure, bulk and surface composition and favorable heat transport through the continuous phase make emulsions ideal as heterophase polymerization reactors[59].
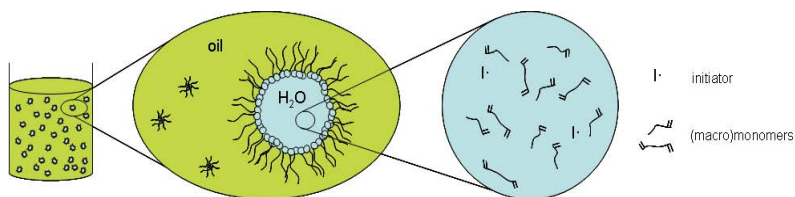

Figure 1.4. *A schematic representation of an inverse emulsion polymerization system, with water-soluble radical initiators and vinyl-containing (macro)monomers. The loci of polymerization are the emulsifier-stabilized aqueous droplets.*

Table 1.1 *Nanoparticles prepared via inverse emulsion polymerization for drug delivery applications.*

Material	Emulsifier(s)	Emulsion type[§]	Remarks	Ref.
Poly(acrylamide)	Aerosol OT (AOT)	IM	Size modulation through controlled dynamics	[61]
	various	IE		[62, 63]
Poly(acrylic acid)	Span®80 & Tween®80	IE	Size-dependence on initiator type (oil vs water soluble)	[64]
		IM	Bimodal size distribution suggests multiple nucleation sites	[65]
Poly(*N*-isopropylacrylamide) & polyelectrolytes or polyampholytes	Polyoxyethylene sorbitan hexaolate & sorbitan sesquioleate	IM	Optimization of surfactant concentrations for different monomer mixtures	[66]
Gelatin	Poly(methyl methacrylate)	IE	Formation of particles via gluteraldehyde cross-linking	[67]
	AOT	IM		[68]
Poly(vinyl pyrrolidone)	AOT	IM	Cross-linking polymerization	[69]
Poly(ethylene glycol) & 2-hydroxyethylacrylate & 2-acryloxythyl trimethylammonium	Laureth-3	IM	Cationic hydrogel nanoparticles for DNA delivery	[70]
Poly(dimethylacrylamide-co-2-acrylamido-2-methyl-1-propanesulfonic acid)	Polyoxyethylene olyelethers	IM	Interesting effect of cross-linker on final hydrodynamic size	[71]
Poly(aspartamide)	Span®85	IM	Photo-initiated cross-linking of functionalized macromonomers	[72]
Poly(acrylamide)	Span®80 & Tween®80	IE	Cross-linking with acid-degradable linker	[36]

[§] IE : Inverse Emulsion, IM : Inverse Microemulsion

Inverse (water-in-oil) emulsions (IE) were initially developed as an alternative to acrylamide polymerization in solution, but soon found their way in the field of hydrophilic nanoparticle formation[73]. Emulsification of the aqueous phase in the oil (commonly consisting of hydrocarbons) is achieved by amphiphiles with low 'hydrophilic lipophilic balance' (HLB) values; the lower the HLB, the more hydrophobic the emulsifier. Stabilization occurs

exclusively through steric effects since dielectric constant of oils is very low. IE are generally thermodynamically unstable and tend to phase separate with time. Thermodynamic stability is achievable (for low aqueous volume fractions) at the expense of high emulsifier concentrations; stable inverse microemulsions usually contain >8% wt. emulsifier, less than 15% v/v aqueous phase and necessitate the presence of co-emulsifiers[60].

The mechanism of polymerization depends strongly on the type of initiator (oil soluble or water soluble) as well as the oil-solubility of monomer(s). For hydrophilic initiators and monomers (homogeneous reaction mixture) the loci of initiation and propagation are the dispersed aqueous droplets, rather than the continuous phase or micellar structures. The obtained particle size distribution is therefore mainly determined by the nanodroplet size distribution of the IE, provided that reaction kinetics are faster than emulsion break-up. For this reason, typically radical polymerization has been selected as the reaction scheme.

Inverse emulsion polymerization is a multi-parameter system, whose potential and versatility in fabricating aqueous-based nanomaterials is already established, and whose optimization may provide better defined colloids for drug delivery applications.

1.7 *In situ* forming biomaterials

In addition to systemic targeted administration, localized drug delivery may be accomplished by introducing a drug depot directly at the target site. A major class of biomaterials, which among other applications (regenerative medicine) have been considered as implantable drug delivery systems, are hydrogels. These hydophilic polymer networks are capable of absorbing great amounts of water while keeping their structural integrity[74]. Their structural similarity to natural extracellular matrix prompted research towards biomedical applications. While use of natural materials containing innate biological signals remains an attractive option, certain drawbacks spurring their development have shifted interest towards biomimetic, synthetic analogues[75].

Implantation of preformed hydrogels necessitates creation of an opening with dimensions at least their size, a source of potential risks and patient discomfort. To overcome this limitation, design focus is being placed on injectable materials with the ability to form in a mild manner 3-dimensional elastic matrices under physiological conditions[76-78]. *In situ* formation may be achieved through specific chemical cross-linking reactions, following

mixing of precursor solutions. Alternatively, gel structuring is triggered by environmental or external stimuli (pH, light, temperature, solvent exchange etc.).

Table 1.2 *Overview of temperature-responsive gelation systems, proposed for biomedical applications*

	Material	Concentration; Temperature range	Remarks	Ref.
PNIPAM	PNIPAM	3-5% ; ~32°C	Transition temperature may be modulated by copolymerization of hydrophilic/hydrophobic monomers	[79]
	PNIPAM-co-AA	>3% ; 30-40°C	Copolymerization of acrylic acid (AA) prevents syneresis	[80]
	NPs of PNIPAM and PAAc	>2.5% ; 32-35°C	Physically bonded nanoparticle network based on interpenetrating networks	[48, 81]
Poloxamers	Poloxamer 407	20-30% ; ~25°C	Transparent gels without syneresis, biocompatible material, easy loading; quick dissolution	[82-84]
	Poloxamer-co-PAAc	0.5-5% ; ~25°C	Bioadhesive because of AA	[85-87]
	Oligo(poloxamers)	20-30%; 20-30°C	Larger aggregates, improved mechanical properties and delayed drug release	[88]
Celluloses	Methylcellulose	1-5% ; 25-50°C	Large pore structures	[89]
	Hydroxylpropyl methylcellulose	1-5% ; 75-90°C	Transition temperature is lowered by reducing the hydroxypropyl molar substitution	[90]
	Ethyl hydroxyethylcellulose with surfactants	1-5% ; 30-40°C	Assosciation is enhanced by micelle formation and clustering	[90, 91]
PLGA-PEG	PEG-PLGA-PEG	15-30% ; ~30°C	Biodegradable polymers; delayed release kinetics	[92-94]
	PEG-g-PLGA & PLGA-g-PEG	15-30% ; ~30°C	Grafted copolymers offer better control of degradation	[95, 96]
Miscellaneous	Chitosan	2% ; ~40°C	Addition of polyol salts transforms pH-dependent gelation to temperature-dependent	[97-100]
	Peptide	2% ; 25-65°C	Gelation temperature controlled by peptide sequence; folding of peptide and self-assembly into fibers.	[101]
	Poly(organophosphazenes)	5-10% ; ~37°C	Modulation of side chains determines gelation temperature	[102]

Besides the advantageous fact that the minimally invasive character of application circumvents surgical operation risks, the liquid nature of the precursors allows enhanced contact and shape-matching with surrounding tissue, thus avoiding the need of a case-to-case tailoring of the implant. Therapeutic agents can be incorporated by simple mixing, covalent attachment to the network through labile bonds, or by encapsulation in carriers (e.g. liposome) entrapped in the final implant.

1.7.1 Thermally responsive materials

Among in situ-forming systems, temperature-induced phase transitions from free-flowing liquids at ambient temperature, to gels at body temperature, have gained considerable attention[76, 77]. They belong to a category of physical transitions which do not require use of organic solvents, chemical cross-linking reactions or externally operated devices (e.g. photo-polymerization), and thus are less likely to induce toxicities to the surrounding tissues and denaturation of the active therapeutic agents to be delivered.

A number of polymers exhibit abrupt changes in their aqueous solubility with increases in temperature; the resulting sol-gel transition occuring at the lower critical solubility temperature (LCST) is characterized by minimal heat production and absence of byproducts. Let us consider the free energy of association (ΔG) between the polymer chains:

$$\Delta G = \Delta H - T \Delta S \qquad (1)$$

where ΔH is the enthalpy term, ΔS the entropy term and T temperature.

Increase over a critical temperature results in a larger value of $T \Delta S$ than the positive enthalpy term (ΔH), and thus a negative ΔG favoring polymer association: chain-chain interactions (hydrophobic effects, hydrogen bonding) dominate over chain-water hydrogen bonding.

Block copolymers containing one block with a LCST at a temperature range where the other block is soluble, self assemble in response to temperature increase. Morphology of the self-assembled structure depends on copolymer architecture and MW; micelles or networks of infinite MW (gels) can be obtained by appropriate design. A recently reported, alternative approach was based on interpenetrating networks of poly(*N*-isopropylacrylamide) (PNIPAM) and poly(acrylic acid) (PAAc), formulated in nanoparticles[48, 81]. The collapse of PNIPAM above its LCST triggered the bonding of the NPs into a network while the repulsion between the charged PAAc chains prevented agglomeration.

A list of developed materials exhibiting thermally-driven phase transitions is given in Table 1.2 One of the oldest and most widely studied materials from this constantly expanding

list, and one which was selected as a primary material in this thesis, is the non-ionic, amphiphilic poly(ethylene glycol)-*bl*-poly(propylene glycol)-*bl*-poly(ethylene glycol) (PEG-PPG-PEG) block copolymer, also refered to as poloxamer or Pluronic®.

1.7.2 Poloxamers - Pluronics®

The poloxamer family consists of more than 30 non-ionic, amphiphilic ABA-type block copolymers, where A is poly(ethylene glycol) (PEG) and B poly(propylene glycol) (PPG) (Figure 1.5). Their physical state (liquid, paste, solid), is governed by their MW and block ratio. Poloxamers are well tolerated (non-toxic), although at high concentrations some side-effects including hypercholesterolemia and hypertrglyceridemia[103,104] suggest that polymer concentration should be kept to a minimum.

Poloxamer temperature-induced aqueous gelation mechanism and gel structure has been elucidated using probe techniques[82,105], light scattering[82], rheometry[83,84,106] and small-angle neutron scattering[106,107] measurements. Micelle formation occurs as a result of PPG dehydration and hydrophobically-driven self-assembly with increasing temperature (at a critical micellar temperature (CMT) and at concentrations above the critical micellar concentration (CMC)). At high enough concentrations, the high density of micelles leads to locking in crystalline structures of hard spheres, a process which is usually, but not accurately, refered to as 'gelation'.
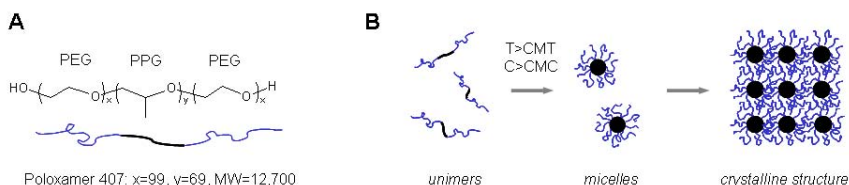
Figure 1.5 *Poloxamer structure (A) and self-assembly (B). The copolymer is in unimer form at low temperature or concentration. With increasing temperature (at concentrations exceeding the CMC) self-assembly into micelles occurs. Close-packing of micelles in crystalline structures, above a concentration threshold, leads to its gel-like behavior.*

Poloxamer 407 (Pluronic® F127) has an LCST at biologically relevent temperature (25°C at 20% wt.), a feature which made it the most popular candidate of the series for biomedical applications. Drug loading is readily achieved by simple mixing; however, an incovenience is the rapid dissolution and release, limiting the use for delivery periods of maximum a few days[108, 109]. Poloxamer 407 gels have been considered for cancer treatment[110],

prevention of postoperative adhesions[111, 112], pain treatment[113], transdermal delivery of insulin[114], peptide delivery[115] among other applications. Their transparency makes them ideal for opthalmic applications[116-119].

1.8 Outline of this thesis

The aim of this thesis was to develop a novel colloidal system for drug delivery applications. We were particularly interested in the production of well-defined, stable nanoparticles via a reproducible and versatile technique, which would allow the accomodation of a variety of therapeutic agents. The emergence of a wide variety of new hydrophilic drugs, combined with the moderate attention of aqueous-based nanoparticles compared to their hydrophobic counterparts, prompted us to design nano-sized hydrogels. Moreover we anticipated a stealth character, given the demonstrated, beneficial properties of hydrophilic surface coatings.

To achieve our goal we selected poly(ethylene glycol) and poloxamer as building blocks. Their established biocompatible, inert and protein repellent character make them ideal for biomedical applications. Both polymers have been used in drug delivery, the former in polymer-drug conjugates and as surface modifier and the latter as injectable *in situ*-forming gels as well as in the form of micellar carriers[120-122]. Moreover, these polymers are available in a range of MW and block ratios (in the case of poloxamer), offering the potential of fine-tuning the material properties.

Here we tackled the task of preparing stable nanostructures based on these polymers, with control over size and architecture. In order to accomplish this, we developed an inverse emulsion polymerization technique where acrylate-functionalized macromonomers were cross-linked through a photo-initiated radical polymerization. Probing the structure of the obtained nanospheres revealed stable hydrophobic nano-domains in the otherwise hydrophilic NPs (Chapter 2).

The need of highly efficient DDS for cancer treatment led us to consider this system for tumor delivery of doxorubicin. The small size (100-300nm in diameter) of the colloids is expected to promote passive targeting through permeable vasculature in tumors (EPR effect), while the hydrophobic pockets allowed drug loading. An *a posteriori* encapsulation protocol was established and *in vitro* release of DOX occurred by diffusion, without burst release, at therapeutically-relevant time scales. In combination with a demonstrated drug protective

effect of the carrier, these NPs proved to be promising candidates for cancer chemotherapy (Chapter 3).

We further explored an alternative initiation scheme, more suitable for scale-up NP fabrication. In order to introduce functionality or reactive groups for *a posteriori* modifications we investigated the copolymerization of low MW, vinyl-containing monomers. Fluorescent labeling served both as a proof of concept of the latter approach and as a tool for subsequent cell studies (Chapter 4).

Incorporation of poloxamer 407 in the cross-linked hydrogel network imparted temperature-responsiveness to the NPs; concentrated aqueous colloidal dispersions (>4% wt.) underwent a physical transition from free-flowing liquids to solid-like materials upon increase in temperature. In chapter 5, the mechanism and implications of this transition are discussed.

In vitro cell-nanoparticle interactions is the subject of chapter 6: having in mind *in vivo* drug delivery applications, such studies are an essential first step to assess the biomaterial's potential. Cytotoxicity of NPs in the form of dilute dispersions or colloidal glasses was found to be negligible. A setup for in vitro internalization studies was established; NP interactions with J774 murine macrophages, used as a model for phagocytic cells of the MPS were here investigated.

Finally, the major characteristics and shortcomings of these hydrogel NPs are summarized. Studies in progress and others envisioned are briefly discussed and clinical applications suitable for our system are suggested (Chapter 7).

1.9 References

1.   M. Ferrari *Cancer nanotechnology: opportunities and challenges* Nature Reviews Cancer 5 **2005** 161-171

2.   T.M. Allen and P.R. Cullis *Drug Delivery Systems: Entering the Mainstream* Science 303 **2004** 1818-1822

3.   K. Kostarelos *Rational design and engineering of delivery systems for therapeutics: biomedical exercises in colloid and surface science* Adv. Colloid Interface Sci. 106 **2003** 147-168

4.   S.M. Moghimi, et al. *Nanomedicine: current status and future prospects* The FASEB Journal 19 **2005** 311-330

5. S.M. Moghimi and J. Szebeni *Stealth liposomes and long circulating nanoparticles: critical issues in pharmacokinetics, opsonization and protein-binding properties* Progress in Lipid Research 42 **2003** 463-478

6. S.M. Moghimi, et al. *Long-Circulating and Target-Specific Nanoparticles: Theory to Practice.* Pharmacol Rev 53 **2001** 283-318

7. S.M. Moghimi and B. Bonnemain *Subcutaneous and intravenous delivery of diagnostic agents to the lymphatic system: Applications in lymphoscintigraphy and indirect lymphography* Adv. Drug Delivery Rev. 37 **1999** 295-312

8. S.M. Moghimi *Exploiting bone marrow microvascular structure for drug delivery and future therapies* Adv. Drug Delivery Rev. 17 **1995** 61-73

9. M. Luck, et al. *Analysis of plasma protein adsorption on polymeric nanoparticles with different surface characteristics.* J. Biomed. Mater. Res. 39 **1998** 478-485

10. V. Olivier, et al. *Uptake of polystyrene beads bearing functional groups by macrophages and fibroblasts* Coll. Surf. B Biointerf. 33 **2004** 23-31

11. R. Gref, et al. *'Stealth' corona-core nanoparticles surface modified by polyethylene glycol (PEG): influences of the corona (PEG chain length and surface density) and of the core composition on phagocytic uptake and plasma protein adsorption* Coll. Surf. B Biointerf. 18 **2000** 301-313

12. H. Otsuka, et al. *PEGylated nanoparticles for biological and pharmaceutical applications* Adv. Drug Delivery Rev. 55 **2003** 403-419

13. F. De Jaeghere, et al. *Cellular uptake of PEO surface-modified nanoparticles: Evaluation of nanoparticles made of PLA : PEO diblock and triblock copolymers* J. Drug Targeting 8 **2000** 143-153

14. S.M. Moghimi and A.C. Hunter *Poloxamers and poloxamines in nanoparticles engineering and experimental medicine.* Trends Biotechnol. 18 **2000** 412-420

15. J.K. Gbadamosi, et al. *PEGylation of microspheres generates a heterogeneous population of particles with differential surface characteristics and biological performance* FEBS Lett. 532 **2002** 338-344

16. P.-A. Oldenborg, et al. *Role of CD47 as a Marker of Self on Red Blood Cells* Science 288 **2000** 2051-2054

17. Y.C. Hsu, et al. *Reduced Phagocytosis of Colloidal Carriers Using Soluble CD47* Pharm. Res. 21 **2003** 1539-1542

18. M.A. Moses, et al. *Advancing the field of drug delivery: Taking aim at cancer* Cancer Cell 4 **2003** 337-341

19.   E. Ruoslahti *Specialization of tumour vasculature* Nature Reviews Cancer 2 **2002** 83-90

20.   H. Maeda, et al. *Tumor vascular permeability and the EPR effect in macromolecular therapeutics* J. Controlled Release 65 **2000** 271-284

21.   H. Hashizume, et al. *Openings between defective endothelial cells explain tumor vessel leakiness* Am. J. Pathol. 156 **2000** 1363-1380

22.   D. Feng, et al. *Ultrastructural Studies Define Soluble Macromolecular, Particulate, and Cellular Transendothelial Cell Pathways in Venules, Lymphatic Vessels, and Tumor-Associated Microvessels in Man and Animals* Microscopy Research and Technique 57 **2002** 289-326

23.   S.K. Hobbs, et al. *Regulation of transport pathways in tumor vessels: Role of tumor type and microenvironment* P. Natl. Acad. Sci. USA 95 **1998** 4607-4612

24.   Y. Bae, et al. *Preparation and Biological Characterization of Polymeric Micelle Drug Carriers with Intracellular pH-Triggered Drug Release Property: Tumor Permeability, Controlled Subcellular Drug Distribution, and Enhanced in Vivo Antitumor Efficacy* Bioconjugate Chem. 16 **2005** 122-130

25.   T.M. Allen *Ligand-Targeted Therapeutics in Anticancer Therapy* Nature Reviews Cancer 2 **2002** 750-763

26.   N. Dinauer, et al. *Selective targeting of antibody-conjugated nanoparticles to leukemic cells and primary T-lymphocytes* Biomaterials 26 **2005** 5898-5906

27.   K. Na, et al. *Self-assembled nanoparticles of hydrophobically-modified polysaccharide bearing vitamin H as a targeted anti-cancer drug delivery system* Eur. J. Pharm. Sci. 18 **2003** 165-173

28.   A. Fahr, et al. *A new colloidal lipidic system for gene therapy* Journal of Liposome Research 12 **2002** 37-44

29.   C.P. Leamon and J.A. Reddy *Folate-targeted chemotherapy* Adv. Drug Delivery Rev. 56 **2004** 1127-1141

30.   S.K. Sahoo and V. Labhasetwar *Enhanced Antiproliferative Activity of Transferrin-Conjugated Paclitaxel-Loaded Nanoparticles is Mediated via Sustained Intracellular Drug Retention* Molecular Pharmaceutics **2005**

31.   L. Nobs, et al. *Current Methods for Attaching Targeting Ligands to Liposomes and Nanoparticles* J. Pharm. Sci. 93 **2004** 1980-1992

32. V.P. Torchilin, et al. *TAT peptide on the surface of liposomes affords their efficient intracellular delivery even at low temperature and in the presence of metabolic inhibitors* Proceeding of the National Academy of Sciences 98 **2001** 8786-8791

33. J. Gruenberg *The endocytic pathway: a mosaic of domains* Nature Reviews Molecular Cell Biology 2 **2001** 721-730

34. K.D. Jensen, et al. *Cytoplasmic delivery and nuclear targeting of synthetic macromolecules* J. Controlled Release 87 **2003** 89-105

35. D. Trentin, et al. *Non-viral gene delivery for local and controlled DNA release* J. Controlled Release 102 **2005** 263-275

36. N. Murthy, et al. *A macromolecular delivery vehicle for protein-based vaccines: Acid-degradable protein-loaded microgels* P. Natl. Acad. Sci. USA 100 **2003** 4995-5000

37. E.R. Gillies and J.M.J. Frechet *pH-Responsive Copolymer Assemblies for Controlled Release of Doxorubicin* Bioconjugate Chem. 16 **2005** 361-368

38. I. Green, et al. *Protein transduction domains: are they delivering?* Trends Pharmacol. Sci. 24 **2003** 213-215

39. J.S. Wadia, et al. *Transducible TAT-HA fusogenic peptide enhances escape of TAT-fusion proteins after lipid raft micropinocytosis* Nat. Med. 10 **2004** 310-315

40. P. Watson, et al. *Intracellular trafficking pathways and drug delivery: fluorescence imaging of living and fixed cells* Adv. Drug Delivery Rev. 57 **2005** 43-61

41. F. Arcamone, et al. *Adriamycin, 14-Hydroxydaunomycin, a New Antitumor Antibiotic from S. peucetius var. caesius* Biotechnol. Bioeng. 11 **1969** 1101-1110

42. J.W. Park *Liposome-based drug delivery in breast cancer treatment* Breast Cancer Research 4 **2002** 95-99

43. A. Gabizon, et al. *Pharmacokinetics of pegylated liposomal doxorubicin - Review of animal and human studies* Clin. Pharmacokinet. 42 **2003** 419-436

44. K.J. Harrington, et al. *Liposomes as Vehicles for Targeted Therapy of Cancer. Part 2: Clinical Development* Clinical Oncology 12 **2000** 16-24

45. J. Panyam and V. Labhasetwar *Biodegradable nanoparticles for drug and gene delivery to cells and tissue* Advanced Drug Delivery Reviews 55 **2003** 329-347

46. K.S. Soppimath, et al. *Biodegradable polymeric nanoparticles as drug delivery devices* J. Controlled Release 70 **2001** 1-20

47. I. Brigger, et al. *Nanoparticles in cancer therapy and diagnosis* Adv. Drug Delivery Rev. 54 **2002** 631-651

48. X. Xia, et al. *Physically bonded nanoparticle networks: a novel drug delivery system* J. Controlled Release 103 **2005** 21-30

49. A. Nori and J. Kopecek *Intracellular targeting of polymer-bound drugs for cancer chemotherapy* Adv. Drug Delivery Rev. 57 **2005** 609-636

50. F. Aulenta, et al. *Dendrimers: a new class of nanoscopic containers and delivery devices* European Polymer Journal 39 **2003** 1741-1771

51. M. Adams, et al. *Amphiphilic Block Copolymers for Drug Delivery* J. Pharm. Sci. 92 **2003** 1343-1355

52. D.E. Discher and A. Eisenberg *Polymer vesicles* Science 297 **2002** 967-973

53. V.C.F. Mosqueira, et al. *Biodistribution of long-circulating PEG-grafted nanocapsules in mice: Effects of PEG chain length and density* Pharm. Res. 18 **2001** 1411-1419

54. V.C.F. Mosqueira, et al. *Poly(D,L-lactide) nanocapsules prepared by a solvent displacement process: Influence of the composition on physicochemical and structural* J. Pharm. Sci. 89 **2000** 614-626

55. J. Kreuter *Evaluation of nanoparticles as drug delivery systems I: preparation methods* Pharmaceutica Acta Helvetiae 58 **1983** 196-209

56. J.J. Marty, et al. *Nanoparticles - New Colloidal Drug Delivery System* Pharmaceutica Acta Helvetiae 53 **1978** 17-23

57. C. Vauthier, et al. *Poly(alkylcyanoacrylates) as biodegradable materials for biomedical applications* Adv. Drug Delivery Rev. 55 **2003** 519-548

58. T. Tadros, et al. *Formation and stability of nano-emulsions* Adv. Colloid Interface Sci. 108-109 **2004** 303-318

59. K. Landfester *Miniemulsions for Nanoparticle Synthesis* Top. Curr. Chem. 227 **2003** 75-123

60. J. Klier, et al. *Properties and applications of microemulsions* Adv. Mater. 12 **2000** 1751-1757

61. N. Munshi, et al. *Size modulation of polymeric nanoparticles under controlled dynamics of microemulsion droplets* J. Colloid Interface Sci. 190 **1997** 387-391

62. J. HernandezBarajas and D. Hunkeler *Heterophase water-in-oil polymerization of acrylamide by a hybrid inverse-emulsion/inverse-microemulsion process* Polymer 38 **1997** 5623-5641

63. J. Hernandez-Barajas and D.J. Hunkeler *Inverse-emulsion polymerization of acrylamide using block copolymeric surfactants: mechanism, kinetics and modelling* Polymer 38 **1997** 437-447.

64. B. Kriwet, et al. *Synthesis of bioadhesive poly(acrylic acid) nano- and microparticles using an inverse emulsion polymerization method for the entrapment of hydrophilic drug candidates* J. Controlled Release 56 **1998** 149-158

65. T.K. De and A.S. Hoffman *A reverse microemulsion polymerization method for preparation of bioadhesive polyacrylic acid nanoparticles for mucosal drug delivery: loading and release of timolol maleate* Artif. Cell. Blood Sub. 29 **2001** 31-46

66. O. Braun, et al. *Synthesis in microemulsion and characterization of stimuli-responsive polyelectrolytes and polyampholytes based on N-isopropylacrylamide.* Polymer 42 **2001** 8499-8510

67. M.G. Cascone, et al. *Gelatin nanoparticles produced by a simple W/O emulsion as delivery system for methotrexate* J. Mater. Sci.-Mater. M. 13 **2002** 523-526

68. A.K. Gupta, et al. *Effect of cellular uptake of gelatin nanoparticles on adhesion, morphology and cytoskeleton organisation of human fibroblasts* J. Controlled Release 95 **2004** 197-207

69. D.J. Bharali, et al. *Cross-linked polyvinylpyrrolidone nanoparticles: a potential carrier for hydrophilic drugs* J. Colloid Interface Sci. 258 **2003** 415-423

70. K. McAllister, et al. *Polymeric nanogels produced via inverse microemulsion polymerization as potential gene and antisense delivery agents.* J. Am. Chem. Soc. 124 **2002** 15198-15207

71. I. Kaneda, et al. *Water-swellable polyelectrolyte microgels polymerized in an inverse microemulsion using a nonionic surfactant* J. Colloid Interface Sci. 275 **2004** 450-457

72. E.F. Craparo, et al. *Preparation of Polymeric Nanoparticles by Photo-Crosslinking of an Acryloylated Polyaspartamide in w/o Microemulsion* Macromol. Chem. Phys. 205 **2004** 1955-1964

73. F. Candau *Inverse Emulsion and Microemulsion Polymerization,* Emulsion Polymerization and Emulsion Polymers **1997,** Ed. P. A. Lovell and M. S. El-Aasser

74. A.S. Hoffman *Hydrogels for biomedical applications* Adv. Drug Delivery Rev. 43 **2002** 3-12

75. M.P. Lutolf and J.A. Hubbell *Synthetic biomaterials as instructive extracellular microenvironments for morphogenesis in tissue engineering* Nature Biotechnology 23 **2005** 47-55

76. E. Ruel-Gariépy and J.-C. Leroux *In situ-forming hydrogels-review of temperature-sensitive systems* European Journal of Pharmaceitics and Biopharmaceutics 58 **2004** 409-426

77. B. Jeong, et al. *Thermosensitive sol-gel reversible hydrogels* Adv. Drug Delivery Rev. 54 **2002** 37-51

78. A. Hatefi and B. Amsden *Biodegradable injectable in situ forming drug delivery systems* J. Controlled Release 80 **2002** 9-28

79. H.G. Schild *Poly(N-isopropylacrylamide): experiment, theory and application* Prog. Polym. Sci. 17 **1992** 163-249

80. C.K. Han and Y.H. Bae *Inverse thermally-reversible gelation of aqueous N-isopropylacrylamide copolymer solutions* Polymer 39 **1998** 2809-2814

81. Z. Hu and X. Xia *Hydrogel Nanoparticle Dispersions with Inverse Thermoreversible Gelation* Adv. Mater. 16 **2004** 305-309

82. P. Alexandridis and T.A. Hatton *Poly(ethylene oxide)-poly(propylene oxide)-poly(ethylene oxide) block copolymer surfactants in aqueous solutions and at interfaces: thermodynamics, structure, dynamics, and modeling* Colloids Surf., A 96 **1995** 1-46

83. A. Cabana, et al. *Study of the gelation process of polyethylene oxide(a) polypropylene oxide(b) polyethylene oxide(a) copolymer (Poloxamer 407) aqueous solutions* J. Colloid Interface Sci. 190 **1997** 307-312

84. J.P. Habas, et al. *Understanding the complex rheological behavior of PEO-PPO-PEO copolymers in aqueous solution* J. Rheol. 48 **2004** 1-21

85. G. Chen and A.S. Hoffman *Graft copolymers that exhibit temperature-induced phase transition over a wide range of pH* Nature 373 **1995** 49-52

86. L. Bromberg *Novel Family of Thermogelling Materials via C-C Bonding between Poly(acrylic acid) and Poly(ethylene oxide)-b-poly(propylene oxide)-b-poly(ethylene oxide)* J. Phys. Chem. B 102 **1998** 1956-1963

87. L. Bromberg *Properties of Aqueous Solutions and Gels of Poly(ethylene oxide)-b-poly(propylene oxide)-b-poly(ethylene oxide)-g-poly(acrylic acid)* J. Phys. Chem. B 102 **1998** 10736-10744

88. D. Cohn, et al. *Improved reverse thermo-responsive polymeric systems* Biomaterials 24 **2003** 3707-3714

89.   M.C. Tate, et al. *Biocompatibility of methylcellulose-based constructs designed for intracerebral gelation following experimental traumatic brain injury* Biomaterials 22 **2001** 1113-1123

90.   A. Carlsson, et al. *Thermal Gelation of Nonionic Cellulose Ethers and Ionic Surfactants in Water* Colloids and Surfaces 47 **1990** 147-165

91.   M. Scherlund, et al. *Nonionic cellulose ethers as potential drug delivery systems for periodontal anesthesia* J. Colloid Interface Sci. 229 **2000** 365-374

92.   B. Jeong, et al. *Drug release from biodegradable injectable thermosensitive hydrogel of PEG-PLGA-PEG triblock copolymers* J. Controlled Release 63 **2000** 155-163

93.   B. Jeong, et al. *Thermoreversible Gelation of PEG-PLGA-PEG Triblock Copolymer Aqueous Solutions* Macromolecules 32 **1999** 7064-7069

94.   M.J. Park and K. Char *Gelation of PEO-PLGA-PEO Triblock Copolymers Induced by Macroscopic Phase Separation* Langmuir 20 **2004** 2456-2465

95.   Y.-M. Chung, et al. *Sol-Gel Transition Temperature of PLGA-g-PEG Aqueous Solutions* Biomacromolecules 3 **2002**

96.   B. Jeong, et al. *Thermogelling Biodegradable Polymers with Hydrophilic Backbones: PEG-g-PLGA* Macromolecules 33 **2000** 8317-8322

97.   E. Ruel-Gariepy, et al. *A thermosensitive chitosan-based hydrogel for the local delivery of paclitaxel* Eur. J. Pharm. Biopharm. 57 **2004** 53-63

98.   E. Ruel-Gariepy, et al. *Characterization of thermosensitive chitosan gels for the sustained delivery of drugs* Internation Journal of Pharmaceutics 203 **2000** 89-98

99.   A. Chenite, et al. *Rheological characterisation of thermogelling chitosan/glycerol-phosphate solutions* Carbohyd. Polym. 46 **2001** 39-47

100.   A. Chenite, et al. *Novel injectable neutral solutions of chitosan form biodegradable gels in situ* Biomaterials 21 **2000** 2155-2161

101.   D.J. Pochan, et al. *Thermally Reversible Hydrogels via Intramolecular Folding and Consequent Self-Assembly of a de Novo Designed Peptide* J. Am. Chem. Soc. 125 **2003** 11802-11803

102.   B.H. Lee, et al. *A Thermosensitive Poly(organophosphazene) Gel* Macromolecules 35 **2002** 3876-3879

103.   W.K. Palmer, et al. *Poloxamer 407-induced atherogenesis in the C57BL/6 mouse* Atherosclerosis 136 **1998** 115-123

104. Z.G. Wout, et al. *Poloxamer 407-mediated changes in plasma cholesterol and triglycerides following intraperitoneal injection to rats.* Journal of Parenteral Science & Technology 46 **1992** 192-200

105. A.V. Kabanov, et al. *Micelle formation and solubilization of fluorescent probes in poly(oxyethelene-B-oxypropyelene-B-oxyethelene) solutions* Macromolecules 28 **1995** 2303-2314

106. R.K. Prudhomme, et al. *Structure and rheology studies of poly(oxyethylene-oxypropylene-oxyethylene) aqueous solution* Langmuir 12 **1996** 4651-4659

107. K. Mortensen and J.S. Pedersen *Structural Study on the Micelle Formation of Poly(ethylene oxide)-Poly(propylene oxide)-Poly(ethylene oxide) Triblock Copolymer in Aqueous Solution* Macromolecules 26 **1993** 805-812

108. B.C. Anderson, et al. *Understanding drug release from poly(ethylene oxide)-b-poly(propylene oxide)-b-poly(ethylene oxide) gels* J. Controlled Release 70 **2001** 157-167

109. T. Moore, et al. *Experimental investigation and mathematical modeling of Pluronic (R) F127 gel dissolution: drug release in stirred systems* J. Controlled Release 67 **2000** 191-202

110. M.M. Amiji, et al. *Intratumoral administration of paclitaxel in an in situ gelling poloxamer 407 formulation* Pharm. Dev. Technol. 7 **2002** 195-202

111. S.H. Oh, et al. *Prevention of postsurgical tissue adhesion by anti-inflammatory drug-loaded Pluronic mixtures with sol-gel transition behavior* J. Biomed. Mater. Res. 72A **2005** 396-316

112. J.L. West and J.A. Hubbell *Comparison of covalently and physically cross-linked polyethylene glycol-based hydrogels for the prevention of postoperative adhesions in a rat model* Biomaterials 16 **1995** 1153-1156

113. A. Paavola, et al. *Controlled release injectable liposomal gel of ibuprofen for epidural analgesia* Int. J. Pharm. 199 **2000** 85-93

114. O. Pillai and R. Panchagnula *Transdermal delivery of insulin from poloxamer gel: ex vivo and in vivo skin permeation studies in rat using iontophoresis and chemical enhancers* J. Controlled Release 89 **2003** 127-140

115. R. Bhardwaj and J. Blanchard *Controlled-release delivery system for the alpha-MSH analog melanotan-I using poloxamer 407* J. Pharm. Sci. 85 **1996** 915-919

116. S.D. Desai and J. Blanchard *In vitro evaluation of pluronic F127-based controlled-release ocular delivery systems for pilocarpine* J. Pharm. Sci. 87 **1998** 226-230

117. S.D. Desai and J. Blanchard *Pluronic (R) F127-based ocular delivery system containing biodegradable polyisobutylcyanoacrylate nanocapsules of pilocarpine* Drug Deliv. 7 **2000** 201-207

118. K. Edsman, et al. *Rheological evaluation of poloxamer as an in situ gel for ophthalmic use* Eur. J. Pharm. Sci. 6 **1998** 105-112

119. A. Bochot, et al. *Liposomes Dispersed Within a Thermosensitive Gel: A New Dosage Form for Ocular Delivery of Oligonucleotides* Pharm. Res. 15 **1998** 1364-1369

120. S. Danson, et al. *Phase I dose escalation and pharmacokinetic study of pluronic-bound doxorubicin (SP1049C) in patients with advanced cancer* British Journal of Cancer 90 **2004** 2085-2091

121. V. Alakhov, et al. *Block copolymer-based formulation of doxorubicin. From cell screen to clinical trials* Coll. Surf. B Biointerf. 16 **1999** 113-134

122. A.V. Kabanov, et al. *Pluronic block copolymers as novel polymer therapeutics for drug and gene delivery.* J. Controlled Release 82 **2002** 189-212

Chapter 2

Amphiphilic Hydrogel Nanoparticles. Preparation, Characterization and Preliminary Assessment as New Colloidal Drug Carriers

Abstract

Inverse emulsion photopolymerization of acrylated poly(ethylene glycol)-*bl*-poly(propylene glycol)-*bl*-poly(ethylene glycol) and poly(ethylene glycol) was successfully employed to prepare stable, cross-linked, amphiphilic nanoparticles. Even at low emulsifier concentrations (2%) and high water-to-hexane to weight ratios (35/65), the stability of the inverse emulsion allowed for the formation of well-defined colloidal material. Inverse emulsion characteristics and polymerization conditions could be controlled to vary the size of the nanoparticles between 50 and 500 nm. The presence of hydrophobic nanodomains within these otherwise hydrophilic nanoparticles was verified by using pyrene as a microenvironmentally sensitive probe. We believe that the complex nano-architecture of these materials makes them a potentially interesting colloidal drug delivery carrier system and that the method should be useful for a number of amphiphilic macromolecular precursors.

2.1 Introduction

The amphiphilic poly(ethylene glycol)-*bl*-poly(propylene glycol)-*bl*-poly(ethylene glycol) polymers, known as Poloxamers or Pluronics, have attracted significant attention for controlled drug delivery applications in the form of micellar nanocontainers[1,2] and physical gels[3,4]. Hydrophobic self-assembly between the central PPG blocks induces polymer assembly into 5-20 nm spherical structures, consisting of a hydrophobic PPG-rich core stabilized by a hydrophilic PEG-rich corona. The core may solubilize lipophilic molecules, and the hydrated PEG corona prevents aggregation, protein adsorption, and recognition of the micelles as foreign bodies by the immune system[5,6]. Low toxicity and weak immunogenic properties have allowed for the use of Pluronic in topical and systemic administration[7,8], including intravenously administered micellar formulations that have reached the level of clinical trials[9].

More general use of Pluronic micellar carriers in the blood stream has been hampered by several factors that may reduce their circulation time: the small dimension of the aggregates and the limited MW of the polymer may allow premature renal excretion of the carrier and penetration through the tight junctions of healthy endothelium. Somewhat larger dimensions would be required for selective penetration only through permeable endothelia (known as the enhanced permeation and retention, EPR, effect[10]), such as those found in most solid tumors[11,12]. Furthermore, higher stability upon dilution in the blood stream, would also be required for prolonged circulation; micellar forms being thermodynamically unstable when overall polymer concentration falls below the critical micellar concentration (CMC).

In an effort to overcome the drawbacks described above, we have considered increasing the size and stability of the nanoscale Pluronic-based carriers while preserving the solubilization and biophysical properties of Pluronic. In work by others, hydrophilic colloidal particles of sub-micron size have been obtained by cross-linking reactions of monomers or functionalized macromonomers in non-interacting compartments or under conditions that ensure size-dependent termination[13-17]. An attractive method, which we have employed, is offered by inverse emulsion polymerization, where a water solution of precursors is dispersed in an oil phase by the use of an appropriate emulsifier, the nature and concentration of which determine the size of the nanoparticle[18, 19]. In a general case, inverse emulsions are less stable than regular emulsions (O/W: oil-in-water), since the low dielectric constant of oils makes electrostatic stabilization ineffective and only steric effects prevent aggregation and drop coalescence. Thermodynamically stable inverse microemulsions are nevertheless possible to obtain by using very high levels of emulsifier and lower aqueous phase volumes[20].

In this study we have employed photo-initiated polymerization of acrylates[21] as a mean to cross-link aqueous solutions of multifunctional macromonomers. This reaction has been successfully used for preparing protein repellent hydrogels in contact with cells and tissues, demonstrating negligible toxicity and fast kinetics[22, 23]. We have applied this approach to Pluronic derivatives in inverse emulsion, monitoring the reaction kinetics and conversion and studying the physical properties of the resulting nanoparticles. We showed the existence of hydrophobic nanophases using pyrene as an environmentally-sensitive probe. Finally, the particles demonstrated colloidal stability even upon freeze drying, a prerequisite for a practical drug delivery formulation.

2.2 Materials & Methods

2.2.1 Materials & Spectroscopy Characterization

Dichloromethane and *n*-hexane (99%) were purchased from LabScan (Oensingen, Switzerland). Tetrahydrofuran, toluene, acryloyl chloride, triethylamine, triethanolamine, pyrene, doxorubicin hydrochloride, Span®65 (sorbitan tristearate, HLB=2.1±1.0) were purchased from Fluka (Buchs, Switzerland). Pluronic® F127, a symmetric triblock copolymer with MW=12700, 70% wt. poly(ethylene glycol) and a central poly(propylene glycol) block, was purchased from Sigma (Buchs, Switzerland). Eosin Y and poly(ethylene glycol) diacrylate $\overline{M}_n$ =575 (PEG575 diacrylate) were purchased from Aldrich (Buchs, Switzerland). All solvents and reagents were used as received unless otherwise mentioned.

^{1}H-NMR spectra were recorded on a 300MHz Bruker spectrometer. FTIR spectra were recorded in ATR mode on a Spectrum One Perkin Elmer Spectrometer. Fluorescence spectra were obtained using a Perkin Elmer LS50b Luminescence spectrometer equipped with a four-position thermostated automatic cell changer with stirrer. UV-Vis spectra were recorded on a Perkin Elmer Lambda 20.

Abbreviations: HLB = Hydrophilic Lipophilic Balance, MWCO = Molecular Weight Cut-Off

2.2.2 Macromonomers

Pluronic® F127 diacrylate (F127 diacrylate) was synthesized as described elsewhere[24], providing a 100% conversion of alcohols to acrylates, with a typical yield of about 80%. Copolymer composition was confirmed by ^{1}H-NMR spectroscopy PEG575 diacrylate was

washed several times (5-7) with n-hexane prior to use in order to remove inhibitors. Composition was confirmed by ^{1}H-NMR spectroscopy and $\overline{M}_n$ by GPC.

The expression "Total Macromonomer" will refer to the sum of the weight % concentrations of all the macromonomers used in the polymerization mixtures.

2.2.3 Inverse emulsion stability

Span$^®$65 was dissolved in 5ml *n*-hexane in 20ml glass vials by sonication (4 min). An aqueous solution of Pluronic F127 was added to the oil phase and sonicated with a tip sonicator (Bandelin Sonoplus) for 1 min. The inverse emulsions were kept at room temperature and were photographed at 5, 15, 30 and 60 min after sonication. The photographs were analyzed to obtain the volume fraction of hexane that phase separated.

$$\text{Fraction of hexane phase separated} = (y/x) / (y_0/x_0) \qquad (2.1)$$

where x and y are the total and phase separated hexane phase heights, respectively, and y_0/x_0 the *n*-hexane-to-total volume ratio (e.g. 0.74 for 65/35 weight ratio). Several emulsifier concentrations (1, 2, 3, 4 % w/w$_{total}$), Pluronic F127 concentrations (0, 1, 5 and 10% w/w$_{aqueous}$) and oil-to-water weight ratios (95/5, 80/20, 65/35, 50/50) were investigated.

2.2.4 Formation of nanoparticles via inverse emulsion polymerization

In a typical experiment, 100 mg Span65 (2.0% w/w$_{total}$) was dissolved in 5ml *n*-hexane by sonication (4 min.). 1.7ml of aqueous precursor solution of F127 diacrylate, PEG575 diacrylate, triethanolamine and eosin Y (6.75%, 6.75%, 2.0%, 0.02% w/w$_{aqueous}$ respectively) were added to the oil phase (oil-to-water weight ratio = 65/35) and an inverse emulsion was formed by sonication for 1 min with a tip-sonicator (Bandelin Sonoplus). The inverse emulsion was illuminated with an Ar ion laser (480-520 nm) for 1 hr, at room temperature, at a flux of around 75mW/s, under magnetic stirring (400 rpm). After illumination, the inverse emulsion was poured into centrifuge tubes containing 35 ml *n*-hexane and 4 ml water. The aqueous phase was extracted with *n*-hexane to remove Span65 and then dialyzed against water (MWCO= 25,000, Spectrum Laboratories) to remove initiator and non-reacted macromonomers.

2.2.5 Preparation of hydrogel discs

Macromonomer precursor solutions were prepared in water with 2.7 mM triethanolamine and 10 µM eosin Y (2.0% and 0.035% w/w$_{aqueous}$ respectively). After addition

of the reagents, the solutions were sonicated for a better mixing (5 min), aliquots of 50 µl were placed between two glass slides, precoated with Sigmacote, and irradiated for 30 min with an Ar ion laser (480-520 nm) at a flux of 75 mW/cm^2. The hydrogel discs were exposed to water for at least 24 hr until equilibrium swelling was reached. The swelling index was calculated as the ratio of the weight of the swollen gel to the weight of the formed gel, for 3 different temperatures: 37ºC, 25ºC and 4ºC. All experiments were performed in triplicate.

2.2.6 Photopolymerization kinetics and conversion measurements

FTIR spectroscopy was used to determine photopolymerization kinetics by monitoring the shift of the ν C=O peak of the acrylate double bond upon reaction (1724→1734 cm^{-1}). The reaction was quenched at different times by the addition of 0.2% wt. hydroquinone aqueous solution.

^{1}H-NMR spectroscopy was used to determine the final double bond conversion at the end of the polymerization by comparing the peaks at δ=5.8, 6.2, 6.4 (double bond protons) and δ=3.5-3.7 (C-CH$_2$-O protons). Samples were prepared by dispersing freeze dried nanoparticles in CDCl$_3$.

2.2.7 Dynamic light scattering (DLS)

Values of hydrodynamic diameter were obtained by dynamic light scattering (DLS) measurements using a Brookhaven instrument (model BI-DSI) equipped with a Lexel 95 laser source (514 nm at room temperature) at a fixed angle of 90°. Prior to analysis, solutions were filtered through a Millex AP 0.4 m filter to remove dust. The digital correlator was operated with 200 channels, a minimum duration of 5 min and an average number of counts per second between 100x10^3 and 700x10^3. Temperature was set at 37ºC unless otherwise noted.

2.2.8 Nanoparticle stability and freeze drying

Purified aqueous suspensions were kept at 4°C and were periodically inspected by DLS. Lyophilized dry nanoparticles were obtained with or without the use of cryoprotectants - glucose (20% wt.) and trehalose (5% & 20% wt.). Samples prepared without cryoprotectants were sonicated with a tip-sonicator (Bandelin Sonoplus); all samples were filtered before DLS.

2.2.9 Pyrene partitioning in nanoparticle aqueous suspensions

Pluronic® F127 or freeze dried nanoparticles were dissolved in aqueous pyrene stock solution (6×10^{-7} M) and left to equilibrate for 2hr. Emission spectra from 351 nm to 450 nm were recorded (excitation: 339 nm) at 37ºC.

2.3 Results & Discussion

2.3.1 Inverse emulsion preparation

Control of ultimate nanoparticle size distribution requires control over the initial inverse emulsion and its stability during polymerization. The formation of inverse emulsions is generally favored by the presence of strongly hydrophobic emulsifiers or mixtures of emulsifiers, which are characterized by low hydrophilic-to-lipophilic balance (HLB) numbers. With an appropriate choice of the emulsifier, the dispersed domains can be sufficiently stable to allow monomers in water to polymerize before macroscopic phase separation takes place. Despite Pluronic® F127 being an amphiphilic structure, its high HLB value (22) requires the presence of a much more hydrophobic surfactant for the formation of an inverse emulsion; we have selected Span 65, HLB=2.1, to give an appropriately low HLB.

Inverse emulsion stability in the time scale of the cross-linking reaction is crucial for good control of the size dispersity of nanoparticles. We have assessed the stability of the inverse emulsions by visual inspection over a period of 1 hr without stirring. Phase separation occurred in all cases in a time frame variable from a few min to 1 hr, producing a pure hexane phase on the top of a second, opaque phase. The kinetics of formation and the relative amount of the excess oil phase were used for a semi-quantitative evaluation of inverse emulsion stability (Figure 2.1).

It should be noted that simple visual inspection in principle does not allow one to distinguish between sedimentation, which can be reversed by stirring, and coagulation, which results in changes of the droplet distribution from their initial states and is to be avoided. However, in all our experiments, redispersion of the droplets could be achieved by gentle shaking or stirring, thus suggesting the phase separation to be mainly caused by sedimentation.
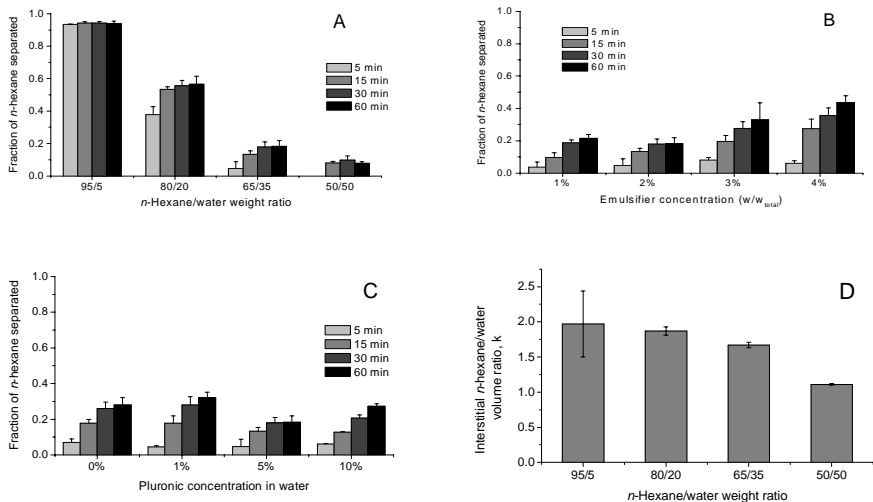
Figure 2.1 *A-C: Volume fraction of n-hexane phase separated from inverse emulsion as a function of time and hexane-to-water weight ratio for 2% Span 65 and 5% Pluronic F127 (A), of % emulsifier for 65/35 hexane-to water weight ratio and 5% Pluronic F127 (B) and of the concentration of Pluronic F127 for 65/35 hexane-to water weight ratio and 2% Span 65 (C). (D): interstitial hexane-to-water volume ratio at complete phase separation (60 min) for the formulations displayed in (A). Mean and S.D. are shown (n=3).*

If coagulation is negligible, phase separation is due to sedimentation of emulsified droplets, which reversibly produce a condensed phase containing hexane in the interstitial space; if this phase is stable, the interstitial hexane/water volume ratio (k) should be constant and should not depend on the overall hexane/water ratio. Under this assumption, when the process of phase separation is complete one should observe the formation of pure hexane in a volume fraction $x_{ph} = 1 - x_{ih} - x_{H2O} = 1 - (1+k)x_{H2O}$, where the indexes *ph* and *ih* stand, respectively, for pure and interstitial hexane. At a critical water volume fraction $x_{H2O}^{cr} = \dfrac{1}{1+k}$, phase separation should no longer occur, all the hexane being present in the interstitial form; finally, at higher water contents coagulation or formation of different phases should take place.

From experiments conducted in excess hexane (65 to 95% in weight), we have indeed observed a roughly constant value of $k \sim 1.8$ (Figure 2.1D), which suggests x_{ph} to possibly

be linearly related to χ_{H2O} (however, a more complex dependence cannot be excluded); the k value should correspond to a critical water volume fraction $\chi_{H2O}^{cr} = 0.35$, that is to an hexane-to-water weight ratio of 55/45 (for 5% Pluronic® F127 and 2% Span® 65). At the highest water content examined (50% wt.), the phase separated system is characterized by a markedly different value of k and by a much higher viscosity.

According to the above considerations and findings, we selected a hexane-to-water weight ratio of 65/35 for further experiments; this ratio is characterized by a high volume of the dispersed water phase (~26% in volume), but still ensures the stability of the aqueous droplets. Increasing levels of emulsifier resulted in increased phase separation (Figure 2.1B). This may arise from a higher content in smaller droplets (connected to a slight change in size distribution), which can pack more densely in the sedimented phase, which will then contain less hexane.

The effect of Pluronic concentration upon inverse emulsion stability was negligible. This suggests that the Pluronic does not participate to the steric stabilization of the droplets, despite its amphiphilic nature. Pluronic molecules are therefore to be found in the bulk of the aqueous droplet solution, most likely in micellar aggregates, since the concentration is always above the CMC at room temperature.

2.3.2 Nanoparticle formation

The aqueous macromonomer nano-droplets in the inverse emulsion are stabilized by subsequent polymerization. Photopolymerization of acrylic derivatives was chosen as a curing reaction, due to its mild character and to the possibility to control the initiation of the reaction, which allows for a good mixing of the reagents in the unreacted state. The aqueous phase, containing eosin Y (sensitizer), triethanolamine (initiator) and Pluronic F127 diacrylate alone or in mixture with the co-macromonomer PEG575 diacrylate, was dispersed in hexane by sonication with the help of Span 65 in the oil-to-water conditions described above. After the photopolymerization, the nanoparticles were purified by removal of the hydrophobic emulsifier through extensive washing with n-hexane (Scheme 2.1). The concentrations of triethanolamine and eosin Y were determined from preliminary experiments to obtain maximum conversion and were set at 2% and 0.02% (w/w$_{aqueous}$) respectively for all experiments.

Scheme 2.1 *Nanoparticle preparation via inverse emulsion photopolymerization*
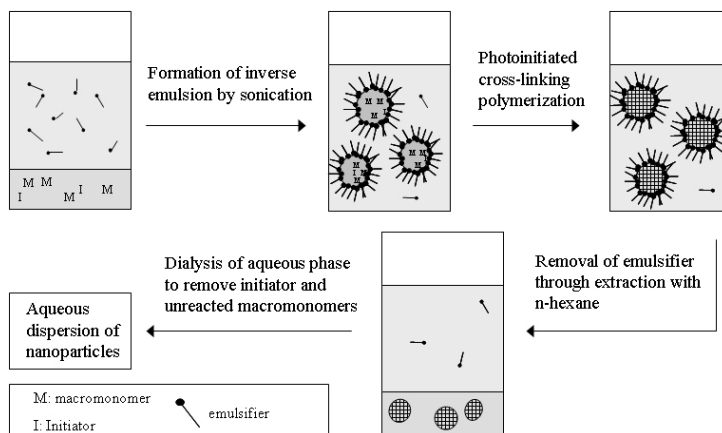
The photopolymerization of PEG diacrylates in bulk and in solution (with the use of N-vinyl pyrrolidone as a co-monomer) is known to proceed very fast (seconds to few minutes)[22, 25]. The wavenumber of the IR carbonyl stretching resonance (ν C=O) shifts from 1724 cm^{-1} to 1734 cm^{-1} upon reaction; by monitoring this peak, it was possible to follow the conversion of double bonds, which showed a plateau in around 30 min (Figure 2.2). ^{1}H-NMR spectroscopy on lyophilized dry nanoparticles resuspended in CDCl$_3$ showed this to correspond to a conversion always greater than 98%. We believe that the necessity for a long irradiation time results from the low effective light intensity, due to the high scattering within the inverse emulsions. For all experiments irradiation time was fixed to 1 hr to ensure complete conversion.
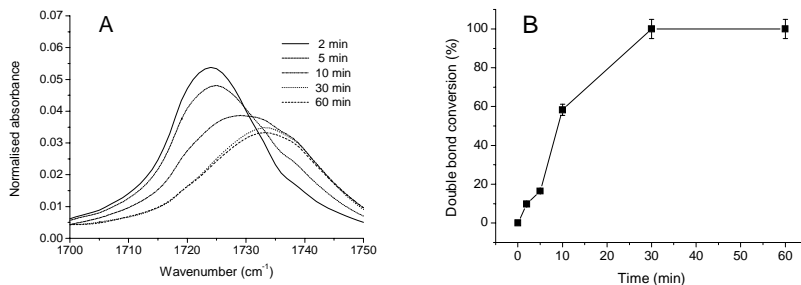
Figure 2.2 *(A) Absorption of ν C=O peak at different reaction times, normalized using the ν$_{as}$ (C-O-C) peak as a reference (1100cm^{-1}) (B) Estimated double bond conversion by (v$_t$-v$_0$)/(v$_f$-v$_0$), where v$_0$, v$_t$, v$_f$ are the wavenumbers of ν(C=O) absorbance maximum at time=0, t, ∞. Mean and S.D. are shown.*

The polymerization of F127 diacrylate without comonomers always produced colloidal objects able to diffuse through dialysis membranes with MWCO of 300,000, despite presenting an apparent hydrodynamic radius of 30-70 nm. We believe that, due to the micellar state of F127, the polymerization produced connected and cross-linked micellar aggregates rather than 'full' hydrogel nanoparticles. Similar objects have already been reported[26]; in our case, however, their size is not controlled, and it is independent of the inverse emulsion characteristics. We have therefore decided to use a water-soluble comonomer (PEG575 diacrylate) to provide polymerization throughout all the water phase of the emulsion droplet and thus generate nanoparticles with controlled size. The copolymerization process provided typical yields of about 80% (measured after emulsifier extraction as weight of dry particles/ initial weight of macromonomers). In principle, also other comonomers can be used in inverse emulsion photopolymerization, provided they contain polymerizable groups and they are soluble in water. The comonomers may differ in distances between polymerizable groups, and/or contain hydrolytically labile moieties, in order to vary mesh size and thus mass transport properties of the nanoparticle hydrogel and to provide degradability to the constructs, respectively.

2.3.3 Particle size

A key feature of the inverse emulsion polymerization process is its ability to control nanoparticle size distribution. The size of the macromonomer inverse emulsion droplets decreased with increasing emulsifier concentration and, assuming a template effect of the emulsions on nanoparticles, we expect the size of the polymerized nanoparticles to reflect this dependence. The nanoparticles indeed showed decreasing diameters with increasing concentrations of Span65 (2-4%), as shown in Figure 2.3 for two different sets of conditions. One can observe that the size of the nanoparticles, as for the nano-droplets in the inverse emulsion, was dramatically influenced by the composition of the polymerizing mixture. For subsequent experimentation, we selected an emulsifier concentration of 2% w/w.
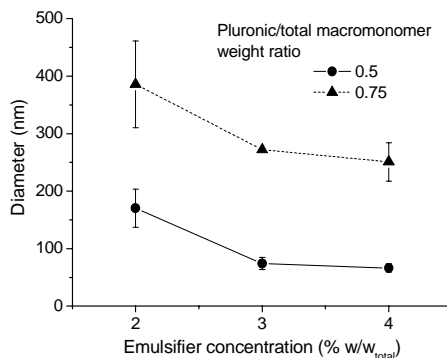

Figure 2.3 *Diameter as a function of emulsifier concentration for nanoparticles prepared with 12.5% wt. total macromonomer concentration. Mean and S.D. are shown (n=3).*

We studied a series of samples with 3 different ratios of Pluronic F127 diacrylate/total macromonomer and at 3 different total macromonomer concentrations (Figure 2.4). A significant increase in diameter was observed upon increasing the relative amount of PEG575 diacrylate, with a more pronounced effect at high total macromonomer concentration. This effect could be ascribed to a pre-polymerization event (on liquid drops), to a post-polymerization one (on gel particles), or it may be a consequence of the polymerization itself. In the last case, the differential size should be related to the different densities of polymerizable groups: however, the polymerization could hardly affect the density of the aqueous droplets, therefore we assume their size to remain unchanged in the transformation to nanoparticles. Two other possible composition-dependant phenomena are A) the swelling of the nanoparticles when exposed to pure water (post-polymerization): when exposed to water,

the nanoparticles may swell, due to the different osmotic pressure developed during photopolymerization. By replacing Pluronic with PEG, both increased hydrophilicity and cross-linking density (PEG575 is more than 20 times smaller than F127) can indeed produce higher osmotic pressure, resulting in ultimately larger, more swollen nanoparticles. B) The combined action of mechanical shear forces and chemical reactivity on droplet collisions in the early stages of photopolymerization (pre-polymerization): the macromonomer solutions have different viscosities and likely different gelation kinetics.
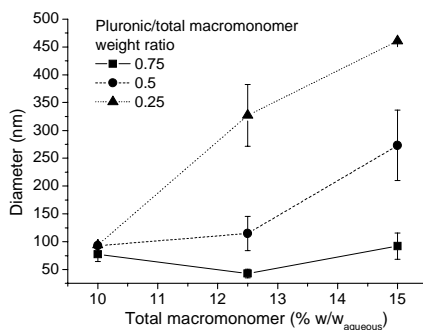

Figure 2.4 *Diameter of nanoparticles at 37°C as a function of the total macromonomer concentration. The nanoparticles were prepared with 2.0% emulsifier. Mean and S.D. are shown (n=3).*

In order to gather more information about the swelling phenomena of the polymer network in the nanoparticles, we have prepared and characterized macroscopic hydrogels with compositions analogous to those of the nanoparticles. Macroscopic hydrogels swelled by decreasing temperature, with a swelling extent proportional to the Pluronic concentration (Figure 2.5A); this has already been seen in other examples of Pluronic-based hydrogels presented in recent literature[24]. DLS experiments on nanoparticles at two different temperatures showed the same trend, with a decrease in diameter resulting from increasing temperature (Table 2.1).

Table 2.1 *Nanoparticle diameters in nanometers (12.5% wt. total macromonomer conc.) at two different temperatures (n=3)*

Pluronic/total macromonomer	0.75	0.50	0.25

| 37ºC | 170.4±3.2 | 169.0±3.0 | 203.4±9.1 |
| 25ºC | 181.4±6.0 | 185.3±2.2 | 203.6±8.0 |

The qualitative agreement between nanoparticle and macroscopic hydrogel temperature-induced swelling indicates that hydrogels can acceptably model the behavior of the amphiphilic nanoparticles However, differently from nanoparticles, in macroscopic hydrogels higher levels of Pluronic resulted in greater swelling, with a steeper dependence with increasing total concentration of macromonomers (Figure 2.5B). This phenomenon may be rationalized by considering that, at constant total macromonomer concentration, the cross-linking density increases with increasing PEG575 diacrylate content, due to its smaller chain length; thus, swelling should be decreased at higher PEG 575 diacrylate content.
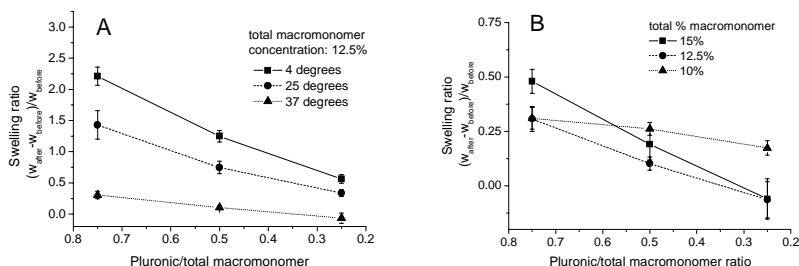

Figure 2.5 *Swelling behavior of hydrogel discs prepared by solution photopolymerization: (A) dependence on temperature, (B) dependence on macromonomer total weight and ratio at 37ºC. Mean and S.D. are shown (n=3).*

The modulation of swelling extent with composition, as observed in the macroscopic hydrogels, cannot explain the much bigger and opposite changes observed in nanoparticle dimensions. For example, one may consider two particles with overall macromonomer contents of 15% and Pluronic fractions of 0.75 or 0.25; applying the swelling ratios recorded on macroscopic hydrogels (0.5 and 0, respectively), the nanoparticles should increase their diameter by a factor 1.15 and 1, respectively. On the contrary, such nanoparticle diameters were observed to increase by a factor 1.19 and 4.95, respectively, demonstrating both an unexpected trend and different magnitude of the phenomenon.

If the dependence of nanoparticle dimensions on comonomer composition cannot be explained on the basis of a post-curing event, such as a differential swelling, it may be due to phenomena happening during photopolymerization that modulate the average size of the polymerizing droplets. It is well known that collisions between droplets are a destabilizing factor for inverse emulsions, and the frequency of collisions can be changed by varying the stirring speed. Indeed we have observed that, in the absence of stirring, the dependence of the particle size on composition completely disappeared and particles always presented an average diameter of 158.5±15.9 (Figure 2.6).

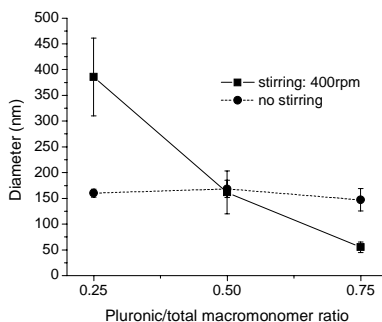Figure 2.6 *Effect of stirring of inverse emulsion during the cross-linking reaction on nanoparticle diameter (2.0% w/w$_{total}$ emulsifier and 12.5% wt. total macromonomer concentration). Mean and S.D. are shown (n=3).*

It is logical to assume that, in a collision, the probability of having an inter-particle chemical reaction, and thus irreversible coalescence, increases with increasing number of reactive groups (acrylates). Our results (Figure 2.7) qualitatively confirmed such an increase. Nevertheless, the higher diameter of high Pluronic content samples observed in the absence of stirring cannot be easily explained and this suggests that processes other than coalescence take place during polymerization under stirring.
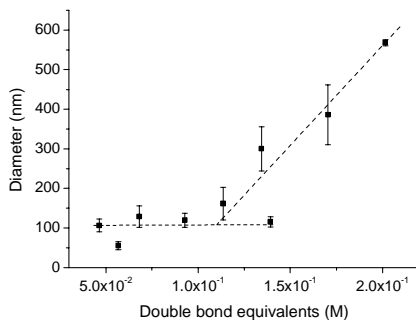
Figure 2.7 *Diameter vs. amount of reactive double bonds (concentration in the water phase) at 400 rpm stirring speed. The line is a guide to the eye. Mean and S.D. are shown.*

Finally, we examined the colloidal stability of our nanoparticle system, as it is essential for intravenous administration considering the dependence of size on biodistribution and cellular uptake and the risk of embolization upon aggregation. Aqueous nanoparticle suspensions were stored at 4°C in pure water; although further experiments using biological fluids are required to simulate conditions *in vivo*, DLS measurements provided promising results and showed no agglomeration for periods of at least one month.

2.3.4 Pyrene partitioning

Photopolymerization of the precursor aqueous solutions can preserve the micellar aggregates of Pluronic F127 in a nanoparticle structure that is insensitive to dilution below Pluronic F127's CMC. Having in mind the incorporation of hydrophobic drugs in the nanoparticles, the amount of loaded 'guest' molecules should depend on the permanence of these micellar structures after photopolymerization and on their number. To prove the above, we have investigated the internal architecture of the nanoparticles using a non-destructive probe technique based on pyrene. Pyrene is a fluorescent probe widely exploited to obtain information on the presence of supramolecular aggregates of amphiphiles[27, 28], the partition coefficients of a probe between solution and aggregate[5, 28], and its release from them[29].

We monitored changes in the intensity ratio of the first to the third vibrational band in the emission spectra of pyrene (I_1/I_3) with increasing aqueous concentrations of nanoparticles. It is known that the I_1/I_3 ratio decreases with decreasing polarity of the microenvironment in which the probe is located. As a control experiment, pyrene emission was examined upon exposure to different concentrations of unreacted Pluronic F127. The measured I_1/I_3 ratios

were plotted against Pluronic concentration (Figure 2.8), since only Pluronic could provide the hydrophobic domains necessary to change the I_1/I_3 ratio. The transition between two plateau I_1/I_3 values (from aqueous solution to the hydrophobic nanoenvironment) with increasing concentrations of nanoparticles confirmed the presence of hydrophobic domains in their structure. Experimental data were fitted with a sigmoidal fit and the inflection points of these fits were used for comparisons (Table 2.2).
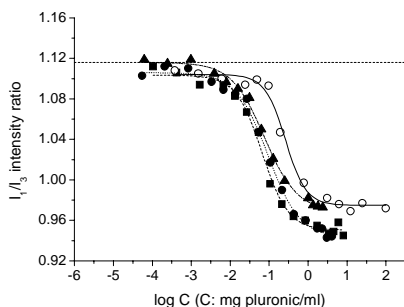

Figure 2.8 *Semilogarithmic plots of the I_1/I_3 fluorescence intensity ratio as a function of Pluronic concentration for various nanoparticles. Symbols represent nanoparticles with 12.5% total macromonomer and Pluronic/total macromonomer ratio of a. 0.75 (■) b. 0.5 (●) c. 0.25 (▲). Unreacted Pluronic (○) is also plotted as well as the value of I_1/I_3 in water (dashed horizontal line).*

In the control experiment, the transition from $I_1/I_3 = 1.10$ to 0.97 is due to the self assembly of the Pluronic unimers into micelles, which takes place in a concentration range between 0.1 and 1 mg/ml. In the case of the nanoparticle suspensions, the increase in the value of I_1/I_3, occurs at lower concentration, confirming that dilution does not destabilize the hydrophobic domains within the cross-linked nanoparticle that composes the nanoparticles. However, a transition eventually does occur, due to the depletion of available sites for solubilization at fixed pyrene concentration. The similar I_1/I_3 values at high concentrations for both Pluronic micelles and nanoparticles confirm our hypothesis that pyrene is solubilized in an environment similar to that of the cores of Pluronic micelles. No dependence of the transition characteristics (I_1/I_3 plateau values, inflection points) upon the Pluronic content of the nanoparticles was observed, demonstrating that the PEG incorporated into the network does not disturb the hydrophobic nanodomains that form from the Pluronic incorporated within the nanoparticle.

We therefore suppose the nanoparticles to contain multiple hydrophobic nano-domains constituted by interacting PPG domains of neighboring Pluronic chains. The hydrophobic domains are 'caged' in a protein-repellent hydrogel, which, contrary to micelles and nano-aggregates, provides stability upon dilution. Similar approaches were recently used to prepare micelle-coated surfaces[30] and self-aggregates with multiple hydrophobic domains for controlled drug delivery applications[31, 32].

Table 2.2 *High-concentration plateau I_1/I_3 intensity ratios and transition concentrations[a] for nanoparticle aqueous solutions and control (free Pluronic)*

Samples[b]	I_1/I_3 intensity ratio	Transition concentration (mg Pluronic/ml)	Transition concentration (mg nanoparticles/ml)
Control	0.97	0.26	-
12.5% / 0.25	0.97	0.08	0.30
12.5% / 0.50	0.94	0.09	0.19
12.5% / 0.75	0.95	0.06	0.09

[a] measured as the inflection points of the sigmoidal fits in Figure 2.8
[b] (% total macromonomer wt. / Pluronic-to-total macromonomer weight ratio)

2.3.6 Freeze drying

The high stability of the nano-droplets in the inverse emulsion and of the nanoparticles in aqueous suspension after purification suggests studies of stability after removal of the aqueous phase and resuspension. Freeze drying indeed offers the possibility to store and even sterilize nanoparticles in the form of a dry powder, which can eventually return to the colloidal state upon rehydration[33]. We freeze dried and rehydrated nanoparticles without using cryoprotectants and monitored the size, in order to determine whether aggregation takes place during this process (Figure 2.9A).

In order to redisperse the nanoparticles, we employed a short sonication step (5-10 min). Interestingly, using 2% emulsifier, the diameter after rehydration decreased, suggesting a break up of the nanoparticles during this sonication step. This effect was not observed however when smaller nanoparticles were prepared with 3% emulsifier, when rehydrated samples showed unchanged dimensions before and after freeze drying. We further investigated the effect of cryoprotectants; trehalose and glucose were selected since both have been previsouly used succesfully in PLGA formulations. In this case dispersion of rehydrated

NPs was achieved by mild shaking only. Between the two cryoprotectants, glucose proved to be effective in preventing aggregation whereas trehalose showed an incomplete concentration-dependent protective effect (Figure 2.9B)

Thus, the nanoparticles appear stable to freeze drying and resuspension in water, allowing long-term storage in a freeze-dried state.
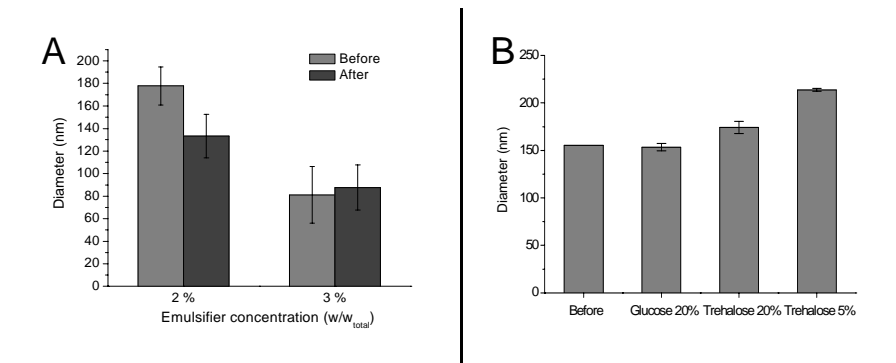

Figure 2.9 *Diameter of nanoparticles before and after freeze drying. Effect of emulsifier concentration in the absence of cryoprotectants (A) and effect of cryoprotectants (B) mean and S.D. are shown (A: n=4, B: n=2).*

2.4 Conclusions

The amphiphilic and biocompatible structure of Pluronic F127 offers an ideal starting point for the design of colloidal carriers for hydrophobic drugs with a prolonged circulation time. In particular, we have tackled the development of Pluronic-based chemically cross-linked nanoparticles, a class of materials characterized by high stability towards dilution and drying and therefore ideal for prolonged storage and use. Such systems, although requiring additional processing in fabrication, offer numerous advantages in use vis-à-vis their parent micellar structures.

We have demonstrated that well-defined Pluronic-based nanoparticles can be obtained via inverse emulsion photopolymerization. Bridging between micelles in the precursor solution, to form macromolecular nanogels with size being determined by processing rather than micelle size, is ensured by copolymerization with a PEG diacrylate. Nanoparticle size

could be controlled through manipulation of polymerization conditions, most notably emulsifier concentration, and the resulting materials were stable upon dilution and resuspension after freeze drying. Hydrophobic nanodomains within the particles remain after polymerization and are potentially capable of absorbing large amounts of hydrophobic drugs.

2.5 References

1. S.M. Moghimi and A.C. Hunter *Poloxamers and poloxamines in nanoparticles engineering and experimental medicine.* Trends Biotechnol. 18 **2000** 412-420

2. A.V. Kabanov, et al. *Pluronic block copolymers as novel polymer therapeutics for drug and gene delivery.* J. Controlled Release 82 **2002** 189-212

3. O. Pillai and R. Panchagnula *Transdermal delivery of insulin from poloxamer gel: ex vivo and in vivo skin permeation studies in rat using iontophoresis and chemical enhancers* J. Controlled Release 89 **2003** 127-140

4. K. Edsman, et al. *Rheological evaluation of poloxamer as an in situ gel for ophthalmic use* Eur. J. Pharm. Sci. 6 **1998** 105-112

5. A.V. Kabanov, et al. *Micelle formation and solubilization of fluorescent probes in poly(oxyethelene-B-oxypropyelene-B-oxyethelene) solutions* Macromolecules 28 **1995** 2303-2314

6. R. Nagarajan *Solubilization of "guest" molecules into polymeric aggregates* Polym. Adv. Technol. 12 **2001** 23-43

7. M.M. Amiji, et al. *Intratumoral administration of paclitaxel in an in situ gelling poloxamer 407 formulation* Pharm. Dev. Technol. 7 **2002** 195-202

8. J.M. Grindel, et al. *Distribution, metabolism, and excretion of a novel surface-active agent, purified poloxamer 188, in rats, dogs, and humans* J. Pharm. Sci. 91 **2002** 1936-1947

9. V. Alakhov, et al. *Block copolymer-based formulation of doxorubicin. From cell screen to clinical trials* Coll. Surf. B Biointerf. 16 **1999** 113-134

10. H. Maeda, et al. *Tumor vascular permeability and the EPR effect in macromolecular therapeutics* J. Controlled Release 65 **2000** 271-284

11. S.K. Hobbs, et al. *Regulation of transport pathways in tumor vessels: Role of tumor type and microenvironment* P. Natl. Acad. Sci. USA 95 **1998** 4607-4612

12. H. Hashizume, et al. *Openings between defective endothelial cells explain tumor vessel leakiness* Am. J. Pathol. 156 **2000** 1363-1380

13. M.G. Cascone, et al. *Gelatin nanoparticles produced by a simple W/O emulsion as delivery system for methotrexate* J. Mater. Sci.-Mater. M. 13 **2002** 523-526

14. K. McAllister, et al. *Polymeric nanogels produced via inverse microemulsion polymerization as potential gene and antisense delivery agents.* J. Am. Chem. Soc. 124 **2002** 15198-15207

15. D.J. Bharali, et al. *Cross-linked polyvinylpyrrolidone nanoparticles: a potential carrier for hydrophilic drugs* J. Colloid Interface Sci. 258 **2003** 415-423

16. B. Kriwet, et al. *Synthesis of bioadhesive poly(acrylic acid) nano- and microparticles using an inverse emulsion polymerization method for the entrapment of hydrophilic drug candidates* J. Controlled Release 56 **1998** 149-158

17. T.K. De and A.S. Hoffman *A reverse microemulsion polymerization method for preparation of bioadhesive polyacrylic acid nanoparticles for mucosal drug delivery: loading and release of timolol maleate* Artif. Cell. Blood Sub. 29 **2001** 31-46

18. F. Candau *Inverse Emulsion and Microemulsion Polymerization,* Emulsion Polymerization and Emulsion Polymers **1997,** Ed. P. A. Lovell and M. S. El-Aasser

19. K. Landfester *Miniemulsions for Nanoparticle Synthesis* Top. Curr. Chem. 227 **2003** 75-123

20. J. Barton *Free-Radical Polymerization in Inverse Microemulsions* Prog. Polym. Sci. 21 **1996** 399-438

21. J.P. Fisher, et al. *Photoinitiated polymerization of biomaterials* Ann. Rev. Mater. Res. 31 **2001** 171-181

22. C.P. Pathak, et al. *Rapid Photopolymerization of Immunoprotective Gels in Contact with Cells and Tissue* Journal of American Chemical Society 114 **1992** 8311-8312

23. G.M. Cruise, et al. *A sensitivity study of the key parameters in the interfacial photopolymerization of poly(ethylene glycol) diacrylate upon porcine islets* Biotechnology and Bioengineering 57 **1998** 655-665

24. F. Cellesi, et al. *Materials for cell encapsulation via a new tandem approach combining reverse thermal gelation and covalent crosslinking* Macromol. Chem. Phys. 203 **2002** 1466-1472

25. J.A. Hubbell *Hydrogel systems for barriers and locla drug delivery in the control of wound healing* J. Controlled Release 39 **1996** 305-313

26. K. Stahler, et al. *Multicompartment polymeric micelles based on hydrocarbon and fluorocarbon polymerizable surfactants* Langmuir 15 **1999** 7565-7576

27. J.R. Lopes and W. Loh *Investigation of self-assembly and micelle polarity for a wide range of ethylene oxide propylene oxide ethylene oxide block copolymers in water* Langmuir 14 **1998** 750-756

28. K.Y. Lee, et al. *Structural determination and interior polarity of self-aggregates prepared from deoxycholic acid-modified chitosan in water* Macromolecules 31 **1998** 378-383

29. J.X. Zhao, et al. *Partitioning of pyrene between "crew cut" block copolymer micelles and H2O/DMF solvent mixtures* Macromolecules 30 **1997** 7143-7150

30. K. Emoto, et al. *Functionality of polymeric micelle hydrogels with organized three-dimensional architecture on surfaces* J. Am. Chem. Soc. 122 **2000** 2653-2654

31. K. Na and Y.H. Bae *Self-assembled hydrogel nanoparticles responsive to tumor extracellular pH from pullulan derivative/sulfonamide conjugate: Characterization, aggregation, and adriamycin release in vitro* Pharm. Res. 19 **2002** 681-688

32. K. Na, et al. *Self-assembled nanoparticles of hydrophobically-modified polysaccharide bearing vitamin H as a targeted anti-cancer drug delivery system* Eur. J. Pharm. Sci. 18 **2003** 165-173

33. Y.N. Konan, et al. *Preparation and characterization of sterile and freeze-dried sub-200 nm nanoparticles* Int. J. Pharm. 233 **2002** 239-252

Chapter 3

Doxorubicin Encapsulation and Diffusional Release from Stable, Polymeric, Hydrogel Nanoparticles

Abstract

We have described the preparation of stable, polymeric nanoparticles, composed of poly(ethylene glycol) and Pluronic®, prepared via inverse emulsion photopolymerization (Chapter 2). In the present chapter we report on the performance of this novel colloidal system as a controlled delivery device for small hydrophobic drugs. Successful encapsulation of doxorubicin occurred through hydrophobic interactions, taking advantage of particle nano-architecture. Loadings of up to 8.7% wt. were achieved using a reproducible, fast procedure. *In vitro* drug release, monitored by fluorescence spectrometry and HPLC, revealed a minor burst (approx. 10% at 37°C) and sustained, diffusional release for over one week; furthermore, drug encapsulation significantly delayed doxorubicin degradation kinetics.

3.1 Introduction

In the field of carrier-mediated drug delivery the optimization of the therapeutic index of each active agent generally requires an *ad hoc* designed system, according to the disease and treatment [1, 2]. The carrier functions can therefore be very diverse, each with application-varying importance, including transport to the targeted tissue, increase of cargo solubilization, protection against degradation or elimination by the mononuclear phagocytic system (MPS) [3]. More sophisticated tasks may be promoted, such as active targeting to specific cells and tissues[4] and control of intracellular distribution[5].

In the development of new colloidal structures as circulating carriers, the assessment of their performance as drug carriers necessarily comprises the knowledge of the loaded amount of drug, its physical state and distribution inside of the carrier, as well as its release kinetics and the influence of environmental factors on it. Although the *in vivo* carrier performance may often differ appreciably, these data provide the first useful information on the mechanism and kinetics can be derived.

In chapter 2, we have reported on the preparation of copolymeric, cross-linked nanoparticles of poly(ethylene glycol)-*bl*-poly(propylene glycol)-*bl*-poly(ethylene glycol) (PEG-PPG-PEG) block copolymers, known as Poloxamers or Pluronics® and poly(ethylene glycol) (PEG), via inverse emulsion photopolymerization[6]. Stable sites for encapsulation of poorly-water soluble agents are present in the formed nanoparticles, due to the hydrophobic domains of PPG. On the other hand, the presence of PEG imparts hydrophilicity and possibly protein repellent character, suggesting long circulation times in body fluids; the sub-micron size, surely contributes to this, while it is also supposed to favor the nanoparticle passive accumulation in regions of impaired vasculature (as in the case of most solid tumors)[7-9]. All these features prompted us to investigate the possibility of developing these nanoparticles as a contolled release drug formulation.

Furthermore, concentrated dispersions of this novel particulate system may produce physical gels (specifically colloidal glasses) upon heating in a biologically relevant temperature range (25-35°C). The ease of application, slow dissolution kinetics (compared to Pluronic micellar gels) and expected low toxicity of the formulation are advantageous features of this system in view of its application as a macroscopic drug depot[10].

In the present chapter we have characterized the encapsulation and release properties of Pluronic nanoparticles using doxorubicin (DOX). The benefits of carrier-mediated DOX

delivery are related to its non-negligible side effects, above all its high cardiotoxicity, which have fuelled research on DOX carriers, e.g. liposomal[11], micellar[12-15] and polymer-DOX conjugates[16]. Despite enhanced therapeutic effects that have led to commercialization of some of these approaches, there is still room for improvement: physically self-assembled structures (liposomes, micelles), where DOX is incorporated due to hydrophobic interactions, face problems deriving from low stability and drug leakiness, whereas polymer-drug conjugates generally require high molecular weight backbones (difficult renal excretion) and suffer from high cost and low drug-to-polymer loading ratios.

Nanoparticles, on the other hand, may circumvent some of the above drawbacks[17]. Micellar structures are present in the bulk of our Pluronic nanoparticles[6], and this nano-architecture allows for a physical encapsulation of the drug in its deprotonated (hydrophobic) state. On the other hand, the chemically cross-linked nature of the carrier provides an enhanced stability in a variety of environmental conditions.

We here present the development of an *a posteriori* drug loading protocol, which avoids the exposure of the drug to the harsh conditions of radical polymerization. We then report on the release behaviour at high dilution, and particularly on kinetics, mechanism and physical state of released drug molecules.

3.2 Materials & Methods

3.2.1 Materials & Spectroscopy Characterization

Acetonitrile and *n*-hexane (99%) were purchased from LabScan (Oensingen, Switzerland). Triethylamine, triethanolamine, potassium iodide, sodium chloride, doxorubicin hydrochloride, Span®65 (sorbitan tristearate, Hydrophilic Lipophilic Balance, HLB=2.1±1.0) were purchased from Fluka (Buchs, Switzerland). Pluronic® F127, a symmetric triblock copolymer with MW=12700, 70% wt. poly(ethylene glycol) and a central poly(propylene glycol) block, was purchased from Sigma (Buchs, Switzerland). Pluronic F127 diacrylate (F127 diacrylate) was synthesized as described elsewhere[18]. Eosin Y, trifluoroacetic acid, sodium dithionite and poly(ethylene glycol) diacrylate $\overline{M}_n$ =575 (PEG575 diacrylate) were purchased from Aldrich (Buchs, Switzerland). Sephadex G25 fine was purchased from

Amersham Biosciences. All solvents and reagents were used as received unless otherwise mentioned.

^{1}H-NMR spectra were recorded on a 300MHz Bruker spectrometer. Fluorescence spectra were obtained using a Perkin Elmer LS50b Luminescence spectrometer equipped with a four-position thermostated automatic cell changer with stirrer or a Tecan Safire[2] microplate reader. UV-Vis spectra were recorded on a Perkin Elmer Lambda 20 or a Tecan Safire[2] microplate reader.

3.2.2 Nanoparticle formation

Nanoparticles were prepared via inverse emulsion photopolymerization as previously described[6]. Briefly, Span65 (2.0% w/w$_{total}$) was dissolved in 2.4 ml n-hexane by sonication (4 min). 0.6 ml of aqueous precursor solution of F127 diacrylate, PEG575 diacrylate, triethanolamine and eosin Y (6.3%, 6.3%, 2.0%, 0.02% w/w$_{aqueous}$ respectively) were added to the oil phase (oil-to-water weight ratio = 72/28) and an inverse emulsion was formed by sonication for 30 sec with a tip-sonicator (Bandelin Sonoplus). The inverse emulsion was illuminated with an Ar ion laser (480-520 nm) for 1 hr, at room temperature, with an intensity of approximately 75 mW/s, under magnetic stirring (200 rpm). After illumination, the inverse emulsion was extracted with n-hexane to remove the emulsifier. The aqueous phase was then dialyzed against water (MWCO: Molecular Weight Cut-Off = 25,000, Spectrum Laboratories) to remove initiator and non-reacted macromonomers.

3.2.3 Dynamic Light Scattering

Values of effective hydrodynamic diameter in dilute dispersions were obtained by dynamic light scattering measurements using a Brookhaven instrument (model BI-DSI) equipped with a Lexel 95 laser source (514 nm at room temperature) at a fixed angle of 90°. Prior to analysis, solutions were filtered through a Millex AP filter (pore size ≈2µm) to remove dust. The digital correlator was operated with 200 channels, a minimum duration of 5 min and an average amount of counts per second between 100x10^3 and 700x10^3. Temperature was set at 37ºC. The determination of diffusion coefficient was calculated by fitting the date with the cumulants method (quartic fit) and diameters were estimated by the Stokes-Einstein equation, assuming a population of non-interactive spherical particles[19].

3.2.4 Evaluation of doxorubicin loading

Doxorubicin-HCl was solubilized in chloroform (CHCl₃) (1mg/ml) containing triethylamine (3 or 5 equivalents in respect to DOX), by sonication (10 min) and subsequently added to an aqueous suspension of nanoparticles (2.5mg/ml). Two different methods for CHCl₃ evaporation were investigated: a) the mixture was kept under magnetic stirring overnight in the dark at 40ºC in an open atmosphere or b) the mixture was placed in a rotary evaporator at 40°C, under slow rotation (35rpm) and reduced pressure (500mmHg for 40min and 200mmHg for 5min). The aqueous suspension was then eluted through a Sephadex G25 fine column to separate DOX-encapsulated nanoparticles from non-encapsulated DOX. Loaded DOX was quantified by measurements of its UV absorbance at 490 nm (extinction coefficient, ε 23.0 cm^2/mg). Loading was expressed as the weight ratio between loaded DOX and nanoparticles and encapsulation efficiency (E.E.) as the weight ratio of encapsulated DOX to total DOX used for encapsulation.

3.2.5 Doxorubicin fluorescence-quenching experiment

The quenching of doxorubicin fluorescence by I⁻ (KI) was monitored in 0.15M NaCl solutions containing a 10^{-5}M antioxidant (Na₂S₂O₄). DOX solutions or separated DOX-loaded nanoparticle dispersions were investigated. All experiments were performed at 27°C. Collisional quenching of fluorescence is described by the Stern-Volmer equation:

$$\frac{I_0}{I_Q} = 1 + K_{SV}[Q], \ K_{SV} = k\tau_0 \quad (3.1)$$

where $[Q]$ is the quencher concentration, K_{SV} the Stern-Volmer constant, k the bimolecular collisional rate, τ_0 the excited-state lifetime of DOX and I_0 and I_Q the fluorescence intensities in the absence and presence of quencher, respectively[20].

3.2.6 In vitro release experiments

The drug (free or encapsulated in nanoparticles) was placed inside a dialysis membrane (MWCO: 25,000) immersed in an aqueous buffer 21 times larger in volume (PBS 10mM, pH 7.4). At predetermined time points the dialysate was sampled and the amount of DOX determined by fluorescence measurements or High Pressure Liquid Chromatography (HPLC). The whole dialysate was replaced every 24 hours.

Experimental data were fitted using a semi-empirical power law equation:

$$\frac{M_t}{M_\infty} = \frac{M_b}{M_\infty} + kt^n \qquad (3.2)$$

where M_t, M_∞ are the amount of drug released at time t and infinite time, M_b the amount of burst released drug, k is the release constant and n is the release exponent. The value of n depends on the geometry of the release device and the mechanism of release. For spheres, n ranges between 0.43 (diffusion-based release) and 0.85 (degradation-based release)[21].

### 3.2.7 HPLC method for quantification of DOX

The amount and degree of degradation of DOX were measured with HPLC using a reversed phase C18 column (Nova-Pak®C18, 3.9×150mm, Waters Associates) operated at room temperature, a Waters 2690 Separation Module (Waters Associates) and a Waters 474 Scanning Fluorescence Detector (Waters Associates). As eluent, 0.1% TFA in water/acetonitrile 25:75 v/v, was used at a flow rate of 1 ml/min and chromatograms were analyzed with Waters Millenium 32 software. A calibration curve was constructed using the Area Under the Curve (AUC) and the total amount of DOX was calculated by summing up all AUC, attributed to DOX and its degradation products.

3.3 Results & Discussion

3.1 Nanoparticle formation

Inverse emulsion photopolymerization is a controllable method for preparing well-defined nanoparticles. The aqueous macromonomer nano-droplets are stabilized by a cross-linking polymerization of acrylic derivatives, which preserves the structure of the previously self-assembled Pluronic micelles (Scheme 3.1). The presence of the segregated hydrophobic nanodomains was confirmed using pyrene as a probe, an experiment that also showed the capacity of incorporating hydrophobic drugs[6].

Scheme 3.1 *Pluronic-containing nanoparticles are prepared through the photopolymerization of water-soluble monomers (PEG and Pluronic diacrlyates) dispersed in inverse emulsion.*
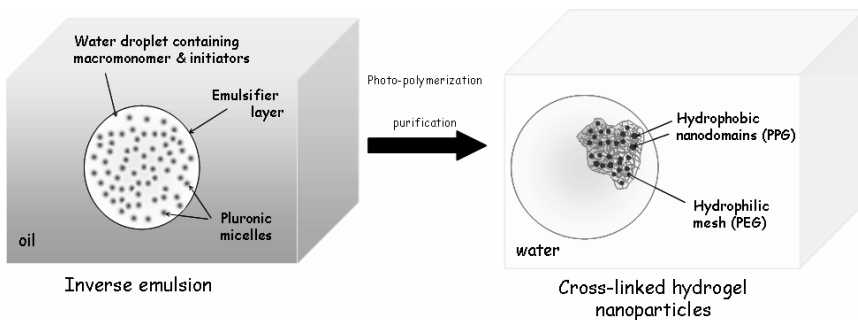
In the present study, we have kept constant composition of the nanoparticles (Pluronic-to-total macromonomer weight ratio: 0.50) and total macromonomer weight content (12.5% wt.). The photopolymerization conversion and the Pluronic content in the nanoparticles were assessed via ^{1}H-NMR on nanoparticle dispersions in D_2O.

The complete disappearance of the peaks at 5.8, 6.1 and 6.4 ppm (3 protons of the acrylate moiety (-O(O)CCH=CH$_2$) confirmed a quantitative conversion of the double bonds within the nanoparticles.

By comparing the resonance at 1.2 ppm (3H of PPG block methyl groups) with that at 3.6 ppm (4H of PEG macromonomer & of PEG blocks in Pluronic), we have recorded a slight enrichment in Pluronic compared to the pre-polymerization mixture (Pluronic macromonomer weight fraction=0.57). A possible interpretation is that Pluronic acrylates may polymerize faster than PEG acrylates, due to their higher local concentration as a result of the micellar organization, and may also provide regions of higher cross-linking density. Another, not necessarily alternative explanation is that PEG acrylate may partially cyclopolymerize (=behaving as a linear monomer instead as a cross-linker) and oligomerize, giving rise to extractable products.

The effect of size on the biological performance of nanoparticles is well documented; an optimal diameter range between 100-200nm is believed to favour prolonged circulation times and passive targeting of carriers thanks to the Enhanced Permeation and Retention (EPR) effect[7-9]. We appropriately selected inverse emulsion conditions to obtain nanoparticles with hydrodynamic diameter of 171 ± 5 nm (mean ± standard deviation), although characterized by a fairly broad dispersion in size (Figure 3.1)
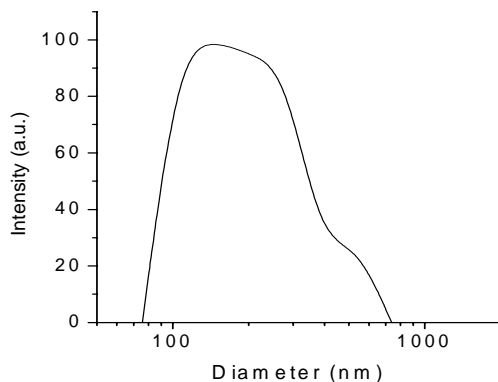
Figure 3.1 *Particle size distribution of nanoparticles prepared by inverse emulsion photo-polymerization and used in this study.*

3.3.2 Physical entrapment of DOX

Physical entrapment, successfully described in a number of cases for Pluronic®
micellar systems[14], is a mild method, applicable to drugs in a vast range of hydrophobicity[22].

We have adopted a literature procedure[23, 24], which, by the use of a base
(triethylamine) that deprotonates the DOX primary ammonium salt, induces the solubilization
of DOX in chloroform; loading by simply equilibrating DOX and supramolecular structures
with hydrophobic domains in water has proven to be ineffective. The organic DOX solution,
mixed with the aqueous nanoparticle dispersion, forms initially a two phase system: a bottom,
clear, organic phase and an opaque aqueous phase, containing chloroform swollen
nanoparticles. Gradually, by chloroform evaporation, the organic phase disappears and the
aqueous phase becomes transparent, and can be later purified via elution on a Sephadex
column to remove non-encapsulated drug (Scheme 3.2). Preliminary experiments showed
higher loading at 40ºC compared to room temperature, most likely due to the increased
hydrophobic character of Pluronics® at higher temperatures.

Scheme 2. *Loading method of DOX in hydrogel nanoparticles.*
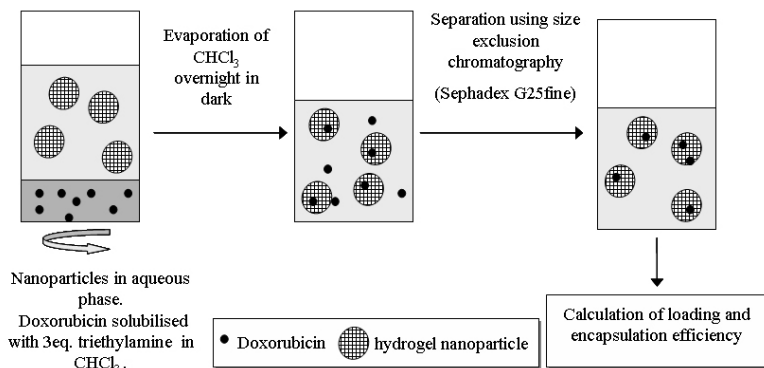
The visible absorption spectrum of encapsulated DOX shows only slight differences from that of the free, protonated DOX in solution, since the protonation site is far from the chromophore; however, the presence of a distinct red-shift of the absorption peak is a clear sign of increased local concentration and thus also of DOX-DOX interactions, likely due to π-π stacking[25]. Much more dramatic is the effect on the fluorescence spectrum, where a clear quenching is recorded; we are fairly sure to ascribe this effect to the increased DOX concentration in the hydrophobic domains of the nanoparticles[26, 27] (Figure 3.2).
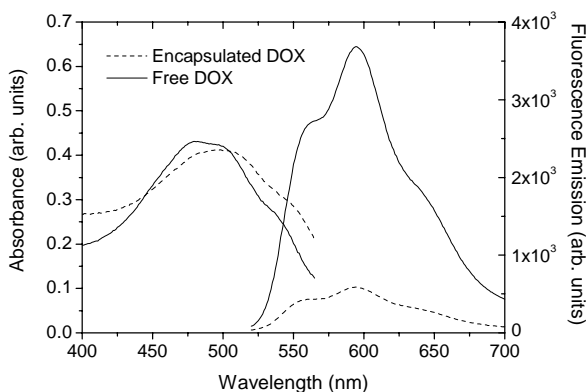

Figure 3.2 *Visible absorption spectra and fluorescence spectra of doxorubicin, encapsulated (39 µg/ml) and free (41µg/ml).*

For a quantitative evaluation of DOX loading, we have used its extinction coefficient at 490 nm in a buffered solution of non-reacted PEG575 diacrylate and Pluronic F127 (in 1:1 weight ratio).

By increasing the relative amount of DOX in the feed, incorporation in the nanoparticles always increased, an indication that nanoparticle saturation was not yet reached (Table 3.1 & Figure 3.2). Encapsulation efficiency seemed to depend on DOX concentration too, with surpisingly low levels at low DOX concentrations, while leveling at higher concentrations. It can be easily shown that pH increases with DOX concentration, since also the amount of base is proportional to that of DOX, and so does also the ratio between deprotonated/hydrophobic and protonated/hdyrophilic DOX. It is also easy to demonstrate that this effect is significant at markedly low concentrations, while it levels off very soon, hence the Indeed, superior loading was obtained when DOX was solubilized with 5 equivalents of triethylamine instead of the 3 equivalents (Table 3.1).

Initial experiments were conducted by slowly evaporating chloroform at atmospheric pressure; this method showed a strong dependence on the vial geometry and on the volume of water phase, thus later we opted for a quicker evaporation with a rotatory evaporator. This second approach resulted in more reproducible loadings of larger volumes in much shorter times (Table 3.1).

Table 3.1 *Doxorubicin loading characteristics as a function of feed loading, amount of based used and evaporation conditions*

Feed loading [a] (%)	Volume of water phase (ml)	Nanoparticle loading [b] (%)	Encapsulation efficiency [c] (%)
5 [d,f]	0.4	0.6±0.1	11.7±1.0
10 [d,f]	0.4	2.3±0.2	22.5±2.2
15 [d,f]	0.4	4.4±0.4	29.2±2.5
20 [d,f]	0.4	5.4±0.4	27.0±1.8
10 [e,f]	1.0	1.1±0.1	11.4±1.1
10 [e,g]	1.0	2.1±0.2	20.3±2.0
20 [e,g]	1.0	8.6±2.0	43.2±9.9
20 [e,g]	2.0	8.7±1.2	43.6±5.9

[a] Weight ratio between total DOX and nanoparticles
[b] Weight ratio between encapsulated DOX and nanoparticles, mean ± standard deviation
[c] Ratio between feed and experimental loading, mean ± standard deviation
[d] evaporation at atmospheric pressure
[e] evaporation at reduced pressure
[f] 3 equivalents of triethylamine in respect to DOX
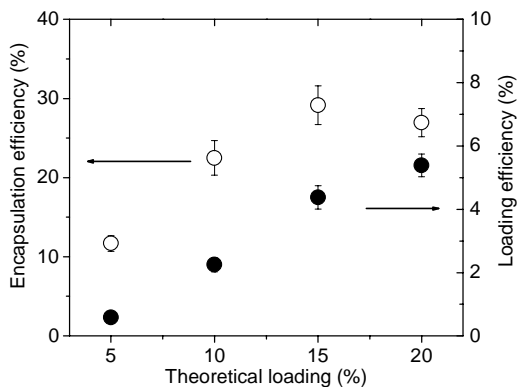[g] 5 equivalents of triethylamine in respect to DOX

Figure 3.2 *Encapulation and loading efficiency at different theoretical loadings, following the first loading protocol (overnight evaporation of CHCl₃). Mean and standard deviations are shown (n=3).*

Evidence of the hydrophobic character of the encapsulation was achieved using fluorescent quenching studies. Large, hydrated, I⁻ ions, used as quenching agents, are not able to penetrate into hydrophobic regions, limiting their quenching activity to DOX molecules in the hydrophilic region and the interface[28, 29].
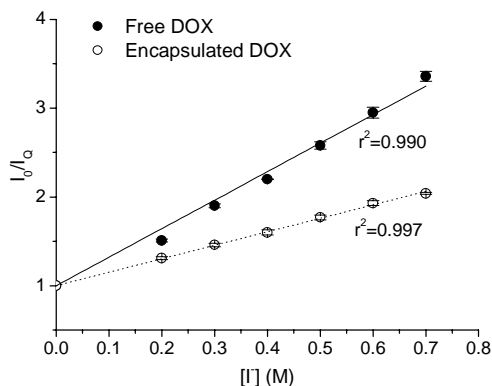

Figure 3.3 *Stern-Volmer plots of free and encapsulated doxorubicin at 27°C. Mean and standard deviations are shown (n=3).*

The slopes of the Stern-Volmer plots for DOX and encapsulated DOX (Figure 3.3) reflect the degree of exposure to the quenching iodide ions. The lower value for encapsulated DOX shows the drugs to be present in hydrophobic, difficultly accessible regions, although partial quenching suggests either an incomplete insertion or some degree of accessibility of I^- in the poly(propylene glycol) domains. Rapoport and Pitina, noticed that although ruboxyl, a paramagnetic analogue of doxorubicin, was entirely inserted in the lipid bilayer of liposomes, a fraction of DOX appeared to reside at the lipid-water interface[29]. Moreover, poly(propylene glycol) is not fully dehydrated in this temperature range[30, 31] and I^- may diffuse through this phase.

3.3.3 Release from nanoparticles

In this study we have simulated 'sink' conditions, placing the loaded nanoparticles in dialysis bag (MWCO: 25,000) and regularly replacing the dialysate every 24 hours. This time is largely in excess for reaching the complete equilibration of DOX solutions on the two sites of the dialysis membrane, as shown in control experiments (Figure 3.4).
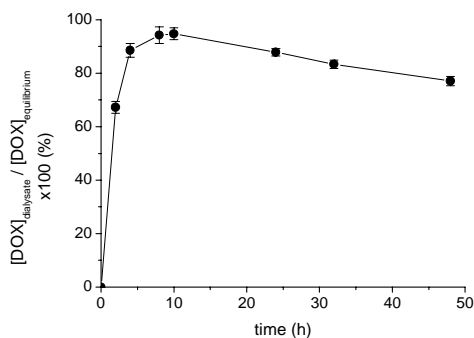

Figure 3.4 *Control equilibration experiment of free doxorubicin through the dialysis membrane (MWCO: 25,000) used in further release studies. The equilibration is complete after 10 hours, then DOX concentration decreases, due to DOX adsorption on glass and other surfaces (dialysis clips, stirrer bars etc.) and DOX degradation and consequent precipitation[32, 33]. Mean and standard deviations are shown (n=3).*

The *in vitro* doxorubicin release profiles at two different temperatures (room temperature and 37°C) are presented in Figure 3.5. Matching results were obtained by both detection methods (HPLC and fluorescence spectroscopy, Figure 3.5A), revealing prolonged drug release over a time scale (7 days) of clinical importance: slower drug release would

require a higher concentration of the delivery system and possibly elevate the risk of drug resistance development, while a more rapid liberation of drug would require more frequent administration.

When dealing with physical encapsulation, small carrier size and in the absence of a switchable barrier, a burst effect is frequently observed, although generally undesired. For our system burst release was evident only at 37°C and accounted for approximately 10% of encapsulated DOX. We suspect that the temperature jump between purification (performed at room temperature) and release (37°C) causes an intraparticle transition leading to drug expulsion; higher Pluronic® content nanoparticles have been shown to exhibit a temperature dependent shrinkage at this temperature range[10], a finding which we believe is also valid in this case.
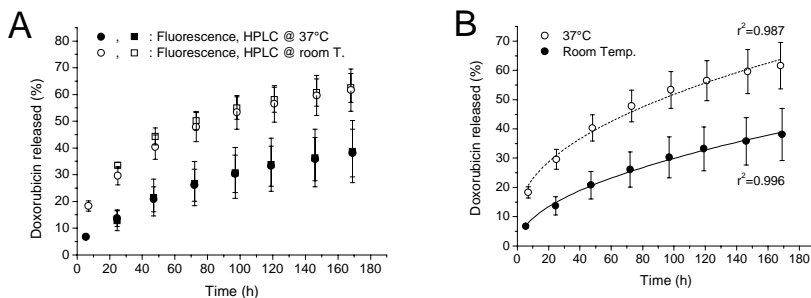

Figure 3.5 *Doxorubicin release profiles from nanoparticles in PBS (10mM, pH=7.4), at room temperature and 37°C. (A) Comparison between the 2 different detection techniques; (B) Fit to the semi-empirical power law equation* $\frac{M_t}{M_\infty} = \frac{M_b}{M_\infty} + kt^n$. *Mean and S.D. are shown (n=3).*

A power law (Equation 3.2) fitted our experimental data well despite its simplicity and assumptions (Figure 3.5B). In the case of release at room temperature no burst effect was included ($\frac{M_b}{M_\infty} = 0$); at 37°C an estimate of $\frac{M_b}{M_\infty} = 0.1$ was taken into account. The values of n (Table 3.2) determined for two different temperatures are close to 0.43. The small deviation may be attributed to invalid assumptions like sink condition maintenance, constant drug diffusivity and high difference between loaded drug concentration and drug solubility[21].

Nevertheless, these results confirm that the main release mechanism is diffusion, an expected finding considering the non-covalent nature of interaction between DOX and nanoparticles.

Table 3.2 *Calculated values for parameters k and n from fitting equation (3.2) to the experimental data.*

Temperature	k	n
Room Temp.	2.99±0.26	0.50±0.02
37°C	5.14±0.07	0.47±0.03

In case of diffusional release, plotting the released amount of drug against the square root of time should yield a linear correlation according to the Higuchi model[21, 34]. Excluding the burst effect by omitting the early time data points (t<24h) good fits were obtained (Figure 3.6). The slopes, which are proportional to an apparent diffusion coefficient, were found to be 3.01±0.71 and 3.98±0.57, for room temperature and 37°C, respectively. Diffusion seems to be faster at 37°C, although the difference is not statistically significant.
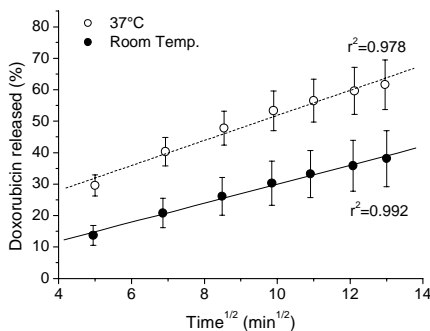

Figure 3.6 *Release of doxorubicin plotted against the square root of time. The early data points corresponding to the burst release are excluded. Linear fits indicate diffusional release. Mean and S.D. are shown (n=3).*

It is well established that PPG hydrophobicity in Pluronic micelles increases with temperature, while water content decreases even if it does not completely disappear[30, 31]. There are therefore two possible effects governing the DOX diffusion out of nanoparticles as a function of increasing temperature: increasing hydrophobicity of the matrix, which should slow down diffusion, and increasing mobility of the molecule, with the opposite effect. Our data apparently support the second effect to overwhelm the first one.

3.3.4 Doxorubicin degradation

In order to investigate the ability of the carrier to perform a protective action, we have used an HPLC method that, in addition to the quantification of the drug release, can also be used to monitor DOX degradation [32, 33, 35]. . Fresh, non-degraded DOX eluted as a single sharp peak after 7.7 min. sharp peak after 7.7 min. Examining DOX released from nanoparticle suspensions, new peaks attributed to DOX degradation products appeared at 6.1 min, 6.4 min and 8.3 min (Figure 3.7A), and increased in intensity with time. The percentage of non-degraded DOX was calculated from the ratio of the AUC of the peak at 7.7 min to the sum of AUC of all peaks (Figure 3.7B).
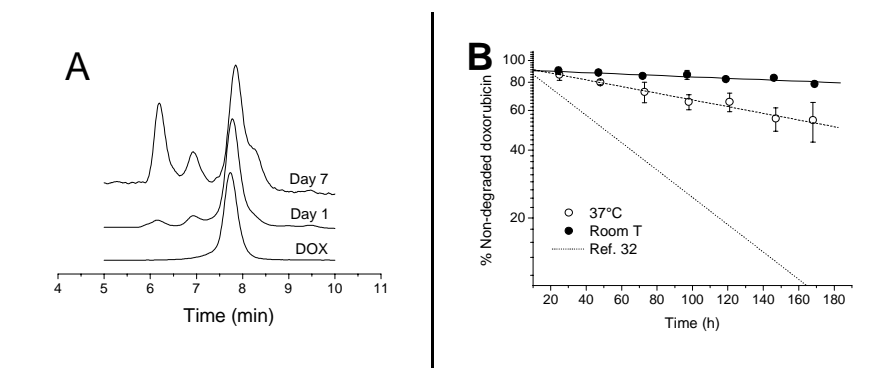

Figure 3.7 *(A) HPLC chromatographs showing peaks attributed to DOX and its degradation products at 37°C. (B) Degradation kinetics of DOX encapsulated in nanoparticles for both temperatures studied. Solid lines are linear fits of the calculated values whereas the dashed line corresponds to degradation of non-encapsulated DOX in PBS at 37°C as obtained from literature (ref. 32).*

Neglecting degradation occuring after release from the carrier in the dialyzate and assuming similar release rates for all species, we were able to estimate the degradation rate of doxorubicin inside the nanoparticles. We have run experiments at room temperature and 37°C, which revealed significant degradation for both temperatures, although more pronounced at 37°C. Comparing however with the degradation rate of DOX at 37°C in PBS (10mM, pH=7.4)[32], we observe that, although encapsulation does not fully protect the drug - most likely because of the presence of water in the hydrophobic domains - it nevertheless delays degradation. The estimated half-life $t_{1/2}$ for encapsulated DOX was 173h, which is much higher than the reported half-life of 50h for DOX in PBS, indicating a protective effect of the

carrier[32]. A detailed study on degradation was not the subject of this study and is currently in progress, using HPLC with a mass spectoscopy detector, capable of identifying the structure of the different metabolites. Concluding, we have also to bear in mind that a quantitative interpretation of these release profiles is also complicated by the fact that different degradation products may have different diffusion properties, in addition to the changes in carrier hydrophobicity and general increase of diffusivity with temperature.

3.3.5 Stability against aggregation

Doxorubicin molecules are known to self-associate through stacking interactions; if the molecules are found on the surface of polymers they may promote aggregation as was shown for polymer-adsorbed DOX[27, 36]. One of our concerns was the possibility of nanoparticle aggregation during the loading and/or release procedure. We confirmed, using DLS, that the diameter of the carrier following loading and release (168 ± 11 nm) is not affected by the experimental protocols used.

3.4 Conclusions

In this chapter we explored the loading and release capabilities of a novel nanoparticulate system, using DOX as an example of a hydrophobic drug. By selecting appropriate macromonomers and inverse emulsion conditions, we were able to prepare colloids with an average size of 170 nm, with internal PPG-rich hydrophobic regions. The successful physical encapsulation of DOX in these domains was confirmed, and it was demonstrated to dramatically alter the *in vitro* pharmacokinetics of the drug. In particular, the use of these systems is attractive since, upon dilution, as would be the case for *in vivo* applications, the hydrophobic regions are stable and are not subject to possible disaggregation as can be the case with micellar systems. Moreover, the hydrophilic nature of the particles can be expected to provide some level of biocompatibility and 'stealth' characteristics. Encapsulation provided sustained release for up to 1 week *in vitro*. Finally, encapsulation of DOX within the hydrophobic core provided substantial protection of the drug against hydrolytic degradation.

3.5 References

1. K. Kostarelos *Rational design and engineering of delivery systems for therapeutics: biomedical exercises in colloid and surface science* Advances in Colloid and Interface Science 106 **2003** 147-168

2. J.A. Hubbell *Enhancing drug function* Science 300 **2003** 595-596

3. T.M. Allen and P.R. Cullis *Drug Delivery Systems: Entering the Mainstream* Science 303 **2004** 1818-1822

4. T.M. Allen *Ligand-Targeted Therapeutics in Anticancer Therapy* Nature Reviews Cancer 2 **2002** 750-763

5. R. Savic, et al. *Micellar nanocontainers distribute to defined cytoplasmic organelles* Science 300 **2003** 615-618

6. D. Missirlis, et al. *Amphiphilic hydrogel nanoparticles. Preparation, characterization and preliminary assessment as new colloidal drug carriers* Langmuir 21 **2005** 2605-2613

7. S.K. Hobbs, et al. *Regulation of transport pathways in tumor vessels: Role of tumor type and microenvironment* P. Natl. Acad. Sci. USA 95 **1998** 4607-4612

8. H. Hashizume, et al. *Openings between defective endothelial cells explain tumor vessel leakiness* Am. J. Pathol. 156 **2000** 1363-1380

9. H. Maeda, et al. *Tumor vascular permeability and the EPR effect in macromolecular therapeutics* J. Controlled Release 65 **2000** 271-284

10. D. Missirlis, et al. *Thermally-induced responses in nanoparticle assemblies: possible formation of a colloidal glass and its perspective applications* Langmuir submitted **2005**

11. A. Gabizon, et al. *Pharmacokinetics of pegylated liposomal doxorubicin - Review of animal and human studies* Clinical Pharmacokinetics 42 **2003** 419-436

12. T. Nakanishi, et al. *Development of the polymer micelle carrier system for doxorubicin* Journal of Controlled Release 74 **2001** 295-302

13. H.S. Yoo and T.G. Park *Folate-receptor-targeted delivery of doxorubicin nano-aggregates stabilized by doxorubicin-PEG-folate conjugate* J. Controlled Release 100 **2004** 247-256

14. V. Alakhov, et al. *Block copolymer-based formulation of doxorubicin. From cell screen to clinical trials* Colloids and Surfaces B: Biointerfaces 16 **1999** 113-134

15. Y. Bae, et al. *Preparation and Biological Characterization of Polymeric Micelle Drug Carriers with Intracellular pH-Triggered Drug Release Property: Tumor Permeability, Controlled Subcellular Drug Distribution, and Enhanced in Vivo Antitumor Efficacy* Bioconjugate Chem. 16 **2005** 122-130

16. A. Nori, et al. *Tat-conjugated synthetic macromolecules facilitate cytoplasmic drug delivery to human ovarian carcinoma cells* Bioconjugate Chem. 14 **2003** 44-50

17. K.S. Soppimath, et al. *Biodegradable polymeric nanoparticles as drug delivery devices* J. Controlled Release 70 **2001** 1-20

18. F. Cellesi, et al. *Materials for cell encapsulation via a new tandem approach combining reverse thermal gelation and covalent crosslinking* Macromol. Chem. Phys. 203 **2002** 1466-1472

19. R. Finsy *Particle sizing by quasi-elastic light-scattering* Adv. Colloid Interface Sci. 52 **1994** 79-143

20. J.R. Lakowicz *Quenching of Fluorescence,* Principles of Fluorescence Spectroscopy **1999,** Ed.

21. J. Siepmann and N.A. Peppas *Modeling of drug release from delivery systems based on hydroxypropyl methylcellulose (HPMC)* Adv. Drug Delivery Rev. 48 **2001** 139-157

22. R. Nagarajan *Solubilization of "guest" molecules into polymeric aggregates* Polym. Adv. Technol. 12 **2001** 23-43

23. G. Kwon, et al. *Block copolymer micelles for drug delivery: loading and release of doxorubicin* J. Controlled Release 48 **1997** 195-201

24. K. Kataoka, et al. *Doxorubicin-loaded poly(ethylene glycol)-poly(beta-benzyl-l-aspartate) copolymer micelles: their pharmaceutical characteristics and biological significance* Journal of Controlled Release 64 **2000** 143-153

25. H. Porumb *The solution spectroscopy of drugs and the drug-nucleic acid interactions* Prog. Biophys. molec. Biol. 34 **1978** 175-195

26. K.K. Karukstis, et al. *Deciphering the fluorescence signature of daunomycin and doxorubicin* Biophysical Chemistry 73 **1998** 249-263

27. E.R. Gillies and J.M.J. Frechet *pH-Responsive Copolymer Assemblies for Controlled Release of Doxorubicin* Bioconjugate Chem. 16 **2005** 361-368

28. G.S. Kwon, et al. *Physical entrapment of adriamycin in AB block-copolymer micelles* Pharm. Res. 12 **1995** 192-195

29.   N. Rapoport and L. Pitina *Intracellular Distribution and Intracellular Dynamics of a Spin-Labeled Analogue of Doxorubicin by Fluorescence and EPR Spectroscopy* J. Pharm. Sci. 87 **1998** 321-325

30.   Y.L. Su, et al. *FTIR spectroscopic investigation of effects of temperature and concentration on PEO-PPO-PEO block copolymer properties in aqueous solutions* Macromolecules 35 **2002** 6426-6431

31.   I. Goldmints, et al. *Structure of (Deuterated PEO)-(PPO)-(Deuterated PEO) Block Copolymer Micelles As Determined by Small Angle Neutron Scattering* Langmuir 15 **1999** 1651-1656

32.   M.J.H. Janssen, et al. *Doxorubicin decomposition on storage. Effect of pH, type of buffer and liposome encapsulation* International Journal of Pharmaceutics 23 **1985** 1-11

33.   J.H. Beijnen, et al. *Aspects of the degradation kinetics of doxorubicin in aqueous-solution* International Journal of Pharmaceutics 32 **1986** 123-131

34.   P.L. Soo, et al. *Incorporation and release of hydrophobic probes in biocompatible polycaprolactone-block-poly(ethylene oxide) micelles: Implications for drug* Langmuir 18 **2002** 9996-10004

35.   G. Zagotto, et al. *Anthracyclines: recent developments in their separation and quantitation* Journal of Chromatography B 764 **2001** 161-171

36.   M.V. Kitaeva, et al. *Doxorubicin-Poly(acrylic acid) Complexes: Interaction with Liposomes* Langmuir 20 **2004** 6575-6579

Chapter 4

An Alternative Initiation Scheme for Inverse Emulsion Polymerization and Addition of Functionality to Nanoparticles

4.1 Introduction

In chapter 2 we have described the use of inverse emulsion cross-linking radical polymerization for the preparation of hydrogel nanoparticles. Initiation occured through light activation of a photo sensitizer (a xanthene dye: eosin Y) followed by electron transfer to a co-initiator (triethanolamine)[1] (Figure 4.1A). Photopolymerization allows easy handling and good mixing of the precursor as well as temporal and spatial control over the reaction[2]; however, it necessitates an external light source and irradiation may damage components of the reaction mixture (e.g. photo-bleaching of fluorescent dyes). Moreover, in heterophase systems, as is the case of inverse emulsions, scattering of irradiated light results in spatially inhomogeneous light intensity.

Therefore, we explored an alternative intiation scheme, namely the redox initiation system consisting of ammonium persulfate (APS) and *N,N,N´,N´*-tetramethylethylenediamine (TEMED), routinely used for preparation of acrylamide gels in gel electrophoresis. Recently it was also succesfully applied for the preparation of acrylamide-based nanogels via inverse emulsion cross-linking polymerization[3]. In this case, initiation is believed to occur via formation of a contact charge transfer complex (CCT) and a cyclic transition state (CTS), yielding three active radical species[4] (I, II & III in Figure 4.1B).

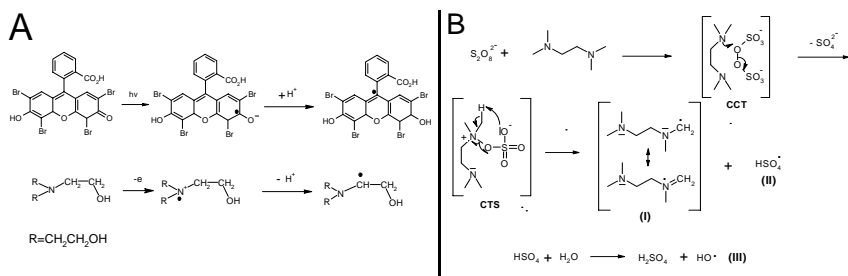Figure 4.1 *Schematic representation of radical formation through photoinitiation by eosin Y and triethanolamine (A) and redox initiation by APS-TEMED (B).*

Interactions of NPs with drugs on one hand and the biological environment on the other, depend highly on the material's chemical identity and structure. Functionality and environmental sensitivity may be further tailored through suitable chemical modifications on

an inert background. Incorporation of functional sites (e.g. reactive or charged groups) in the carrier provides them with additional drug loading and labeling capabilities.

Drugs covalently bound via specific, cleavable linkers are released in response to environmental changes[5], whereas ionizable groups are able to interact with opposite charged molecules and may allow pH-responsive release. Furthermore, introduction of labels via stable linkages, allows detection and visualization of the colloids; for instance, fluorescent tags may be used to track the intracellular location and environment of NPs[6, 7], and even provide information on cell biomechanics[8].

The reaction scheme we have used in this thesis to prepare non-ionic, hydrogel NPs is based on the solution, cross-linking polymerization of diacrylate macromonomers. The nature of the vinyl-containing group is known to influence the monomer's reaction kinetics[9]. Nevertheless, incorporation of various comonomers, of different MW and charge, has been verified in similar reaction conditions, for the preparation of graft copolymers[10], as well as hydrogels[11-13], microgels[14] and nanogels[15, 16]. We used this strategy to copolymerize monomers containing a double bond (an acrylamide or a methacrylamide group) linked to a functional group. Following NP formation, pendant groups were present in the three-dimensional (3D) nanogel matrix, which could be used for subsequent reactions. Having in mind the need to accurately quantify NPs at very low concentrations, as well as the ability to image through fluorescence spectroscopy the otherwise invisible NPs, we fluorescently labeled the colloids.

4.2 Materials & Methods

4.2.1 Materials

Poly(ethylene glycol) diacrylate $\overline{M}_n$ =575 (PEG575 DA), di(ethylene glycol) diacrylate), triethylamine, dimethyl sulfoxide (DMSO), Sephadex G25 (fine), agarose, ammonium persulfate (APS) and fluorescein isothiocyanate (FITC) were purchased from Sigma-Aldrich (Buchs, Switzerland). Span®65 (sorbitan tristearate, Hydrophilic Lipophilic Balance=2.1±1.0), *N,N,N',N'*-Tetramethylethylenediamine (TEMED), triethanolamine and eosin Y were purchased from Fluka (Buchs, Switzerland). *N*-hexane (99%) was purchased from LabScan (Oensingen, Switzerland). N-(3-aminopropyl) methacrylamide hydrochloride (APMA) was purchased from Polysciences Inc. Fluorescamine was purchased from Applichem.

Pluronic® F127, a symmetric triblock copolymer with MW=12700, 70% wt. poly(ethylene glycol) and a central poly(propylene glycol) block, was purchased from Sigma (Buchs, Switzerland). Pluronic® F127 was functionalized with acrylate groups (F127 DA) as described elsewhere[17].

Phosphate Buffer Saline (PBS, 10mM, pH 7.4) was prepared by dissolving 0.2g KCl, 0.2g KH_2PO_4, 1.15g Na_2HPO_4 and 8g NaCl in 1L of milliQ grade water. Carbonate buffer (0.5M, pH 9.5) was prepared by dissolving 17g Na_2CO_3 and 28g $NaHCO_3$ in 1L of milliQ grade water.

4.2.2 Spectoscopic characterization

^{1}H-NMR spectra were recorded on a 300MHz Bruker spectrometer. FTIR spectra were recorded in ATR mode on a Spectrum One Perkin Elmer Spectrometer. Fluorescence and UV-Vis spectra were obtained using a Safire 2 well plate reader.

4.2.3 Nanoparticle formation

Nanoparticles were prepared via inverse emulsion radical polymerization using two different initiation mechanisms.

Photo-initiation was employed as previously described in detail (Chapter 2). Briefly, Span®65 (44mg, 2.0% w/w_{total}) was dissolved in 2.4 ml n-hexane by sonication (4 min). 0.6 ml of aqueous precursor solution of F127 DA, PEG575 DA, triethanolamine and eosin Y (6.3%, 6.3%, 2.0%, 0.02% $w/w_{aqueous}$ respectively) were added to the oil phase (oil-to-water weight ratio = 72/28) and an inverse emulsion was formed by sonication for 30 s with a tip-sonicator (Bandelin Sonoplus). The inverse emulsion was illuminated with an Ar ion laser (480-520 nm) for 1 hr, at room temperature, with an intensity of approximately 75 mW/s, under magnetic stirring.

Alternatively, APS was used as initiator and TEMED as accelerator. In this case, the aqueous precursor solution, containing F127 DA and PEG575 DA (0.28ml, 6.3% and 6.3% $w/w_{aqueous}$ respectively), was added to the oil phase containing the emulsifier. TEMED (100µl, 3.7% wt.) was then added and an inverse emulsion formed by sonication for 30s. To initiate the reaction, APS solution (0.22ml, 5.5% wt. aqueous solution for a final aqueous concentration of 2% $w/w_{aqueous}$) was added, and immediately the inverse emulsion was sonicated for another 30s in order to disperse the initiator. The polymerization was left to proceed for 2h, at room temperature and under magnetic stirring. In order to test the

possibility of scaling up the procedure, samples were additionally prepared with 5 times larger quantities.

Nanoparticles containing co-monomers were formed by dissolving appropriate amounts in the aqueous macromonomer precursor solution. Photopolymerization was employed for preparation of AMPS-containing NPs, whereas APMA-containing NPs were prepared using both initiation mechanisms.

After reaction completion, the emulsifier was extracted with *n*-hexane and the aqueous phase was dialyzed against water (molecular weight cut-off: 25,000, Spectrum Laboratories) for 2-3 days to remove initiator and non-reacted macromonomers.

4.2.4 Quantification of amine groups in nanoparticles and FITC conjugation

The concentration of primary amines was determined using fluorescamine, which upon reaction with the amine group yields a fluorophor[18]. Fluorescamine (20µl of 3 mg/ml acetone solution) was added in a 96-well plate containing dispersions of functionalized nanoparticles (200µl) in PBS (10mM, pH=7.4) and left 15min at room temperature to react. Emission intensity was read at 475nm (excitation at 390nm, 30°C) and NH_2 concentration was calculated using a calibration curve constructed with unreacted APMA solutions.

The amine groups present in the nanoparticles were then used for fluorescent labeling. 40 equiv FITC (1 mg/ml in DMSO) was added in 1.5ml eppendorf tubes containing 0.5ml nanoparticle dispersions (2-4mg/ml in 0.25M carbonate buffer). The reaction was left to proceed overnight at 4°C, under dark and conjugated nanoparticles were separated from unreacted FITC by size exclusion chromatography (Sephadex G25) followed by dialysis for at least 2 days (Spectrum Laboratories, MWCO: 25,000). Conjugation efficiency was determined using fluorescence spectroscopy (excitation wavelength: 488nm, emission wavelength: 525nm) and a calibration curve constructed with unreacted FITC in PBS.

Particles were imaged with a confocal microscope after embedding in an agarose gel. Briefly, an aqueous fluorescent NP dispersion (5µl) was mixed with 200µl agarose solution (1% w/v) in a microscope chamber slide (Lab-Tek, Nalge Nunc International) at 45°C; upon cooling to room temperature a gel was formed, entrapping NPs and inhibiting their rapid thermal motion.

4.3 Results & Discussion

4.3.2 Redox initiation

We initially selected eosin Y and triethanolamine as photo-sensitizer and initiator respectively, because of their low toxicity and fast reaction kinetics[9, 19]. However, scattering of light by the opaque inverse emulsion, a high dependance on reactor geometry and the need for specialized light sources led us to develop an alternative polymerization protocol based on a different initiation scheme, namely the redox system of ammonium persulfate (APS) and N,N,N',N'-tetramethylethylenediamine (TEMED).

In view of the fact that radical formation in presence of both APS and TEMED is rapid and polymerization occurs in the confined space determined by the dimensions of the aqueous droplets, we decided to disperse one initiator in a pre-formed inverse emulsion already containing the other one; addition of both initiators simultaneously prior to sonication, resulted in extremely fast macroscopic gel formation at the concentrations used here. From preliminary experiments we observed that the addition sequence was critical for controlled and reproducible formation of NPs with low polydispersity, with initial addition of TEMED providing better results. We also noticed that TEMED affected inverse emulsion characteristics: at high concentrations (3.7% wt.), sonication resulted in the formation of a semi-transparent inverse emulsion, an indication of reduced aqueous droplet size, suggesting a role of TEMED as co-emulsifier. Indeed, the average hydrodynamic diameter of particles prepared using this initiation scheme was lower compared with those prepared by photo-initiated polymerization, having the same macromonomer ratio and composition (Table 4.1).

The initiator concentrations were selected in order to ensure the formation of monodisperse NPs as well as the complete double bond conversion: an increase in initiating species results in an increase of cross-linking kinetics which help stabilize faster the NPs and reduce the possibility of interparticle reactions during aqueous droplet coalescence. Completion of the reaction was verified by ^{1}H-NMR spectroscopy on lyophilized NPs redispersed in CDCl$_3$: the characteristic proton peaks of the acrylate group (δ=5.8, 6.2 and 6.4) were absent.

An additional advantage of this initiation scheme was the possibility of preparing larger NP quantities (scale up). Typically 3ml of inverse emulsion were polymerized; sample TH-NH-B was prepared in 15ml and exhibited the same average diameter.

Sample	APMA concentration (% w/w$_{NP}$)	Inverse emulsion volume (ml)	Hydrodynamic diameter (nm)	Polydispersity index
PH-ST-1[a]	-	3.0	144.7±11.7	0.12
PH-NH-1[a]	0.08	3.0	153.0±4.9	0.27
PH-NH-2[a]	0.40	3.0	161.3±13.2	0.23
TH-ST-1[b]	-	3.0	102.4±16.7	0.22
TH-NH-1[b]	0.40	3.0	137.1±3.5	0.18
TH-NH-B[b]	0.40	15.0	132.9±2.0	0.30

[a] Photo-initiation
[b] Redox initiation

The above results show that it was indeed feasible to prepare NPs using the redox initiation system APS-TEMED in a reproducible manner, with full double bond conversion and independently of batch volume. However handling of the precursor mixture in this case requires more attention: dispersion of APS in the aqueous droplets of the inverse emulsion needs to be rapid and uniform over its whole volume.

4.3.3 Bulk functionalization of NPs

The three-dimensional network of the hydrogel NPs accomodates large amounts of water and has a characteristic mesh-size which can be controlled by the length of the macromonomers and the cross-linking density (determined mainly by the macromonomer concentration)[20]. Studies have not yet been undertaken to determine the mesh-size of the NPs presented in this thesis; however, similar polymerization conditions resulted in hydrogels which permitted diffusion of low MW molecules within their structure[13, 20, 21]. Moreover, it was shown in chapter 3 that doxorubicin (MW=580) was able to diffuse through the NP matrix. Therefore, we assumed that small drugs or labels could readily diffuse and interact with elements present in the bulk of the NPs.

Aiming to incorporate such functional elements, we introduced in the polymerization scheme two different, low MW, vinyl-containing comonomers: 2-acrylamido-2 methyl propan-sulfonic acid (AMPS) and N-(3-aminopropyl) methacrylamide hydrochloride (APMA) (Figure 4.2).
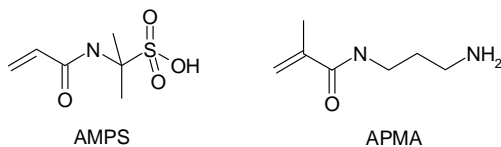
Figure 4.2 *Chemical structure of functional co-monomers containing reactive vinyl groups used in this study.*

AMPS is known to spontaneously polymerize in acidic environment[22]; for this reason, it was neutralized before its addition to the precursor solution. Its incorporation at three different concentrations in the NPs was confirmed by FTIR spectroscopy (Figure 4.3). Although there was no attempt to retrieve quantitative results, it is evident that increased amounts of AMPS were co-polymerized with increasing feed amounts.
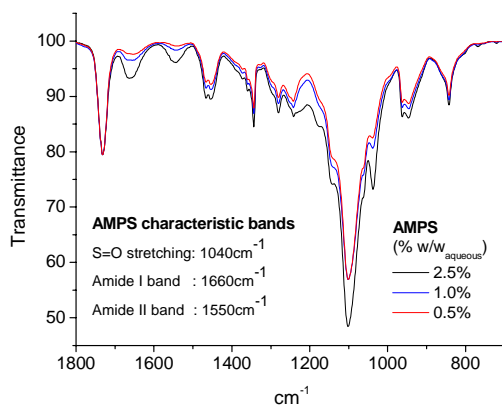

Figure 4.3 *FTIR spectra of NPs prepared with various AMPS precursor concentrations (region between 700 and 1800cm^{-1} normalized to the C=O stretching resonance is shown). Increase of comonomer characteristic peaks with increasing concentration, verifies proportional incorporation in the NPs.*

At physiological pH, the presence of AMPS in the NPs renders them negatively charged; electrostatic interactions between the sulfate groups and positively charged molecules could be used for loading purposes.

The second comonomer selected was APMA (Figure 4.2); its structure consists of a methacrylamide group on one side and a primary amine on the other side of a small (C3)

alkane chain. The concentration of primary amines and therefore the degree of incorporation of this comonomer was quantified using a fluorescamine assay: APMA was succesfully co-polymerized and the final amine concentration in the nanoparticles was in good agreement with that of the feed composition (Table 4.2).

Table 4.2 *Incorporation of APMA comonomer in NPs and conjugation efficiency of FITC coupling to the amines present in NPs.*

Sample	Theoretical APMA concentration (% w/w$_{NP}$)	Calculated AMPA concentration (% w/w$_{NP}$)	FITC conjugation efficiency (%)
PH-NH-1	0.08	0.13±0.04	15±1
PH-NH-2	0.40	0.45±0.03	11±1
TH-NH-1	0.40	0.42±0.01	11±3

The *a posteriori* covalent attachment of a low MW, amine reactive molecule to the nanoparticles was demonstrated using fluorescein isothiocyanate (FITC). Conjugation efficiencies were in the range of 10-15% (Table 4.2); we believe these low values are mainly due to FITC instability in aqueous media. The limited diffusion in the interior of the highly cross-linked networks of the nanoparticles may constitute an additional obstacle. Nevertheless, fluorescent NPs were succesfully isolated and imaged using a confocal microscope (Figure 4.4), confirming the feasibility of the functionalization strategy proposed.
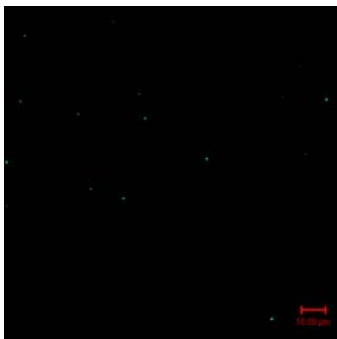

Figure 4.4 *Fluorescently labeled NPs (fluorescein) embedded in agarose gel and visualized by confocal microscopy.*

4.4 Conclusions

We have here presented an alternative initiation scheme for the radical cross-linking polymerization of PEG and Pluronics in inverse emulsion. Redox initiation by APS-TEMED

resulted in complete double bond conversion and formation of sub-micron particles, in a similar manner as photo-initiation. Therefore it can replace the former method in cases when substances that are incompatible with laser irradiation are used.

In order to functionalize the bulk of the NPs, comonomers were introduced in the reaction scheme; their efficient co-polymerization provided reactive groups for further modification, as was demonstrated by the covalent attachment of fluorescein. We believe these results may be extended for various functional, water-soluble molecules possessing at least one vinyl group in their structure.

4.5 References

1.   A. Zakrzewski and D.C. Neckers *Bleaching Products of Rose Bengal Under Reducing Conditions* Tetrahedron 43 **1987** 4507-4512

2.   J.P. Fisher, et al. *Photoinitiated polymerization of biomaterials* Ann. Rev. Mater. Res. 31 **2001** 171-181

3.   N. Murthy, et al. *A macromolecular delivery vehicle for protein-based vaccines: Acid-degradable protein-loaded microgels* P. Natl. Acad. Sci. USA 100 **2003** 4995-5000

4.   X.D. Feng, et al. *Study of the initiation mechanism of the vinyl polymerization with the system persulfate/N,N,N´,N´-tetramethylethylenediamine* Makromolekulare Chemie-Macromolecular Chemistry and Physics 189 **1988** 77-83

5.   K.D. Jensen, et al. *Cytoplasmic delivery and nuclear targeting of synthetic macromolecules* J. Controlled Release 87 **2003** 89-105

6.   P. Watson, et al. *Intracellular trafficking pathways and drug delivery: fluorescence imaging of living and fixed cells* Adv. Drug Delivery Rev. 57 **2005** 43-61

7.   R.P. Kulkarni, et al. *Single Cell Kinetics of Intracellular, Nonviral, Nucleic Acid Delivery Vehicle Acidification and Trafficking* Bioconjugate Chem. 16 **2005** 986-944

8.   Y. Tseng, et al. *Micromechanical Mapping of Live Cells by Multiple-Particle-Tracking Microrheology* Biophysical Journal 83 **2002** 3162-3176

9.   E. Andrzejewska *Photopolymerization kinetics of multifunctional monomers* Prog. Polym. Sci. 26 **2001** 605-665

10.   H.N. Xiao, et al. *Preparation and kinetic characterization of copolymers of acrylamide and poly(ethylene glycol) (meth)acrylate* Polymer 37 **1996** 1201-1209

11.   R.A. Scott and N.A. Peppas *Kinetics of copolymerization of PEG-containing multiacrylates with acrylic acid* Macromolecules 32 **1999** 6149-6158

12.   A.A.A. Abdel-Azim, et al. *Preparation and properties of two-component hydrogels based on 2-acrylamido-2-methylpropane sulphonic acid* Polym. Adv. Technol. 9 **1998** 282-289

13.   M.B. Mellott, et al. *Release of protein from highly cross-linked hydrogels of poly(ethylene glycol) diacrylate fabricated by UV polymerization* Biomaterials 22 **2001** 929-941

14.   C.M. Nolan, et al. *Phase Transition Behavior, Protein Adsorption, and Cell Adhesion Resistance of Poly(ethylene glycol) Cross-Linked Microgel Particles* Biomacromolecules **2005**

15.   K. McAllister, et al. *Polymeric nanogels produced via inverse microemulsion polymerization as potential gene and antisense delivery agents.* J. Am. Chem. Soc. 124 **2002** 15198-15207

16.   C.D. Vo, et al. *Preparation of thermosensitive nanogels by photo-cross-linking* Colloid Polym. Sci. 280 **2002** 400-409

17.   F. Cellesi, et al. *Materials for cell encapsulation via a new tandem approach combining reverse thermal gelation and covalent crosslinking* Macromol. Chem. Phys. 203 **2002** 1466-1472

18.   S. Udenfriend, et al. *Fluorescamine: A Reagent for Assay of Amino Acids, Peptides, Proteins, and Primary Amines in the Picomole Range* Science 178 **1972** 871-872

19.   C.P. Pathak, et al. *Rapid Photopolymerization of Immunoprotective Gels in Contact with Cells and Tissue* J. Am. Chem. Soc. 114 **1992** 8311-8312

20.   G.M. Cruise, et al. *Characterization of permeability and network structure of interfacially photopolymerized poly(ethylene glycol) diacrylate hydrogels.* Biomaterials 19 **1998** 1287-1294

21.   A.W. Watkins and K.S. Anseth *Investigation of Molecular Transport and Distributions in Poly(ethylene glycol) Hydrogels with Confocal Laser Scanning Microscopy* Macromolecules 38 **2005** 1326-1334

22.   O.A. Kazantsev, et al. *Spontaneous polymerization of 2-acrylamido-2-methylpropanesulfonic acid in acidic aqueous solutions* Russian Journal of Applied Chemistry 75 **2002** 465-469

Chapter 5

Thermally-Induced Responses in Nanoparticle Assemblies: Possible Formation of a Colloidal Glass and its Perspective Applications

Abstract

We here discuss a temperature-induced sol-gel phenomenon observed for concentrated water dispersions of amphiphilic hydrogel nanoparticles, which are composed of covalently cross-linked Pluronic F127 and PEG. We interpret this transition as related to a change in the state of individual nanoparticles, turning from soft, deformable objects into hard spheres. The change in nanoparticles' mechanical properties determines a structural arrest of the dispersion, which turns into a glassy state. We also discuss the implications of this phenomenon for applications in biomaterials and controlled release.

5.1 Introduction

We here discuss a new kind of colloidal hydrogel, prepared through the thermo-switchable assembly (vitrification) of nanoparticles.

Hydrogels are almost ubiquitous biomedical materials, with applications ranging from topical controlled drug delivery to permanent or provisional tissue substitution and regeneration. The attention of researchers and clinicians is increasingly focusing on hydrogels formed *in situ* from liquid precursors; these materials are advantageous because of the minimally invasive formation and the optimal contact and shape-matching with the surrounding tissues. A variety of systems have been developed for these applications[1-3], with fluid-to-solid (*sol-gel*) transition resulting from the formation of chemical cross-links (chemical gelation) or from a change in physico-chemical interactions (physical gelation).

Materials that exhibit a lower critical solution temperature (LCST) near physiological temperature are very attractive candidates for *in situ sol-gel* applications, because of the mild character of the transition (negligible heat production, no byproducts), and indeed a number of them have been investigated, for example poly(*N*-isopropylacrylamide)[4] (pNIPAm), the amphiphilic poly(ethylene glycol)-*bl*-poly(propylene glycol)-*bl*-poly(ethylene glycol) (PEG-PPG-PEG) block copolymers, known as Poloxamers or Pluronics[5-7] and PEG-PLGA block copolymers[3, 8]. In a recent report, a natural polymer formulation based on chitosan showed promising results *in vitro* as well as *in vivo*[9, 10].

We are specifically interested in Pluronics-containing materials. Pluronics show excellent biocompatibility, can be easily functionalized and loaded with drugs; in most cases, they can be excreted, thus avoiding long-term accumulation. A non-negligible inconvenience is, however, the rapid kinetics of dissolution of their physical gels; furthermore, this process determines a simultaneous release of any encapsulated payload[11], hindering the use of these materials for applications that require a long-term sustained release. Several approaches have been pursued to overcome this problem, including the use of different polymer additives (PEG, PVP, different cellulose and others)[12, 13], the incorporation of preformed loaded nanoparticles[14] or liposomes[15, 16] and the preparation of higher molecular weight polymers containing segments of PEG and PPG[17]. The chemical cross-linking of physical gels with hydrolytically-sensitive groups can also be used to prolong the stability of Pluronic gels[18]. However, all these systems lack of the simplicity of a system based on purely physical gelation of only one component.

It is important to recall that Pluronic sol-gel transition is a phenomenon of colloidal self-assembly: an increase in temperature, concentration, or both, make Pluronic unimers associate into micelles, which then crystallize into a cubic phase[5, 19, 20]. It is therefore more appropriate to describe these systems as 'micellar crystals' rather than gels, and the process is better termed a reverse thermal hardening (or gelation) rather than a simple LCST transition.

Having in mind that also other colloidal systems can undergo sol-gel transitions and that the kinetics of dissolution processes is related to the diffusion coefficients of the colloids, and thus inversely proportional to their size, we focused our attention on larger objects (nanoparticles), whose gels should therefore show slower solubilization than micellar systems. The sol-gel processes of concentrated nanoparticles dispersions have indeed attracted considerable attention [21-23]: if these dispersions can behave as liquids at low volume fractions (φ), upon concentration the particles' motion starts to correlate with that of their neighbors; finally, at a specific volume fraction a structural arrest takes place, limiting the diffusion of the individual nanoparticles. In a model of elastic hard spheres, at $\varphi=0.49$ a fluid becomes a two-phase system composed of the fluid with a face-centered-cubic crystal. At $\varphi\sim0.58$ a glass transition takes place, before reaching the random close-packed volume fraction of $\varphi=0.67$. It is generally assumed that the individual particles are dynamically arrested within a cage formed by their neighbours ("cage effect"), conferring an elastic character to the material.

This picture is valid under the assumption of hard, non-interacting spheres. The presence of attractive forces may on the contrary cause a glass-like gelation at lower volume fractions[24], while soft, swellable, interpenetratable and/or deformable particles may flow even at higher volume fractions[25-27]. In an attempt to rationalize these colloidal fluid-to-solid transitions, different methodologies have been introduced, including the 'jamming' phase diagram concept[24, 28] and the glass paradigm approach[29].

Although colloidal sol-gel transitions have been studied from a physicochemical perspective, such systems have not been explored extensively for biomedical applications. Studies have been performed mostly on non-aqueous solvents and on colloids that are well-characterized but of limited biological interest.

We have here tackled the task of producing a thermoreversible colloidal gel-like solid, by providing thermal sensitivity (through a Pluronic structure) to nanoparticles and studying the influence of temperature on their self-assembly. In terms of biomedical goals, we wished to prepare a system that would (1) form an elastic material with enhanced mechanical properties from injectable, fluid precursors through a temperature gradient; (2) exhibit slow

dissolution kinetics, because of the slower dynamics of nanoparticles compared to micelles, and in this way (3) decouple the release kinetics of a payload from that of the gel dissolution.

Specifically, we have employed materials composed of copolymeric cross-linked gels of Pluronics and PEG, which were produced in form of nanoparticles via inverse emulsion photopolymerization[30]. The nanoparticles preserve the amphiphilic (micellar) structure of Pluronic, even rendering it more stable towards dilution, and thus feature hydrophobic sites for encapsulation of poorly-water soluble drugs.

5.2 Materials & Methods

5.2.1 Materials

Dichloromethane and *n*-hexane (99%) were purchased from LabScan (Oensingen, Switzerland). Toluene, acryloyl chloride, triethylamine, triethanolamine, span65 (sorbitan tristearate, HLB=2.1±1.0) were purchased from Fluka (Buchs, Switzerland). Pluronic F127, a symmetric triblock copolymer with MW=12700, 70% wt. poly(ethylene glycol) and a central poly(propylene glycol) block, was purchased from Sigma (Buchs, Switzerland). Pluronic F127 was functionalized with acrylate moieties (F127 diacrylate) as described elsewhere[31]. Eosin Y and poly(ethylene glycol) diacrylate $\overline{M}_n$ =575 (PEG575 diacrylate) were purchased from Aldrich (Buchs, Switzerland). All solvents and reagents were used as received unless otherwise mentioned.

5.2.2 Nanoparticle preparation

Nanoparticles were prepared via inverse emulsion photopolymerization as described in chapter 2. Briefly, Span65 (2.0% w/w$_{total}$) was dissolved in 2.4 ml *n*-hexane by sonication (4 min). 0.6 ml of aqueous precursor solution of F127 diacrylate, PEG575 diacrylate, triethanolamine and eosin Y (9.4%, 3.1%, 2.0%, 0.02% w/w$_{aqueous}$ respectively) were added to the oil phase (oil-to-water weight ratio = 72/28) and an inverse emulsion was formed by sonication for 30 sec with a tip-sonicator (Bandelin Sonoplus). The inverse emulsion was illuminated with an Ar ion laser (480-520 nm) for 1 hr, at room temperature, with an intensity of around 75 mW/s, under magnetic stirring (200 rpm). After illumination, the inverse emulsion was extracted with *n*-hexane to remove the emulsifier. The aqueous phase was then

dialyzed against water (MWCO= 300,000, Spectrum Laboratories) to remove initiator and non-reacted macromonomers.

5.2.3 Preparation of hydrogel discs

Macromonomer precursor solutions were prepared in water with 2.7 mM triethanolamine and 10 μM eosin Y (2% and 0.035% w/w$_{aqueous}$ respectively). Aliquots of 50 μl were placed between two glass slides, precoated with Sigmacote, and irradiated for 5 min with an Ar ion laser (480-520 nm) at a flux of 75 mW/s. The formed hydrogel discs were weighed in air and ethanol after cross-linking and after swelling to equilibrium for 48 hr in water. The swelling index was calculated as the ratio weight of the swollen gel to the dry weight, for different temperatures (n=4) and density was calculated using the formula:

$$d_{gel} = \frac{w_{swollen}}{\left(w_{swollen} - w_{ethanol}\right)} d_{ethanol} , \text{ with } d_{ethanol}\text{=0.79 g/ml.}$$

5.2.4 Spectroscopic characterization

^{1}H-NMR spectra were recorded on a 300 MHz Bruker spectrometer. FTIR spectra were recorded in ATR mode on a Spectrum One Perkin Elmer Spectrometer. Fluorescence spectra were obtained using a Perkin Elmer LS50b Luminescence spectrometer equipped with a four-position thermostated automatic cell changer with stirrer. UV-Vis spectra were recorded on a Perkin Elmer Lambda 20.

5.2.5 Dynamic light scattering (DLS)

Values of effective hydrodynamic diameter in dilute dispersions were obtained by dynamic light scattering measurements using a Brookhaven instrument (model BI-DSI) equipped with a Lexel 95 laser source (514 nm at room temperature) at a fixed angle of 90°. Prior to analysis, solutions were filtered through a Millex AP filter (pore size ≈2µm) to remove dust. The digital correlator was operated with 200 channels, a minimum duration of 5 min and an average amount of counts per second between $100x10^3$ and $700x10^3$. Temperature was set at 37°C unless otherwise noted. Different analysis types were used to fit the autocorrelation function: a cumulant quartic fit for calculation of mean diameter and an inverse Laplace transform algorithm (CONTIN) for determination of size distributions. In

order to minimize any variation in data due to batch-to-batch differences in nanoparticle size distribution, all production batches were pooled for further experimentation.

5.2.6 Rheometry

All rheometry measurements were performed on a Bohlin 120 HR rheometer with parallel plate geometry (gap size 500-800 μm). Samples were placed on the lower plate in liquid form and silicon oil was applied on the surface to prevent evaporation. Temperature was controlled in the range 5-50°C with an accuracy of ± 0.1°C. Steady shear viscometry was performed at 37°C. From oscillatory measurements, the storage modulus G' (elastic modulus) and loss modulus G'' (viscous modulus) were determined in the linear viscoelastic region (with the 3-dimensional network of the material intact). Temperature scans at a rate of 1°C/min were performed using a frequency of 1 Hz and an applied stress of 10 Pa. The fluid-to-solid transition point was defined as the crossing point of the G' and G'' curves. Angular frequency was varied between 0.01 and 100 rad/s and stress sweeps were performed at 1 Hz (37°C). All experiments were performed in triplicate and the nanoparticle concentration values were expressed as weight % of solid material.

5.2.7 Dissolution studies

The dissolution rates of concentrated polymer gels and nanoparticle glasses, were compared by determining their interface eroding velocities in water as described elsewhere[32]. Briefly, dyed aqueous solutions of Pluronic F127 or dispersions of nanoparticles (0.5 ml) were poured into 5 × 40 mm tubes at 4°C and left for 30 min at 4°C to solubilize gel possibly formed on the tube walls as well as to obtain a smooth flat surface. Samples were then equilibrated at 37°C before being inverted and placed in a 37°C water bath (0.5 l). The height of the gel/glass in the tubes was measured using a digital micrometer (±0.01 μm).

5.3 Results & Discussion

5.3.1 Nanoparticle preparation

We have previously reported the preparation and characterization of Pluronic-based nanoparticles via inverse emulsion photopolymerization[30]. When acrylated Pluronics were

copolymerized with PEG diacrylates in inverse emulsions, it was possible to form colloidal nanoparticles in which the PPG-rich hydrophobic nanodomains of Pluronic micelles could be permanently stabilized in the form of a nanogel (Scheme 5.1). In the present study, we focused our attention on high Pluronic content nanoparticles (Pluronic-to-total macromonomer weight ratio: 0.75). In order to determine the degree of conversion of the cross-linking reaction and the actual Pluronic content in the nanoparticles, we performed ^{1}H-NMR analysis on the nanoparticle dispersions in D_2O. The disappearance of the peaks at 5.8, 6.1 and 6.4 ppm (3 protons of the acrylate moiety -CH=CH$_2$) confirmed the complete conversion of the double bonds. The Pluronic-to-total copolymer ratio was calculated by comparing the peak at 1.2 ppm (3H of the PPG block methyl group -CH$_3$) with the main peak at 3.6 ppm (PEG backbone). The determined value of 0.79 is in good agreement with the theoretical value of 0.75 of the precursor mixture.

Scheme 5.1 *A schematic representation of how the inverse emulsion photopolymerization of acrylated macromonomers stabilizes the aqueous nanodroplets into hydrogel nanoparticles.*
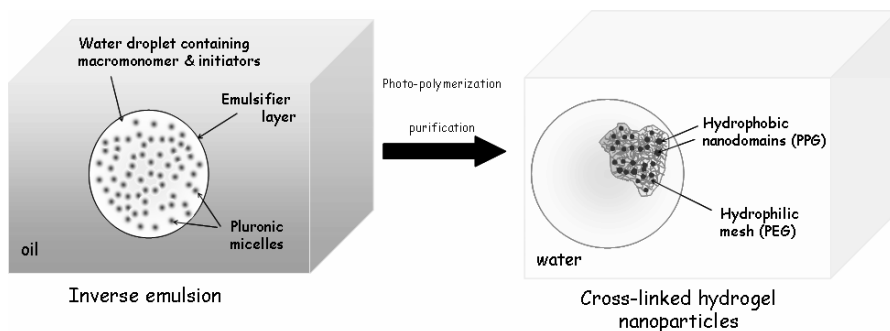
5.3.2 Temperature-dependent swelling; nanoparticles vs. macroscopic gels

As mentioned above, our previous studies demonstrated that the PPG chains of the Pluronic macromonomer formed stable hydrophobic domains in the cross-linked nanoparticles. This chain segregation, apart from offering loading sites for poorly-water soluble drugs through hydrophobic interactions (with the PPG domains), can have an interesting effect on the mechanical properties (i.e. size and elasticity) of the nanoparticles with temperature.

As for any LCST-related phenomenon, at the basis of Pluronic reverse gelation there is entropy-driven release of bound water. It is expected that Pluronic-containing materials (not only these nanoparticles) shrink with increasing temperature.

Through the same photopolymerization process, we have prepared macroscopic hydrogels with composition identical to the nanoparticles and studied their water-uptake at different temperatures. The gel swelling showed a clear transition in the 15-40°C temperature range (Figure 5.1). Similar results were obtained for composite hydrogels of hyaluronic acid and Pluronic[33] and for microgels of Pluronic-modified poly(acrylic acid)[34]. Thus, as much as the self-association of PPG chains in micelles is retained in the cross-linked nanoparticle, the thermal properties are still present too. The correlation between swelling of cross-linked hydrogels and their mechanical properties is well described in literature; decreased swelling corresponds to higher elasticity[31].

We expected the above results to relate to nanoparticles' behaviour as well. Indeed dynamic light scattering analysis showed a distinct reduction in size upon heating (Table 5.1). This corresponds to a real temperature-induced shrinkage, since there is no significant changes in the width of the broad size distributions (Figure 5.2). Qualitatively, the degree of temperature-induced de-swelling on nanoparticles, calculated as a reduction in volume, is analogous to that measured on macrogels.

Table 5.1 *Mean nanoparticle hydrodynamic diameter before and after freeze drying based on a cumulant quartic fit (n=3)*

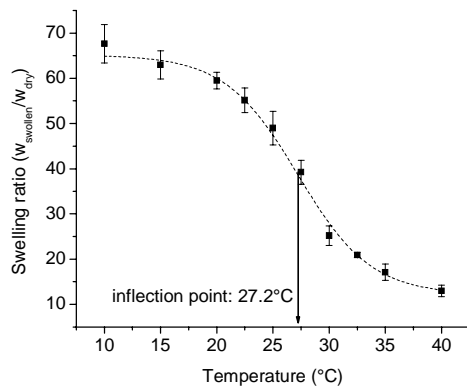| Temperature (°C)	Before freeze drying	After freeze drying
15	217.2±3.7	-
25	149.4±9.9	-
37	101.5±7.4	97.9±15.1

Figure 5.1 *Swelling of macroscopic hydrogels prepared with a Pluronic-to-total macromonomer weight ratio of 0.75 and with 12.5% total polymer weight ($w/w_{aqueous}$). The data are well fitted with a sigmoidal function ($r^2=0.997$, n=4), showing an inflection point indicative of the temperature sensitivity of the material. Mean and S.D. are shown.*
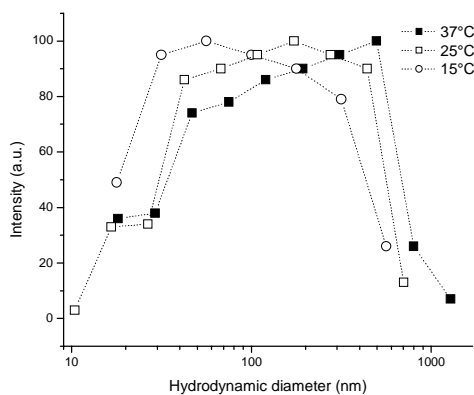

Figure 5.2 *Size distribution of nanoparticles as a function of temperature (dynamic light scattering with CONTIN analysis).*

On the basis of the above findings and due to the absence of specific interparticle interactions (these are dilute colloidal dispersions and the surface does not present ionic or strongly H-bonding groups), we therefore assume the temperature increase to mainly cause

size reduction due to water expulsion which, by analogy to the macroscopic hydrogels, should be accompanied by an increase in elastic modulus.

5.3.3 Concentration-dependent solidification at 37°C

Semi-dilute and concentrated colloidal dispersions are generally characterized by non-linearities in their macroscopic physical properties, e.g. in viscosity. In the specific case of colloidal dispersions, above a critical volume fraction, which depends on nanoparticle interactions, temperature and solvent characteristics, a dispersion can turn from a free-flowing liquid into a visco-elastic solid.

Our hydrogel nanoparticles indeed show a rapid increase in viscosity and in storage modulus (Figure 5.3) above a critical concentration, which at 37°C corresponds to roughly 4% wt in dry material. Also the shear rate dependence of viscosity shows dramatic changes around this concentration, with a Newtonian behaviour below 4% wt. and shear-thinning above (Figure 5.4). A similar behavior has been reported for other semi-solid systems, including Pluronic aqueous (micellar) solutions[20] and dispersions of polysaccharide nanoparticles chemically derivatized to render them hydrophobic[35].
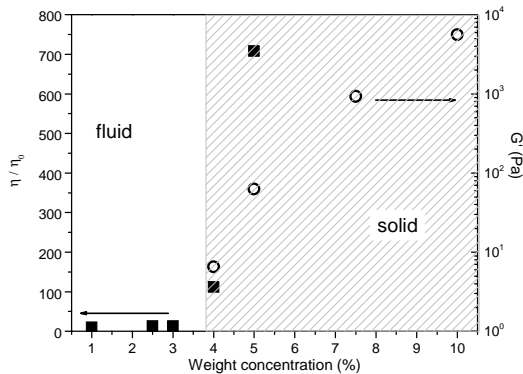

Figure 5.3 *Concentration dependence of reduced zero-shear viscosity η/η₀ and elastic modulus G' at 37°C for hydrogel nanoparticles. The shaded area identifies the supposedly 'solid' region.*
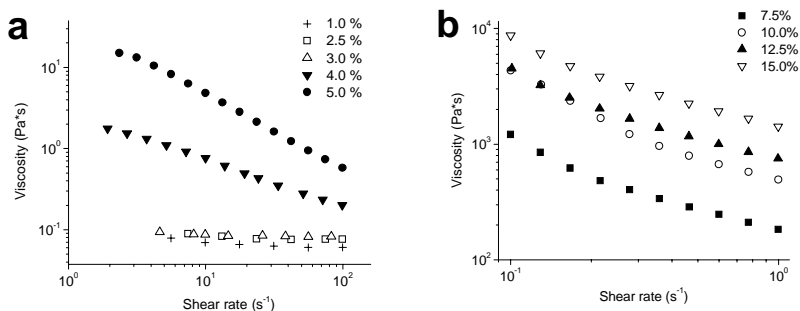
Figure 5.4 *Shear rate dependence of steady shear viscosity for fluid nanoparticle dispersions of different concentration (left). The mechanical integrity of the more concentrated samples was compromised at high shear rates, thus their shear-thinning behaviour was proofed for a different rate range (right).*

In order to better understand this phenomenon, it is of the essence to convert the critical concentration of 4% wt. to a volume fraction. Assuming that macroscopic hydrogels and nanoparticles prepared with the same initial polymer concentration would swell in a comparable manner, we have employed the values of swelling index and density measured for the hydrogels. With a swelling index of roughly 15:1 and a density at 37°C of 1.01 g/ml, the resulting conversion factor of 15 ml/g provides estimated volume fractions of $\varphi_{3\%}=0.45$ and $\varphi_{4\%}=0.60$, respectively for 3 and 4% wt. dispersions.

These values fall in the same range of concentrations that the hard sphere model would predict to be on the edge of a glass transition (see introduction); in our case we have non-covalently linked nanoparticles with little or no interparticle attraction, but, in order interpret our transition as a structural arrest at high volume fractions, we need to clarify whether they can be considered elastic and "hard". Interestingly, we know (see above) that Pluronic materials change their swelling degree and therefore also their mechanical properties with temperature; in particular, they become harder with increasing temperature[31]. If a hard sphere model can rationalize the solidification, the conditions of the structural arrest should depend on the elastic modulus of the colloids and thus, in this case, on their swelling degree.

It is noteworthy that nanoparticle volume fractions for higher weight concentrations, would quickly exceed unity. These are clearly unrealistic values obtained assuming the nanoparticles to have the same value of equilibrium swelling as in dilute conditions; on the

contrary, they are likely forced into sub-equilibrium swelling and thus smaller dimensions than those recorded via DLS on dilute dispersions.

5.3.4 Temperature-dependence of the sol-gel transition

At low temperature (e.g. 4°C) all the dispersions in the concentration range studied (1-15%) could flow freely and be easily loaded into a syringe, suggesting therefore the occurrence of a thermally induced transition, at least for the more concentrated samples. Temperature-induced gel points, defined as the point where G' = G'' in oscillatory rheological measurements (Figure 5.5), were indeed recorded for these systems, with a monotonical decrease in the gel temperature with increasing concentration (Figure 5.6). Correspondingly, G' increased in a gradual but marked fashion over almost 4 orders of magnitude.
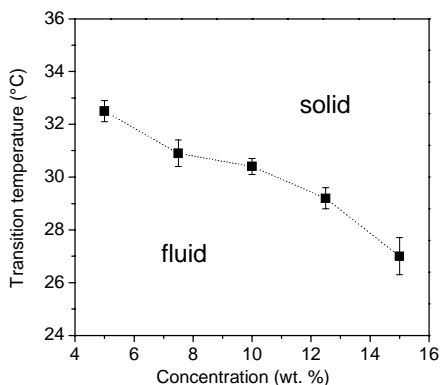

Figure 5.5 *Dependence of transition temperature on weight concentration of nanoparticle dispersion.*
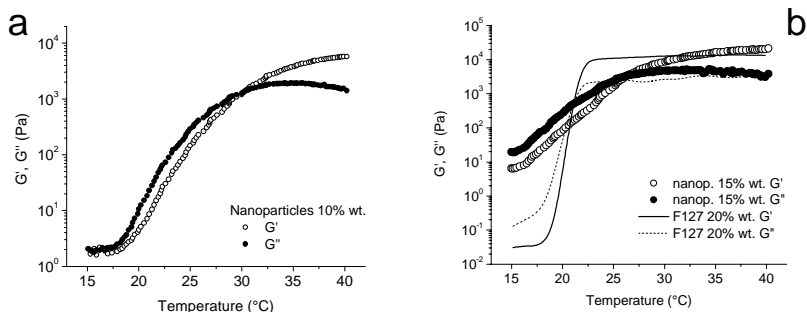
Figure 5.6 *Temperature-dependent gelation of Pluronic nanoparticle dispersions at (a) 10% wt. and (b) 15% wt. concentration. 1°C/min scans were performed at a fixed frequency of 1 Hz and 10 Pa applied stress. A 20% wt. aqueous Pluronic F127 solution is compared in (b) to the 15% wt. nanoparticle dispersions, which shows similar final values for both moduli.*

In the comparison to micellar Pluronic F127 solutions (Figure 5.6b), it is apparent that the transition is not as sharp and the temperature range is wider; in addition, also the dependence on concentration is clearly less steep: 14°C difference between 15 and 25% wt. Pluronic F127 solutions[31], vs. 6°C between 5 and 15% wt. nanoparticles suspensions. We believe these differences to stem from the polydispersity of our samples, but also from the markedly different transition mechanisms between these two systems, as discussed below.

5.3.5 Thixotropy at 37°C

The evaluation of the mechanical properties at the target temperature (37°C) revealed a clear thixotropic character of the colloidal dispersions, which always presented a flow region (G''>G') at low frequencies, followed by a crossover point and a plateau with a predominant elastic behavior (up tot 20 kPa for the most concentrated samples) at higher frequencies (Figure 5.7). Both the location of the cross-over point and the plateau G' values depended on concentration, with a monotonic decrease and increase, respectively, with increasing concentration (Table 5.2). These results are analogous to those obtained by Habas et al. for PEO-PPO-PEO block copolymers[19]: these authors examined the frequency dependence of micellar copolymer solutions in the organized phase at increasing temperatures and observed a decrease in the angular frequency ω_C, at which the G' and G'' curves intersect. This frequency delimits two domains in the behavior of the material, namely the viscoelastic

solid region and the viscous fluid. From their results the authors argued that their structured system is not a gel but a fluid with a long relaxation time[19], a definition we believe to be applicable for Pluronic nanoparticles too.

Table 5.2 *Dependence of the G', critical frequencies and terminal relaxation times plateau values on the concentration of nanoparticles dispersions at 37°C*

Concentration (wt. %)	Storage modulus (Pa)	ω_C (rad/s)	τ (s)
4.0	n.a.[a]	4.13	0.04
5.0	71	0.49	0.33
7.5	997	0.16	1.02
10.0	5960	0.17	0.95
12.5	13.0×10^3	0.10	1.60
15.0	20.1×10^3	0.02	10.0

[a] value affected by excessive variability

Alternatively, the relaxation kinetics of these materials can be expressed by the 'terminal relaxation time', which is defined as $\tau = 1/\omega_C$ and is physically related to the time the system needs to reach the flow zone. Pluronic nanoparticles show an increase of τ (decrease in ω_C) with increasing concentration, indicating the increased elasticity of the nanoparticle dispersions (Table 5.2).
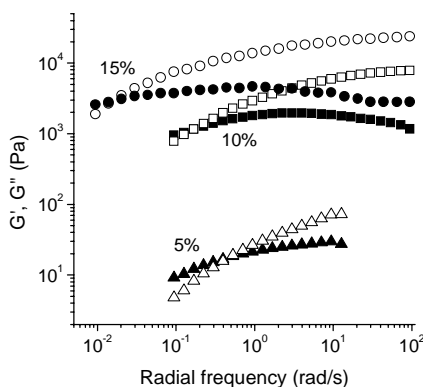

Figure 5.7 *Frequency dependence of the storage (G', open circles) and loss (G'', closed circles) moduli for aqueous nanoparticle dispersions of different concentrations at 37°C.*

The thixotropic character of these dispersions was further confirmed by the shear-thinning behavior (Figure 5.4) and by the presence of a flow-zone at low stress. The 'soft' nature of the interactions between nanoparticles (no chemical bond formation, no electrostatic, strong dipolar or H-bond interaction) suggests that when the applied stress exceeds a critical value, the three-dimensional network will cease to respond in an elastic manner and will deform plastically. Oscillatory measurements at 1 Hz with increasing stress values indeed confirmed G' to be independent on the applied stress only up to a critical and concentration-dependent value, above which G' decreases quite abruptly (Figure 5.8).
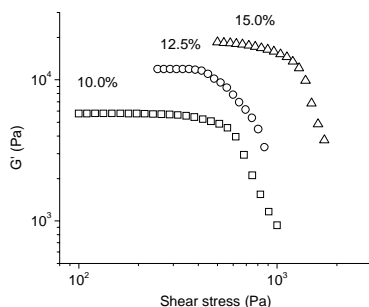
Figure 5.8 *Dependence of applied shear stress on storage modulus during dynamical (oscillation) measurements at a fixed frequency of 1 Hz and 37°C.*

It is important to state that all previous rheological measurements presented here were performed in the linear viscoelastic region, where the dynamic moduli are not a function of the applied stress.

5.3.6 Proposed mechanism: colloidal glass formation

We would like here to summarize a number of issues:

(1) The nanoparticle surface does not present dangling or charged polymer chains, which would give rise to interparticle attractive forces as a result of an increase in temperature, thus it is unlikely that the transition results from the development of attractive interparticle interactions, as would be the case in a classical colloidal gelation[36].

(2) At high volume fractions, the nanoparticles are in mechanical 'contact' with their neighbours (independently of temperature); at super-critical concentrations, we even suppose

the nanoparticles to be in a less-than-equilibrium swelling state, due to constraints of limited space availability.

(3) Macroscopic hydrogels and diluted nanoparticles exhibit a de-swelling phenomenon in the same temperature range where the fluid-to-solid transition takes place in concentrated nanoparticle dispersions. It is noteworthy that, as an effect of this phenomenon, macroscopic hydrogels become harder and the same is likely to happen for nanoparticles.

(4) The nanoparticle population is polydisperse, which excludes the possibility that the bulk transition induces the formation of a crystalline phase[37], as has been seen in other (monodisperse) colloidal systems, including Pluronic micellar solutions.

(5) The colloidal sol-gel transition cannot be caused by an arrest (vitrification) due to increase in the nanoparticle size and thus volume fraction, because, on the contrary, their size decreases, rather than increases, upon warming. It is noteworthy that this decrease in dimensions is not such to dramatically change the particle volume fraction, due also to the polydisperse nature of the samples (Figure 5.2: the size distribution substantially overlap below and above the transition).

(6) The solidification is mechanically reversible and the material flows plastically if the applied stress exceeds a critical value, indicating the lack of long relaxation time interactions between the colloidal particles.

Based upon preceding observations, we are inclined to believe that the macroscopic sol-gel transition is primarily a result of an intra-particle event, namely a transition from soft and deformable hydrogel nanoparticles to more elastic spheres. The limited possibilities of motion of a collection of concentrated and non-deformable colloidal objects would then induce a structural arrest, giving rise to the solid-like behavior of the material. In these concentrated colloidal dispersions and at temperatures above the transition temperature (25-30°C), any particle would be trapped in the 'cage' formed by its non-deformable neighbors, while at low temperatures the particles could escape by deformation (Scheme 5.2). By applying a sub-critical stress, the network will be (elastically) distorted, while at higher stresses, sufficient to exploit the residual deformability of the nanoparticles, the material will flow.

Scheme 5.2 *Schematic representation of the thermally-induced fluid-to-solid transition*

Colloidal dispersion → ΔT, shear → Colloidal glass

Deformability
Long-range movements

Elasticity
Entrapment
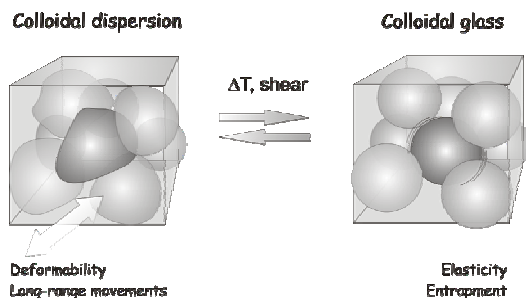
We would also expect (but we have not yet recorded) a solid-to-fluid transition to happen at higher temperatures, that is in the presence of a high enough thermal agitation.

We would finally like to point out an only apparent incongruence: the application of the MCT (Mode-Coupling-Theory) approach to hard sphere colloid glasses does predict an exponential divergence of the elastic modulus by increasing the colloid volume fraction above critical values[38]. Figure 5.3 seems on the contrary to suggest our system to show a much slower increase, with a final asymptotic value. We have however, to bear in mind that our empiric calculations set the transition concentration range (where the exponential regime should take place, $\varphi_c=0.5-0.7$) in the range 3-5% wt., where an exponential increase may indeed take place.

We would like thus to summarize that such a colloidal glass transition is therefore qualitatively different from the Pluronic sol-gel transition, where an increase in temperature induces firstly micellization and then crystallization of the micelles. Additionally, we prefer not to strictly define our system as a "colloidal gel", because we assume our particles to lack of short-range inter-particle attractive forces; we fully recognize, however, that this assumption should be proved by using much less polydisperse samples and studying their non-ergodicity possibly via dynamic light scattering.

5.3.7 Colloidal glasses exhibit slower dissolution than Pluronic gels

One of the targets of this research was to obtain materials that are similar to Pluronic in terms of advantageous characteristics, but feature a slower dissolution kinetics in excess water. By comparing a 25% wt. Pluronic F127 gel to a 12.5% wt. colloidal glass (based on 75% Pluronic F127 and 25% PEG575 diacrylate), it was apparent that this target was achieved. The micellar gel was already approx. 50% dissolved after 6 hr of exposure to excess

water; on the contrary, after a lag time of 24 hr, was recorded, the colloidal glass followed an apparent zero order kinetics with 50% of the gel being dissolved after around 180 hr (n=2).

We ascribe the slower dissolution kinetics of the nanoparticle glass primarily to the slower diffusive mobility of the nanoparticles, which are 1-2 orders of magnitude larger than Pluronic F127 micelles (10-20nm) and unimers.

It is noteworthy that, based upon data presented above, the 12.5% wt. nanoparticle glass is far below its equilibrium swelling. Thus, it might be expected that the material first swell and subsequently dissolve, due to diffusion of nanoparticles in the medium. The apparent absence of any swelling in these measurements, however, can be due to the contemporary incipient dissolution; this can thus also explain the occurrence of a lag time at the beginning of the experiments.
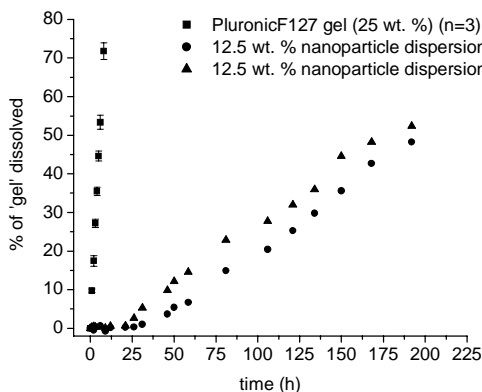
Figure 5.9 *Dissolution rate for PluronicF127 gel (25 % w/w) and two identical nanoparticle dispersions (12.5% w/w).*

5.4 Conclusions

In this chapter we present a new water-based thermally hardening system. This system consists of cross-linked hydrogel nanoparticles based on polymeric precursors of well-known biocompatibility (PEG and Pluronic). The biomedical use of one of them (Pluronic) is often related to its temperature-induced fluid-to-solid transition.

Pluronic-based nanoparticles undergo a temperature-induced solidification too, in a temperature range suitable for *in vivo* hydrogel formation. We suggest this transition to generate a gel in form of a colloidal glass (rather than a crystal or a gel), due to the modification of the nanoparticles mechanical properties from soft to hard spheres, which reach a state of arrested mobility.

The absence of strongly attractive interparticle forces determines the solubilization of the glass upon dilution; this process, however, is much slower than for Pluronic gels, likely due to the much retarded dynamics of the nanoparticles compared to the smaller micelles.

It is noteworthy that this feature in principle allows to extend the use of Pluronic-based systems for drug sustained release applications; indeed, due to the slower process, the release kinetics of a loaded drug would be decoupled from that of the material dissolution, and would therefore depend solely on molecular properties (e.g. partition between Pluronic hydrophobic domains and water).

5.5 References

1.   A. Hatefi and B. Amsden *Biodegradable injectable in situ forming drug delivery systems* Journal of Controlled Release 80 **2002** 9-28

2.   J.L. West and J.A. Hubbell *Comparison of Covalently and Physically Cross-Linked Polyethylene Glycol-Based Hydrogels for the Prevention of Postoperative Adhesions in a Rat Model* Biomaterials 16 **1995** 1153-1156

3.   B. Jeong, et al. *Thermosensitive sol-gel reversible hydrogels* Advanced Drug Delivery Reviews 54 **2002** 37-51

4.   H.G. Schild *Poly (N-Isopropylacrylamide) - Experiment, Theory and Application* Progress in Polymer Science 17 **1992** 163-249

5.   A. Cabana, et al. *Study of the gelation process of polyethylene oxide(a) polypropylene oxide(b) polyethylene oxide(a) copolymer (Poloxamer 407) aqueous solutions* Journal of Colloid and Interface Science 190 **1997** 307-312

6.   M.M. Amiji, et al. *Intratumoral administration of paclitaxel in an in situ gelling poloxamer 407 formulation* Pharmaceutical Development and Technology 7 **2002** 195-202

7.   O. Pillai and R. Panchagnula *Transdermal delivery of insulin from poloxamer gel: ex vivo and in vivo skin permeation studies in rat using iontophoresis and chemical enhancers* Journal of Controlled Release 89 **2003** 127-140

8.   B. Jeong, et al. *Biodegradable block copolymers as injectable drug-delivery systems* Nature 388 **1997** 860-862

9.   E. Ruel-Gariepy, et al. *A thermosensitive chitosan-based hydrogel for the local delivery of paclitaxel* European Journal of Pharmaceutics and Biopharmaceutics 57 **2004** 53-63

10.   A. Chenite, et al. *Novel injectable neutral solutions of chitosan form biodegradable gels in situ* Biomaterials 21 **2000** 2155-2161

11.   T. Moore, et al. *Experimental investigation and mathematical modeling of Pluronic (R) F127 gel dissolution: drug release in stirred systems* Journal of Controlled Release 67 **2000** 191-202

12.   R. Bhardwaj and J. Blanchard *Controlled-release delivery system for the alpha-MSH analog melanotan-I using poloxamer 407* Journal of Pharmaceutical Sciences 85 **1996** 915-919

13.   S.D. Desai and J. Blanchard *In vitro evaluation of pluronic F127-based controlled-release ocular delivery systems for pilocarpine* Journal of Pharmaceutical Sciences 87 **1998** 226-230

14.   S.D. Desai and J. Blanchard *Pluronic (R) F127-based ocular delivery system containing biodegradable polyisobutylcyanoacrylate nanocapsules of pilocarpine* Drug Delivery 7 **2000** 201-207

15.   A. Paavola, et al. *Controlled release injectable liposomal gel of ibuprofen for epidural analgesia* International Journal of Pharmaceutics 199 **2000** 85-93

16.   A. Bochot, et al. *Liposomes dispersed within a thermosensitive gel: A new dosage form for ocular delivery of oligonucleotides* Pharmaceutical Research 15 **1998** 1364-1369

17.   D. Cohn, et al. *Improved reverse thermo-responsive polymeric systems* Biomaterials 24 **2003** 3707-3714

18.   F. Cellesi, et al. *Towards a fully-synthetic substitute of alginate: development of a new process using thermal gelation and chemical cross- linking* Biomaterials 25 **2004** 5115-5124

19.   J.P. Habas, et al. *Understanding the complex rheological behavior of PEO-PPO-PEO copolymers in aqueous solution* Journal of Rheology 48 **2004** 1-21

20. R.K. Prudhomme, et al. *Structure and rheology studies of poly(oxyethylene-oxypropylene-oxyethylene) aqueous solution* Langmuir 12 **1996** 4651-4659

21. F. Sciortino *Disordered materials - One liquid, two glasses* Nature Materials 1 **2002** 145-146

22. K.N. Pham, et al. *Multiple glassy states in a simple model system* Science 296 **2002** 104-106

23. D. Quemada and C. Berli *Energy of interaction in colloids and its implications in rheological modeling* Advances in Colloid and Interface Science 98 **2002** 51-85

24. V. Prasad, et al. *Universal features of the fluid to solid transition for attractive colloidal particles* Faraday Discussions 123 **2003** 1-12

25. M. Kapnistos, et al. *Reversible thermal gelation in soft spheres* Physical Review Letters 85 **2000** 4072-4075

26. E. Stiakakis, et al. *Kinetic arrest of crowded soft spheres in solvents of varying quality* Physical Review E 66 **2002** art. no.-051804

27. C.L.A. Berli and D. Quemada *Rheological modeling of microgel suspensions involving solid- liquid transition* Langmuir 16 **2000** 7968-7974

28. V. Trappe, et al. *Jamming phase diagram for attractive particles* Nature 411 **2001** 772-775

29. K.A. Dawson *The glass paradigm for colloidal glasses, gels, and other arrested states driven by attractive interactions* Current Opinion in Colloid & Interface Science 7 **2002** 218-227

30. D. Missirlis, et al. *Amphiphilic hydrogel nanoparticles. Preparation, characterization and preliminary assessment as new colloidal drug carriers* Langmuir **2005**

31. F. Cellesi, et al. *Materials for cell encapsulation via a new tandem approach combining reverse thermal gelation and covalent crosslinking* Macromolecular Chemistry and Physics 203 **2002** 1466-1472

32. B.C. Anderson, et al. *The effect of salts on the micellization temperature of aqueous poly(ethylene oxide)-b-poly(propylene oxide)b-poly(ethylene oxide) solutions and the dissolution rate and water diffusion coefficient in their corresponding gels* Journal of Pharmaceutical Sciences 91 **2002** 180-188

33. M.R. Kim and T.G. Park *Temperature-responsive and degradable hyaluronic acid/Pluronic composite hydrogels for controlled release of human growth hormone* Journal of Controlled Release 80 **2002** 69-77

34. L. Bromberg, et al. *Dually responsive microgels from polyether-modified poly(acrylic acid): Swelling and drug loading* Langmuir 18 **2002** 4944-4952

35. K. Kuroda, et al. *Hierarchical self-assembly of hydrophobically modified pullulan in water: Gelation by networks of nanoparticles* Langmuir 18 **2002** 3780-3786

36. J. Bergenholtz and M. Fuchs *Gel transitions in colloidal suspensions* Journal of Physics-Condensed Matter 11 **1999** 10171-10182

37. G. Petekidis, et al. *Yielding and flow of colloidal glasses* Faraday Discussions 123 **2003** 287-302

38. K.S. Schweizer and E.J. Saltzman *Activated hopping, barrier fluctuations, and heterogeneity in glassy suspensions and liquids* Journal of Physical Chemistry B 108 **2004** 19729-19741

Chapter 6

In Vitro Cell–Nanoparticle Interaction Studies

6.1 Introduction

The use of nanoparticles (NPs) to increase the therapeutic effect of chemotherapeutic agents after intravenous injection, through passive or active cancer targeting has shown promising results[1-3]. Essential for the success of carrier-mediated, tumor-targeted delivery is the prevention of colloid capture by the mononuclear phagocyte system (MPS), particularly the hepatic Kuppfer cells and spleen macrophages; long circulation times help increase the amount of delivered drug[4, 5]. Moreover, the release of cytotoxic drugs in the host's defense cells may lead to their hazardous depletion.

The exact mechanisms of recognition of foreign particulate matter by cells of the MPS remain elusive. *In vitro* and *in vivo* observations have shown that the fate of the carrier depends largely on its physicochemical properties[6], and more specific size[7,8], hydrophobicity[9-11] and surface charge[10, 12, 13]. These characteristics affect adsorption of serum components on the colloids (opsonization) and thus influence phagocytosis. Hydrophobic surfaces and particles with large zeta potential absolute values are typically more susceptible to recognition and capture by phagocytic cells. Deviations from this trend may arise by the presence of chemical groups or molecules displayed on the carrier exterior and which are responsible for altering the adsorbed protein pattern[9]: favoring adsorption of molecules that reduce the phagocytic response known as dysopsonins (e.g. albumin), while preventing or delaying adsorption of certain opsonizing factors (e.g. immunoglobin G, fibronectin etc.), enhances the stealth character of the carriers.

Most nanoparticulate systems studied in respect to their MPS-evading capacities and circulation life-time are based on hydrophobic materials, like poly(lactic acid) (PLA) and poly(lactic-co-glycolic acid) (PLGA)[11,12,14,15], poly(ε-caprolactone), poly(cyanoacrylate)[16], poly(styrene)[13] and poly(methyl methacrylate)[7,17]. Consequently, surface modification strategies have been explored in order to mask the hydrophobic and/or charged particle core. A hydrophilic corona is formed, which results in decreased protein adsorption and/or interaction with macrophages, and increases the in *in vivo* circulation times of the carrier.

Poly(ethylene glycol) remains the most popular choice for surface modification due to its higly hydrated, flexible, non-ionic chains that efficiently shield the carrier interior[18]. However, complete, uniform coverage of colloids with small size and high curvature has proven to be challenging; incomplete shielding may be responsible for removal from circulation of a substantial percentage of dose[19]. Another promising biomimetic approach

recently reported was the attachment of CD47 on the carrier surface, which is believed to function as a marker of self, inhibiting in this way phagocytosis[20].

We have previously presented (in chapters 2 and 4) the preparation of polymeric nanoparticles based on poly(ethylene glycol) and poly(ethylene glycol)-*bl*-poly(propylene glycol)-*bl*-poly(ethylene glycol) copolymers. Considering their hydrophilic and non-ionic character, we anticipated a protein repellent character and low interactions with cells. In this chapter, we employ J774A.1 murine macrophages as model phagocytic cells in order to investigate the particle-cell interactions and assess the potential of the NPs as long circulating carriers.

Practical interest exists in the *in vitro* evaluation of MPS-evading properties of colloidal carriers. Although the pattern and quantity of adsorbed proteins is critical, binding studies from plasma or serum have proven to be poor simulators of the dynamic events occuring during protein adsorption/desorption, with weak capability to predict *in vivo* particle longevity. The exact role of the adsorbed proteins, the time-dependent adsorption patterns and the effect of incubation medium need to be clarified in order to obtain satisfying translation to physiological behavior. On the other hand, colloid-cell interaction studies have provided insight on uptake mechanisms and more reliable translation of results in physiological situations.

The cell line we have selected (J774) for our study, has previously been used to investigate the mechanism of binding and internalization of colloidal systems, mainly liposomes[21-23] but also polymeric colloids[17, 24]. These studies have shown that charged (positive or negative) liposomes are internalized to a greater extent than neutral ones, independent of the nature of the charged groups. Uptake is a two-step process with initial binding (rate determining step) and subsequent endocytosis. Chenevier et al. showed that for cationic liposomes, the first binding step involves the presence of two different binding sites[23]. The protective effect of PEG has also been demonstrated using this cell line: Mosquiera et al. used poly(lactide) nanocapsules to study in detail the effect of PEG length and concentration on macrophage-colloid interactions, reported decreased cell association of PEGylated carriers[24]. In order to quantify NPs at very low concentrations and visualize their interactions with the cells, we previously introduced amine groups in the nanoparticle structure and fluorescently labeled them *a posteriori* using versatile and mild chemistry (chapter 4).

Finally, having in mind clinical applications of the NPs proposed in this thesis, we aimed at resolving another important concern using cell studies, the toxicity of the carrier.

Development of several polymeric systems has been hampered by their non-specific toxicity; here, as a first indication of the non-toxic character of the material, proliferation of HeLa cells was evaluated in the absence and presence of NPs.

6.2 Materials & Methods

6.2.1 Nanoparticle formation

Nanoparticles were prepared as described in chapters 2 and 4; conditions of the different samples used in this study are presented in Table 6.1. In all cases hexane-to-aqueous phase weight ratio was set at 72:28, emulsifier (Span$^®$65) concentration at 2% wt. and total macromonomer weight ratio in the aqueous phase at 12.5% w/w$_{aqueous}$. For photo-initiated polymerization concentration of triethanolamine and eosin Y were set at 2.0% and 0.02% w/w$_{aqueous}$ respectively, whereas for initation using APS and TEMED concentrations were set at 2.0% w/w$_{aqueous}$ and 3.7% w/w$_{total}$.

Table 6.1 *Inverse emulsion polymerization parameters for preparation of NPs used in this chapter.*

Sample	Pluronic-to-total macromonomer weight ratio	APMA concentration (% w/w$_{NP}$)	Initiation type
PH-ST-1	0.50	-	Photo-initiation
TH-ST-1	0.50	-	Redox-initiation
TH-NH-1	0.50	0.40	Redox-initiation
TH-ST-G	0.75	-	Redox-initiation

6.2.2 Zeta potential and fluorescence spectroscopy measurements

Zeta potential was determined in 1mM phosphate buffer (pH=7.4) using a Malvern Nano-ZS zetasizer instrument. Fluorescence spectra were obtained using a Tecan Safire[2] microplate reader.

6.2.3 Cell Culture

The murine macrophage cell line J774A.1 (ATCC) and HeLa cells were cultured as exponentially growing subconfluent monolayers in DMEM and MEM-alpha media respectively. Both culture media were supplemented with 10% bovine growth serum

(Hyclone) and 0.1% antibiotic-antimycotic (Invitrogen), unless otherwise stated. Cells were grown at 37°C, humidified atmosphere and 5% CO_2.

6.2.4 Cytotoxicity assays

Cell proliferation of HeLa cells was monitored using the MTS assay with a *CellTiter 96 AQ_{ueous} One Solution Cell Proliferation Assay* kit from Promega. MTS stands for a novel tetrazolium compound that is bioreduced by cells into a colored formazan product, soluble in tissue culture medium. HeLa cells were seeded in 96-well plates at a density of 16×10^3 cells/cm^2, left overnight to adhere and then incubated with nanoparticle dispersions in medium (ranging from 40 to 1000 µg/ml). After 24h incubation at 37°C and 5% CO_2, 20µl of MTS solution was added and the absorbance was recorded at 490nm after 1 hr. Results are reported as proliferation relative to controls (absence of NPs in medium).

Viability of cells during the formation of a colloidal glass from a concentrated nanoparticle dispersion was assessed using calcein and ethidium homodimer-1 as a *LIVE/DEAD viability/cytotoxicity kit* from Molecular Probes. HeLa cells were seeded in chamber slides at a density of 16×10^3 cells/cm^2. A cold dispersion of NPs (12.5% wt; 100µl) in MEM-Alpha (serum-free) was then added until complete coverage of the cell layer; the chamber slide was incubated for 30 min followed by addition of 200µl culture medium. After an additional 4.5 h incubation cells were stained with calcein and ethidium homodimer-1 to visualize live and dead cells.

6.2.5 Cell-nanoparticle association studies

Association of fluorescent nanoparticles with J774A.1 macrophage-like cells was studied using fluorescence spectroscopy and fluorescent activated cell-sorting (FACS) analysis.

Cells were seeded in 24-well plates at a density of 125×10^3 cells/cm^2, allowed to attach overnight and incubated with NPs or fluospheres$^®$ (100nm, carboxylated; Molecular Probes) in supplemented culture medium (unless otherwise mentioned) for 4h, at 37°C.

For fluorescence association experiments cells were then washed twice with PBS and lysed using CelLytic™ (Sigma) lysis reagent (200 µl/well, 10min). Each well was rinsed with PBS (200µl) to give a final cell lysate volume of 400 µl. Additional experiments were carried out at 4°C and using the phagocytosis inhibitor sodium azide (Fluka); in the former case

HEPES was added in culture medium, whereas in the latter, cells were preincubated with NaN$_3$ (0.1% w/v) 30 min prior to NP addition.

Protein content was measured using the BIO-RAD Protein Assay kit, with albumin as standard. Nanoparticle concentration was determined by fluorescence spectroscopy measurements using calibration curves prepared in control cell lysates (absence of NPs).

For the FACS analysis, after incubation with NPs, cells were washed twice with PBS and scraped off the well plates mechanically. Cell suspensions were divided in two parts; in one part Trypan blue (Invitrogen) was added to quench external fluorescence (20µl in 200µl cell suspension). Analysis by FACS was performed using a CyAn ADP analyzer and a total of 10,000 cells per sample was analyzed.

6.2.6 Confocal Laser Scanning Microscopy (CLSM)

Cells were seeded in chamber slides (Lab-Tek, Nalge Nunc International) at a density of 125×10^3 cells/cm^2, allowed to attach overnight and incubated with NPs or fluospheres® in supplemented culture medium for 4h, at 37°C. Subsequently, cells were washed two times with PBS and inspected immediately in PBS solution without any fixation using a Zeiss LSM 510 META confocal laser scanning microscope.

Cell membrane and nucleus of live cells were visualized using an *Image iT LIVE Plasma Membrane and Nuclear Labeling Kit* (Molecular Probes). After washing a solution of Hoechst dye and fluorescently labeled agglutinin were added, the cells incubated 10min and inspected immediately after.

6.3 Results & Discussion

6.3.1 Nanoparticle characterization

It is well established that NPs with diameter between 50-200nm are better-suited as long-circulating carriers[5]. We concentrated our focus on this size range to assess cytotoxicity and probe the stealth character of PEG-Pluronic NPs (Table 6.2). For all samples prepared, double bond conversion was complete, as evidenced by the absence of the corresponding proton signals in ^{1}H-NMR spectra (δ=5.8, 6.2 and 6.4 of -OC(O)CH=CH$_2$); toxic, unreacted acrylate presence was therefore negligible.

The surface charge of the colloids used in our experiments was determined using zeta potential measurements. Slightly negative values close to zero for PEG-Pluronic NPs indicate

that particles are practically electroneutral. Incorporation of APMA comonomer containing a primary amine did not affect ζ-potential, most likely due to its low surface concentration (approx. 3% of dry weight). On the other hand, carboxylated fluospheres® were negatively charged at physiological pH (Table 6.2).

Table 6.2. *Hydrodynamic diameter determined by DLS and zeta potential of the nanoparticles used in our studies*

Sample	Hydrodynamic diameter (nm)[a]	Polydispersity index[b]	Zeta potential (mV)
PH-ST-1	145±12	0.12	-6.7±1.1
TH-ST-1	102±17	0.22	-5.1±0.8
TH-NH-1	137±4	0.18	-6.5±0.5
TH-NH-G[c]	118	0.27	-
Fluospheres®	124±2	0.02	-53.2±2.2

[a] average and standard deviation (n=3)
[b] average values(n=3)
[c] n=1

6.3.2 Cytotoxicity of nanoparticle formulations

Poly(ethylene glycol) and Poloxamers are generally viewed as non-toxic; we were here interested in testing the cytotoxicity of NPs based on these polymers. The fabrication process requires functionalization of macromonomers, as well as use of initiators and an organic solvent (*n*-hexane), which are all potentially toxic to the cells.
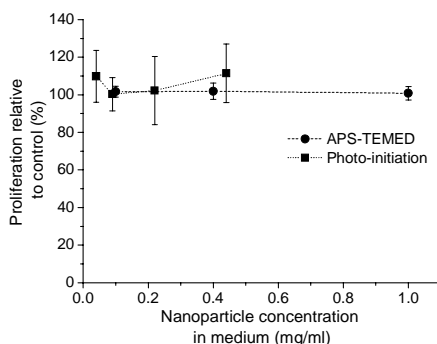

Figure 6.1. *Mitochondrial activity measured by the MTS assay, indicative of cell viability and proliferation, at different NP concentrations in the culture medium for NP prepared by radical polymerization using two different initiation schemes.*
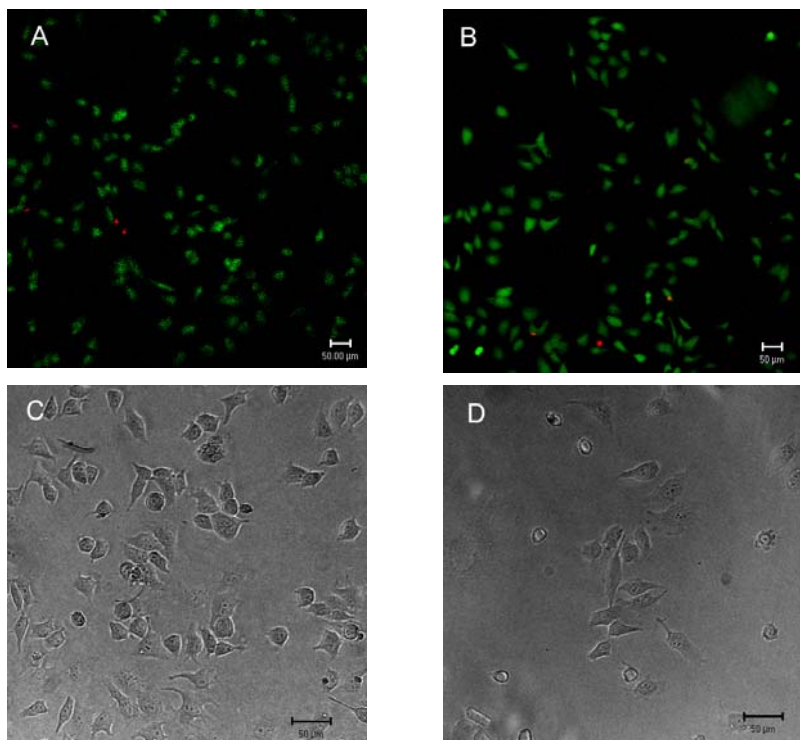
Figure 6.2. *Effect of thermally-induced physical transition on HeLa cell viability and morphology. Cells were either covered with the colloidal glass and incubated for 5h (A,C) or simply incubated (control: B,D) in non-supplemented cell culture medium. Live (green)/dead (red) stain cytotoxicity assay revealed similar results for cells in contact with the thermogelling material (A) and control (B). Cells remained attached and well spread under the colloidal glass (C).*

Viability of HeLa cells, measured as their mitochondrial metabolic activity, in presence of nanoparticles (PH-ST-1 and TH-ST-1) at concentrations as high as 1mg/ml, was equal to controls for NPs prepared by both initiation mechanisms (Figure 6.1). We can therefore conclude that the production and purification protocols used, resulted in non-toxic NPs.

We were also interested to see whether the thermally-induced glass transition (described in chapter 5) is compatible with viable cells. To this end, a cold (~5°C) NP dispersion (12.5 %wt in MEM-Alpha culture medium) was applied on top of attached HeLa

cells; incubation at 37°C triggered the formation of a semi-solid covering the cells. Qualitatively (using a live/dead stain), cytotoxocity was found to be negligible compared to controls (Figure 6.2 A,B); cell morphology was also unaffected by the physical transition (Figure 6.2 C,D).

6.3.3 Nanoparticle uptake studies

Given the significance of long circulation times and the important role of macrophages on the removal of foreign particulate matter from the bloodstream, we decided to probe the interactions of our NPs with a macrophage-like cell line to assess their stealth character. J774 cells were selected as model phagocytic cells of the MPS and fluorescently labeled NPs were used for detection and quantification of uptake.

Different concentrations of NPs were incubated with cells for 4 hr and fluorescence associated with cells was normalized to total protein content; parallel experiments were performed with commercially available carboxylated fluospheres®. We should note at this point, that the quantification through fluorescence spectroscopy of particles associated with cells, makes no distinction between internalized and adsorbed NPs.
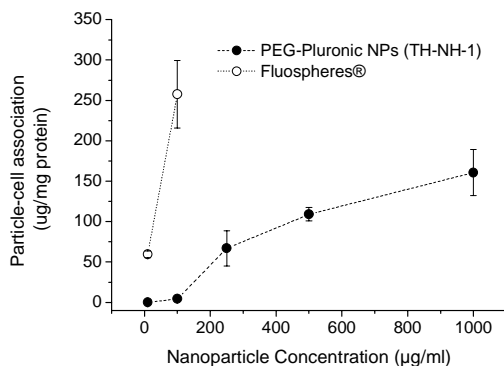
Figure 6.3. *Effect of nanoparticle concentration in serum-supplemented growth medium on association with J774A.1 macrophages. Colloids were incubated for 4h at 37°C and 5% CO_2. Values represent mean and standard deviation from 3 independent experiments.*

The interaction of NPs with macrophages was dose-dependent, with the saturation limit not being reached at the highest concentration studied here (Figure 6.3). In the case of fluospheres®, concentrations above 100 µg/ml resulted in fluorescence values above the detection limit of the experimental setup. We interpret the markedly reduced phagocytosis of

hydrogel NPs compared to fluospheres® on the basis of their dissimilar physicochemical properties: the absence of considerable charge and the hydrophilic character of the PEG-Pluronic colloids reduce direct binding, and/or binding after adsorption of serum proteins to cells, a key, first step of colloidal uptake.

In order to examine the effect of opsonization, we incubated the colloids in serum-free culture medium (Figure 6.4). For PEG-Pluronic NPs we did not observe any significant change in cell-NP association in the absence of serum: this finding supports our hypothesis that protein adsorption is minimal and therefore has a negligible role on the interactions of these NPs with cells. On the other hand, a slight increase in internalization of fluospheres® was observed. Presence of serum could lead to protein adsoption and screening of the negative suface charge reducing in this way phagocytosis.
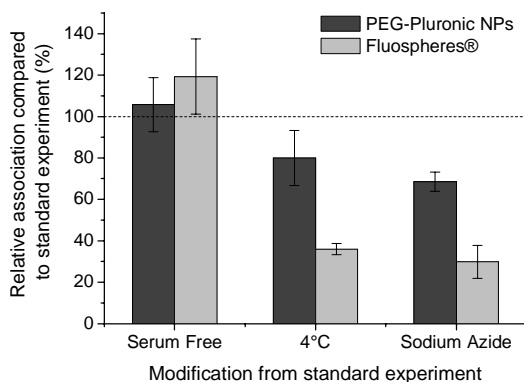
Figure 6.4. *Effect of various manipulations in respect to the standard internalization experiment; J774A.1 cells were incubated 4h in the absence of serum, at 4°C or in the presence of 0.1% w/v sodium azide. Concentration was set at 0.25mg/ml for PEG-Pluronic NPs and at 0.10mg/ml for fluospheres®. Values represent mean and standard deviation from 3 independent experiments.*

Associated fluorescence may either be due to internalized NPs or NPs merely bound to the cell surface. To distinguish between these two possibilities we selectively quenched fluorescence of NPs attached to the cell membrane of live cells, using a membrane impermeable quencher. Trypan blue completely quenched fluorescence of FITC-labeled nanoparticle dispersions at the concentrations used in our study. FACS analysis showed that essentially all NPs after washing the cells were internalized (Figure 6.5A). This finding was

not unexpected considering the absence of charge or targeting groups, which would allow a firm binding to cell surface. The use of FACS analysis to compare quantitavely the uptake of hydrogel NPs and fluospheres was not possible since the fluorescence emission per particle is different; an agreement with the fluorescence spectroscopy data was however evident (Figure 6.5B)
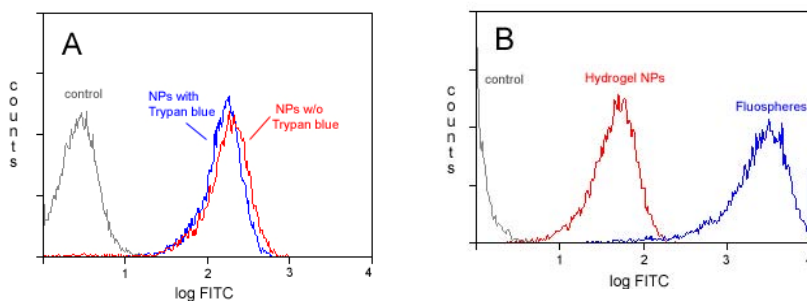

Figure 6.5 *Frequency distributions of fluorescence intensity in J774A.1 cells incubated for 4 hr with colloids. The presence of Trypan blue, which is able to quench fluorescence of colloids attached to the cell surface, did decrease only slightly the frequency distribution of FITC-labeled, hydrogel NPs (A). The fluorescence intensity of cells incubated with fluospheres (100 µg/ml) was much higher than that of cells incubated with hydrogel NPs (250 µg/ml). A direct comparison is however not possible since the fluorescent intensity per particle is different for these two colloids,*

Some internalization processes of colloidal objects by cells involve energy consumption. We have studied the contribution of these energy-dependent routes by using physical and chemical inhibitors. Both low temperature and energy depletion by sodium azide (NaN_3) are known to block endocytosis. However, incubation at 4°C is known to additionally rigidify the lipid cell membrane and moreover, the physicohemical properties of the thermally-sensitive NPs are different at this temperature (chapter 5). For the above reasons, we additionally used NaN_3 to obtain unambiguous results.

Both treatments resulted in a similar decrease of particle uptake. The magnitude of reduction was however different for the two colloids tested: fluosphere® inhibition was 65-70% compared to approx. 30% for the hydrogel NPs (Figure 6.4). Low but significant inhibition observed for PEG-Pluronic NPs, suggests that endocytosis is not the primary way of internalization.

There are several remaining possible endocytic pathways through which NPs may be internalized and trafficked in the cell. Determination of the predominant mechanisms is possible by two main approaches.

The first approach is based on inhibition of specific pathways or cell functions: reduced uptake in the presence of inhibitors demonstrates involvement of these processes. Nystatin and β-cyclodextrin, sequester and deplete respectively, cholesterol, disrupting in this way lipid-raft mediated pathways[25]. Filipin inhibits caveola-coated pit endocytosis, cytochalasin D actin polymerization and nocodazole microtubule formation[26]. Inhibition of clathrin-coated pit endocytosis is possible with brefeldin A or chlorpromazine[27]. However, intrepreting of the results obtained should be treated with caution since a number of these molecules have multiple actions. The second approach utilizes fluorescent markers of intracellular targets: co-localization with the drug carrier corroborates their active participation[28, 29]. In this case, care should be taken to avoid artifacts caused by cell fixation; for this reason live-cell microscopy is better-suited for these studies.

The experimental setup we have developed allows the implementation of the first approach and studies are currently under way. Considering the second approach, we initially incubated cells in the presence of the colloids only. Laser confocal images of live cells corroborated our findings from the fluorescence association studies (Figure 6.6). Although virtually all macrophages incubated with fluospheres® showed high levels of internalization, very low fluorescence was detected with NPs. The low amounts of internalized NPs, their weak fluorescence and rapid photo-bleaching of fluorescein, render visualization of colloids difficult. Moreover, fluorescein emission depends highly on pH: approx. 97% reduction in intensity was observed at pH 5.5 (acetate buffer) compared to pH 7.4 (phosphate buffer). Given the pH drop in cellular compartments during endocytosis it is probable that NPs located in organelles of low pH (e.g. lysosomes) are not visible. We believe a switch to a more stable, pH-insensitive fluorophore and an increase of the conjugated amount to NPs are necessary for obtaining better images and revealing the intracellular localization of NPs. Nevertheless, our microscopy data confirmed our findings from fluorescence association experiments and FACS analysis showing low uptake and intracellular distribution on the NPs.
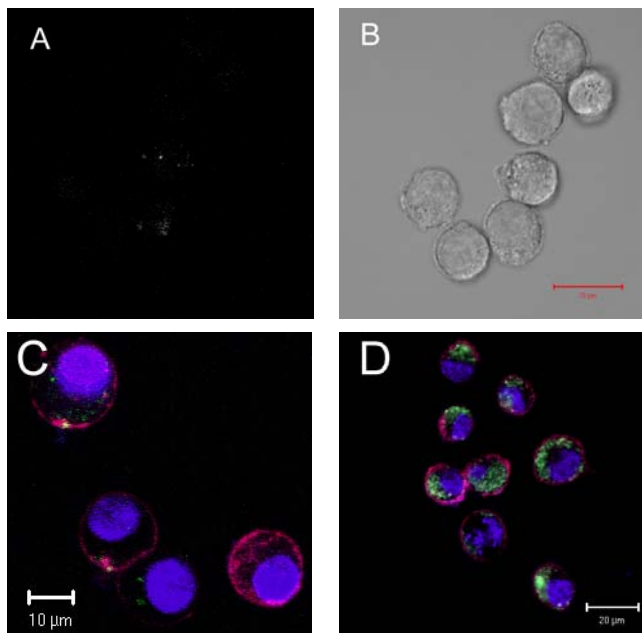
Figure 6.6 *Internalization of fluorescent nanoparticles in J774A.1 cells after 4 hr incubation. Very weak fluorescence emission was observed for FITC-labeled, hydrogel NPs (A): a CLSM image of a section in the middle of the cells shown in (B). (C,D): CLSM images of live cells with internalized FITC-labeled NPs (C) or fluospheres® (D) (red: cell membrane, blue: nucleus, green: NPs).*

6.4 Conclusions

Removal of foreign particulate matter by phagocytic cells of the MPS poses a substantial obstacle to effective carrier-mediated, targeted drug delivery. In this chapter we have demonstrated that hydrogel nanoparticles, formulated by non-ionic and inert polymers, interacted a great deal less with J774 cells than model hydrophobic and charged colloids (Fluospheres®). The presence of opsonic factors did not affect uptake while a slight decrease of association was observed after inhibition of energy-dependent processes. Based on the above results, and the absence of toxicity of the NPs, we conclude that these colloids carriers hold potential as long-circulating carriers and *in vivo* circulation studies should be undertaken.

6.5 References

1.   I. Brigger, et al. *Nanoparticles in cancer therapy and diagnosis* Adv. Drug Delivery Rev. 54 **2002** 631-651

2.   M. Ferrari *Cancer nanotechnology: opportunities and challenges* Nature Reviews Cancer 5 **2005** 161-171

3.   S. Sengupta, et al. *Temporal targeting of tumour cells and neovasculature with a nanoscale delivery system* Nature 436 **2005** 568-572

4.   S.M. Moghimi and J. Szebeni *Stealth liposomes and long circulating nanoparticles: critical issues in pharmacokinetics, opsonization and protein-binding properties* Progress in Lipid Research 42 **2003** 463-478

5.   S.M. Moghimi, et al. *Long-Circulating and Target-Specific Nanoparticles: Theory to Practice.* Pharmacol Rev 53 **2001** 283-318

6.   F. Ahsan, et al. *Targeting to macrophages: role of physicochemical properties of particulate carriers-liposomes and microspheres-on the phagocytosis by macrophages* J. Controlled Release 79 **2002** 29-40

7.   O. Gonzalez, et al. *Effect of size, concentration, surface area, and volume of polymethylmethacrylate particles on human macrophages in vitro* J. Biomed. Mater. Res. 30 **1996** 463-473

8.   V.J. Tomazic-Jezic, et al. *Significance of the type and the size of biomaterial particles on phagocytosis and tissue distribution* J. Biomed. Mater. Res. 55 **2001** 523-529

9.   A. Gessner, et al. *Nanoparticles with decreasing surface hydrophobicities: influence on plasma protein adsorption* Int. J. Pharm. 196 **2000** 245-249

10.   M. Luck, et al. *Analysis of plasma protein adsorption on polymeric nanoparticles with different surface characteristics.* J. Biomed. Mater. Res. 39 **1998** 478-485

11.   S. Prior, et al. *In vitro phagocytosis and monocyte-macrophage activation with poly(lactide) and poly(lactide-co-glycolide) microspheres* Eur. J. Pharm. Sci. 15 **2002** 197-207

12.   R. Gref, et al. *'Stealth' corona-core nanoparticles surface modified by polyethylene glycol (PEG): influences of the corona (PEG chain length and surface density) and of the core composition on phagocytic uptake and plasma protein adsorption* Coll. Surf. B Biointerf. 18 **2000** 301-313

13. V. Olivier, et al. *Uptake of polystyrene beads bearing functional groups by macrophages and fibroblasts* Coll. Surf. B Biointerf. 33 **2004** 23-31

14. V.C.F. Mosqueira, et al. *Biodistribution of long-circulating PEG-grafted nanocapsules in mice: Effects of PEG chain length and density* Pharm. Res. 18 **2001** 1411-1419

15. E. Allemann, et al. *Kinetics of blood component adsorption on poly(D,L-lactic acid) nanoparticles: Evidence of complement C3 component involvement* J. Biomed. Mater. Res. 37 **1997** 229-234

16. M.T. Peracchia, et al. *Visualization of in vitro protein-rejecting properties of PEGylated stealth polycyanoacrylate nanoparticles* Biomaterials 20 **1999** 1269-1275

17. N. Jaulin, et al. *Reduction of the Uptake by a Macrophagic Cell Line of Nanoparticles Bearing Heparin or Dextran Covalently Bound to Poly(methyl methacrylate)* J. Drug Targeting 8 **2000** 165-172

18. H. Otsuka, et al. *PEGylated nanoparticles for biological and pharmaceutical applications* Adv. Drug Delivery Rev. 55 **2003** 403-419

19. J.K. Gbadamosi, et al. *PEGylation of microspheres generates a heterogeneous population of particles with differential surface characteristics and biological performance* FEBS Lett. 532 **2002** 338-344

20. Y.C. Hsu, et al. *Reduced Phagocytosis of Colloidal Carriers Using Soluble CD47* Pharm. Res. 21 **2003** 1539-1542

21. C.R. Miller, et al. *Liposome-Cell Interactions in Vitro: Effect of Liposome Surface Charge on the Binding and Endocytosis of Conventional and Sterically Stabilized Liposomes* Biochemistry 37 **1998** 12875-12883

22. K.D. Lee, et al. *Quantitative Analysis of Liposome-Cell Interactions in Vitro: Rate Constants of Binding and Endocytosis with Suspension and Adherent J774 Cells and Human Monocytes* Biochemistry 32 **1993** 889-899

23. P. Chenevier, et al. *Interaction of Cationic Colloids at the Surface of J774 Cells: A Kinetic Analysis* Biophysical Journal 79 **2000** 1298-1309

24. V.C.F. Mosqueira, et al. *Interactions between a Macrophage Cell Line (J774A1) and Surface-modified Poly($_{D,~L}$-lactide) Nanocapsules Bearing Poly(ethylene glycol)* J. Drug Targeting 7 **1999** 65-78

25. J.S. Wadia, et al. *Transducible TAT-HA fusogenic peptide enhances escape of TAT-fusion proteins after lipid raft micropinocytosis* Nat. Med. 10 **2004** 310-315

26. J. Panyam, et al. *Rapid endo-lysosomal escape of poly(DL-lactide-co-glycolide) nanoparticles: implications for drug and gene delivery* FASEB Journal 16 **2002** 1217-1226

27. S.B. Sieczkarski and G.R. Whittaker *Dissecting virus entry via endocytosis* Journal of General Virology 83 **2002** 1535-1545

28. C. Foerg, et al. *Decoding the Entry of Two Novel Cell-Penetrating Peptides in HeLa Cells: Lipid Raft-Mediated Endocytosis and Endosomal Escape* Biochemistry 44 **2005** 72-81

29. P. Watson, et al. *Intracellular trafficking pathways and drug delivery: fluorescence imaging of living and fixed cells* Adv. Drug Delivery Rev. 57 **2005** 43-61

Chapter 7

Outlook

7.1 Important features of PEG-Pluronic hydrogel nanoparticles

The main features of the nanoparticles presented in this thesis are here summarized.

We have synthesized a novel colloidal system based on Pluronic® F127 and poly(ethylene glycol) of various molecular weights (575-3400). Both polymers are biocompatible, with FDA approval for pharmaceutical purposes. We were interested in formulating these polymers in robust, nano-sized structures to overcome limitations in size control, loading capacity and stability.

The inverse emulsion polymerization technique selected for the production of NPs is simple, versatile and easy to scale-up. A number of different monomers may be included in the cross-linked, hydrogel network of the NPs, providing a flexible way of regulating material properties and introducing functionality; incorporation of electrostatically charged and reactive groups was demonstrated by copolymerization of appropriate monomers. The use of the latter for modification with a fluroescent dye yielded fluorescent NPs, able to be detected *in vitro*.

Inverse emulsion additionally allowed for size control in the sub-micron diameter range; regulation of emulsifier concentration is a potent way to adjust the size of the aqueous droplets, which template the final hydrogel particles formed. High polydispersity is however a challenge that remains to be resolved.

Long-term storage is possible through lyophilization of aqueous NP dispersions, an important requirement when envisioning commercial pharmaceutical formulations.

A closer look on structure revealed that the aggregated state of Pluronic micelles in water was preserved during the stabilizing cross-linking reaction. The particles can thus be visualized as nanoscale, three-dimensional, polymeric networks consisting of PPG-rich, hydrophobic domains surrounded by a hydrophilic, PEG-rich matrix. The permanence of domains similar in hydrophobicity to Pluronic micellar cores, but insensitive to dilution under the CMC, allows the encapsulation of hydrophobic drugs. As an example, a fast and efficient solvent evaporation technique was developed to partition doxorubicin in the NPs. Physically entrapped drug molecules are partially protected from degradation and diffuse out of the NPs without a burst, over one week under sink conditions. We aniticipate that this *a posteriori* loading approach, which has the advantage of avoiding possible deactivation of the drug in the reaction environment, may be applied to a variety of low MW, poorly water-soluble

drugs. Alternative drug loading approaches have not yet been explored but are nevertheless possible with the NPs described here and are discussed later on.

The chain segregation of incorporated Pluronic, apart from offering drug loading sites, imparts the hydrogel NPs with interesting temperature-responsive mechanical properties. Bound water is released from the hydrogel NPs with increasing temperature, reducing their dimensions and transforming them into more elastic spheres. At concentrations above which there is physical contact of neighboring particles, this intra-particulate event is manifested as a macroscopic, fluid-to-solid transition; NPs are dynamically arrested within a 'cage' formed by their neighbors. The mild and reversible transition occurs at a clinically-relevant temperature range, with no syneresis or by-product formation, and is compatible with living cells. The colloidal macroscopic drug depot will give rise, upon dissolution in bodily fluids, to a colloidal nanoparticle dispersion; however, it is notable that the processes of drug release within the NPs and dissolution are independent and may be tailored on a case-to-case basis.

Biomaterials intend to come in contact with tissue and therefore *in vitro* cell-nanoparticle interactions studies were undertaken. Absence of cytotoxicity is a promising finding and substantiates not only the non-toxic character of the precursors but also that of the fabrication method. The hydrophilic and protein repellent nature of the particles are responsible for low association with a macrophage-like cell line. Although is difficult to extrapolate our data to *in vivo* situations, we believe it is reasonable to anticipate a stealth character and long circulation times.

The above mentioned characteristics of this novel drug delivery system provide a platform for further studies and exploitation for therapeutic purposes.

7.2 Suggestions for improvements and further development

In the previous paragraph we presented methodologies leading to the development of novel drug delivery systems, in the form of nanoparticles or colloidal glasses. On the long road towards clinical applications, a number of additional issues need to be addressed, some critical, others less. Improvements on existing characteristics are also valuable and would enhance the quality and effectiveness of these NPs as therapeutic products. Here we briefly discuss these areas, providing strategies and preliminary results.

7.2.1 Biodegradability

The hydrogel network of the NPs presented so far is itself nondegradable under physiological conditions. The ester bonds present in the acrylate moieties of PEG and Pluronic cross-linkers are hydrolyzed extremely slowly in PBS, rendering the hydrogels prepared through radical polymerization stable for very long periods[1].

In order to avoid accumulation of the material in the body we propose the alternate use of PEG-based biodegradable cross-linkers compatible with the preparation scheme. Degradation can be based on protease sensitive substrates[2-4] or hydrolyzable (poly)ester[5] or anhydride[2,6] groups, incorporated in the polymeric structure. In addition to the above opportunities, we decided to design novel, degradable, linear polymers, which would function both as macronomonomers and cross-linkers; their resemblance to the macromonomers used in our studies should allow the trivial replacement of our model system with a biodegradable one (compound iii, Scheme 7.1).

Labile ester bonds are introduced following Michael-type addition of thiols onto acrylates[7]; the presence of electronegative sulfur atoms in close proximitiy of the ester bond leads to an increase in hydrolytic sensitivity [8]. As Schoenmakers et al. have shown, the hydrolysis kinetics show a dependance on the number of methylene units between the sulfide and the ester bond. In the case of a 3-sulfanylpropionyl linker an estimated half life of 4.2±0.1 days was reported [8], although this value is expected to be influenced by the microenvironment's hydrophobicity.

Use of this chemisty has been implemented in preparing degradable hydrogels via a step-growth mechanism[9], and recently also through a combined step-growth and chain-growth polymerization scheme[10].

Synthesis of compound (iii) with poly(ethylene glycol) (MW=3400) as the backbone was succesful and is currently being optimized. Macroscopic hydrogel discs based on this macromer were prepared and are being studied in respect to their degradation kinetics whereas the final step of preparing fully resorbable particles is being planned.

For a degradable network prepared by radical polymerization of macromonomers with the strructure of compound (iii), the degradation products would be comprised of the original macromonomer core and the kinetic chains generated during polymerization. Provided the molecular weight of the latter is below the renal threshold barrier (20-30,000), the polymers can be excreted from the body. For this reason, we are planning to investigate the molecular weight distribution of the kinetic chains after fully degrading the hydrogels using GPC.

Scheme 7.1
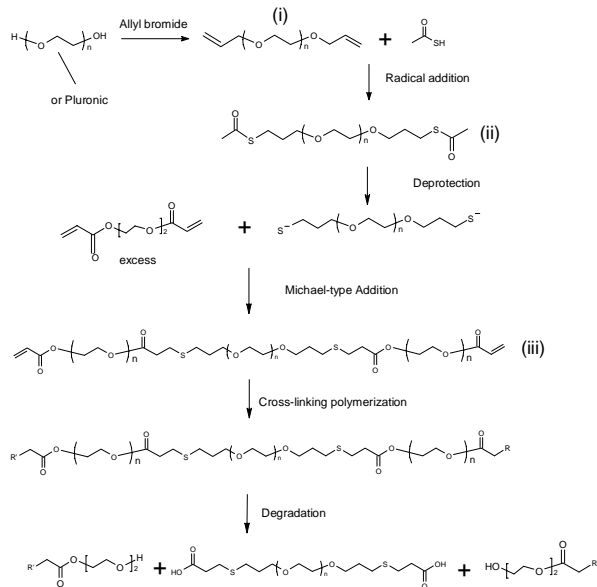
7.2.2 Surface functionalization

The potential that active targeting confers to colloidal drug carriers was briefly discussed in the introductory chapter. Emulsion techniques are ideal for engineering nanoparticles with different surface from bulk properties through the use of emulsifiers which are incorporated (linked, adsorbed or entangled) in the NPs. Introduction of reactive groups selectively on the surface is the first step of attaching specific ligands.

Inconveniently, in inverse emulsion the amphiphiles intented to provide surface functionality, expose their hydrophobic part outwards, rendering the formed colloids unstable against aggregation when exposed to aqueous environment and prone to opsonization. To overcome this problem we suggest a strategy which would make use of cleavable co-emulsifiers containing a reactive double bond on their hydrophilic segment. After NP formation and while in inverse emulsion the hydrophobic part of the linked emulsifier could be removed, exposing reactive groups. Crucial considerations for this approach are the ability of the co-emulsifier to partition in the interface and participate in the polymerization as well as the conditions of cleavage, which should not affect the bulk of the NPs.

7.2.3 Polydispersity issues

The effect of size distribution on the *in vivo* fate of NPs is well documented. In our work we were able to control the average size through proper adjustment of inverse emulsion parameters; however, we were not able to obtain particles with very narrow polydispersity. We believe this incapacity is due to emulsion instability issues. Switching to a thermodynamically stable inverse microemulsion template at the expense of higher emulsifier concentrations and lower aqueous volume ratios, would not necessarily solve this problem. It is known that in microemulsions water droplets are in constant collision with each other[11, 12]: uncontrolled reactions between transient droplets would result in a polydisperse population, of course with a lower average diameter. On the other hand, the transparent nature of inverse microemulsions might allow faster photopolymerization kinetics and quicker stabilization of the colloids.

Based on the above considerations, we believe it is worthwhile attempting the switch to a microemulsion-based scheme, with the aim of enhanced control over size distribution, of even smaller particles.

7.2.4 Drug loading

In terms of drug loading the succesful physical encapsulation of doxorubicin and the covalent linking of fluorescein established the proof of principle of two different loading strategies.

The former approach has not yet been tested in relation to its long-term stability. After purification of the loaded NPs the equilibrium is shifted and release takes place. In order to ensure an efficient pharmaceutical formulation, the ability to obtain a freeze-dried drug-loaded product, which upon rehydration retains its drug loading, needs to be confirmed.

Concerning the latter approach, the necessity of releasing the active agent after covalent linking has to be addressed. The copolymerization of monomers containing labile linkers is certainly an option as it has already been used for formation of cross-linked PEG hydrogels via photopolymerization[8,13]. Alternatively, the drug may be linked after NP production via a labile moiety.

Another possibility accessible by the NPs presented in this thesis is the electrostatic binding of molecules. Nucleic acids and certain therapeutic peptides[14] are charged and would therefore interact with modified PEG-Pluronic NPs. Adsorption throughout the particle volume or selectively on the surface has already been demonstrated using PEG-based

nanogels[15, 16]. To enhance binding it might be beneficial to pre-adsorb high MW, opposite charged polyelectrolytes[17].

Finally, entrapment of high MW therapeutics or antigens (for vaccines), is an option which merits investigation; recent studies using inverse emulsion polymerization in the presence of proteins showed their succesful entrappment in the degradable or non-degradable hydrogel matrix of NPs[17, 18].

Each of the above loading approaches will determine the mechanism of drug release; combined loading of more than one agents and/or use of multiple loading approaches might prove beneficial in targeting several aspects of a particular disease[19].

7.2.5 Drug delivery from colloidal glass

Drug delivery from individual NPs in the form of dilute dispersions can be engineered by proper selection of agent, particle characteristics and loading approach. The formation of physically bonded colloidal solids offers an additional possibility for the delivery of high MW therapeutics (e.g. proteins). Mixing of such macromolecules in the cold precursor solution would lead in their entrapment in the formed colloidal glass upon heating to body temperature. Release would then occur upon dissolution into a colloidal dispersion or via diffusion through the interparticle pores[20]. Combined release of macromolecules and drugs incorporated in the NPs could also be implemented (Figure 7.1).
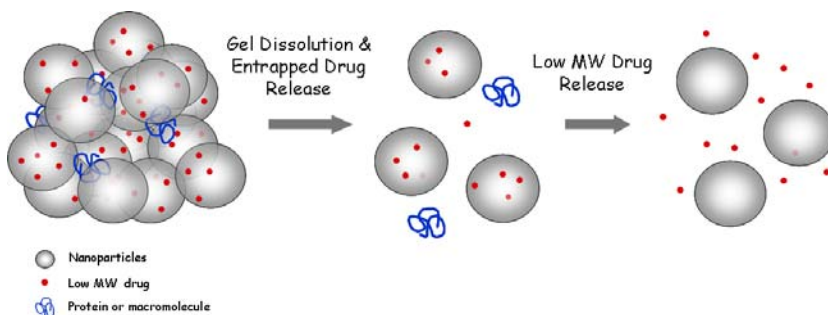

Figure 7.1. *Schematic representation of combined release of low and high MW drugs from colloidal glass*

As a first step we are currently performing *in vitro* release experiments of albumin and fluorescently labeled dextrans (of different MW) entrapped in colloidal glasses.

7.2.6 Stealth character

The *in vitro* cell studies presented in chapter 6 have shown low interactions of the hydrogel NPs with a macrophage-like cell line, intended to act as a model of MPS macrophages; these results imply a 'stealth' character. A key experiment will be the determination of the *in vivo* blood circulation times of the carriers proposed here.

7.3 Potential biomedical applications

Initially, we sought to develop NPs as carriers for drug delivery through parenteral administration. Focus was placed on the physicochemical characterization of dilute colloid dispersions, their drug loading capabilities and their interactions with cells as individual particles. Anticancer therapy being a primary target application, we concentrated our efforts in obtaining NPs with appropriate size for passive targeting and loaded with potent chemotherapeutics.

The thermal properties of the colloids, and especially the thermally-induced, sol-gel transition of their concentrated dispersions, made us consider additional applications of our system as injectable *in situ* forming biomaterials. We here briefly present some potential applications exploiting the unique characteristics of the NPs portrayed in this thesis.

7.3.1 Tumor therapy

Two different administration routes may be employed using our doxorubicin-loaded colloidal system for the treatment of cancer: parenteral injections or injections directly at the tumor.

In the case of parenteral injections, the size range of the NPs would allow their passive accumulation in tumor tissue thanks to the EPR effect. Drug molecules would then be released in the intestitial space and diffuse into the cells (bigger fraction), or would get liberated after uptake of the NPs by tumor cells (smaller fraction). Release is not dependent on destabilizing factors (as in the case of liposomal formulations) and is expected to proceed continuously until drug depletion. However, the risk of multidrug resistance development might pose a significant obstacle to this tactic.

Direct, local injection is an alternative approach which might circumvent certain complications of systemic administration. Taking advantage of the liquid-to-solid transition,

drug-loaded NPs could be introduced and remain within (or in close proximitiy of) tumors, releasing locally their payload. Similar approaches have already been reported using microparticles[21, 22], thermo-responsive[23, 24] or protease-sensitive[25] hydrogels. Although administration becomes more complicated, high drug concentrations at the target site and reduction of side effects might make this approach better-suited for certain applications.

7.3.2 Prevention of postoperative adhesions

Abdominal and pelvic adhesions are abnormal fibrous structures bridging surfaces of the peritoneal and pelvic cavities. They form following abdominal surgery (>30%) or inflammation and might cause bowel obstruction, pain and infertility in women[26, 27].

Peritoneal adhesions are certainly the most known, but not the only ones; postoperative adhesions and fibrosis may also lead to spinal cord tethering after neurosurgery. Different strategies have been proposed to prevent adhesion formation: use of fibrinolytic agents[26, 28], biodegradable materials acting as physical barriers[29], controlled antiproliferative drug delivery[30, 31] or combination of these. We considered using the drug loading capabilities of the NPs combined with the trivial formation of colloidal hydrogels to locally administer rapamycin, a potent antiproliferative agent. The slow dissolution kinetics of our system, its ease of application and the biocompatible character of the material make it an ideal candidate for the application in mind. Experiments are in planning in collaboration with Dr. H. Schmoekel at the EPFL using experimental animal models.

7.4 References

1. C.P. Pathak, et al. *Rapid Photopolymerization of Immunoprotective Gels in Contact with Cells and Tissue* J. Am. Chem. Soc. 114 **1992** 8311-8312

2. A. Kelner and E. Schacht *Tailor-made polymers for local drug delivery: release of macromolecular model drugs from biodegradable hydrogels based on poly(ethylene oxide)* J. Controlled Release 101 **2005** 13-20

3. B.K. Mann, et al. *Smooth muscle cell growth in photopolymerized hydrogels with cell adhesive and proteolytically degradable domains: synthetic ECM analogs for tissue engineering* Biomaterials 22 **2001** 3045-3051

4.   S. Halstenberg, et al. *Biologically Engineered Protein-graft-Poly(ethylene glycol) Hydrogels: A Cell Adhesive and Plasmin-Degradable Biosynthetic Material for Tissue Repair* Biomacromolecules 3 **2002** 710-723

5.   D.K. Han and J.A. Hubbell *Synthesis of polymer network scaffolds from L-lactide and poly(ethylene glycol) and their interaction with cells* Macromolecules 30 **1997** 6077-6083

6.   A.S. Sawhney, et al. *Bioerodible hydrogels based on photopolymerized poly(ethylene glycol)-co-poly(alpha-hydroxy acid) diacrylate macromers* Macromolecules 26 **1993** 581-587

7.   M.P. Lutolf, et al. *Systemic Modulation of Michael-Type Reactivity of Thiols through the Use of Charged Amino Acids* Bioconjugate Chem. 12 **2001** 1051-1056

8.   R.G. Schoenmakers, et al. *The effect of the linker on the hydrolysis rate of drug-linked ester bonds* J. Controlled Release 95 **2004** 291-300

9.   M.P. Lutolf and J.A. Hubbell *Synthesis and physicochemical characterization of end-linked poly(ethylene glycol)-co-peptide hydrogels formed by Michael-type addition* Biomacromolecules 4 **2003** 713-722

10.   A.E. Rydholm, et al. *Degradable thiol-acrylate photopolymers: polymerization and degradation behavior of an in situ forming biomaterial* Biomaterials 26 **2005** 4495-4506

11.   P.D.I. Fletcher, et al. *The kinetics of solubilisate exchange between water droplets of a water-in-oil microemulsion* J. Chem. Soc., Faraday Trans. I 83 **1987** 985-1006

12.   S. Clark, et al. *Interdroplet exchange-rates of water-in-oil and oil-in-water microemulsion droplets stabilised by $C_{12}E_5$* Langmuir 6 **1990** 1301-1309

13.   D.L. Elbert and J.A. Hubbell *Conjugate Addition Reactions Combined with Free-Radical Cross-Linking for the Design of Materials for Tissue Engineering* Biomacromolecules 2 **2001** 430-441

14.   S. Lien and H.B. Lowman *Therapeutic peptides* Trends Biotechnol. 21 **2003** 556-562

15.   G. Lambert, et al. *Nanoparticulate systems for the delivery of antisense oligonucleotides* Adv. Drug Delivery Rev. 47 **2001** 99-112

16.   K. McAllister, et al. *Polymeric nanogels produced via inverse microemulsion polymerization as potential gene and antisense delivery agents.* J. Am. Chem. Soc. 124 **2002** 15198-15207

17. S. Jain, et al. *Synthesis of Protein-Loaded Hydrogel Particles in an Aqueous Two-Phase System for Coincident Antigen and CpG Oligonucleotide Delivery to Antigen-Presenting Cells* Biomacromolecules **2005**

18. N. Murthy, et al. *A macromolecular delivery vehicle for protein-based vaccines: Acid-degradable protein-loaded microgels* P. Natl. Acad. Sci. USA 100 **2003** 4995-5000

19. S. Sengupta, et al. *Temporal targeting of tumour cells and neovasculature with a nanoscale delivery system* Nature 436 **2005** 568-572

20. X. Xia, et al. *Physically bonded nanoparticle networks: a novel drug delivery system* J. Controlled Release 103 **2005** 21-30

21. S. Nsereko and M. Amiji *Localized delivery of paclitaxel in solid tumors from biodegradable chitin microparticle formulations* Biomaterials 23 **2002** 2723-2731

22. E. Harper, et al. *Enhanced Efficacy of a Novel Controlled Release Paclitaxel Formulation (PACLIMER Delivery System) for Local-Regional Therapy of Lung Cancer Tumor Nodules in Mice* Clinical Cancer Research 5 **1999** 4242-4248

23. E. Ruel-Gariepy, et al. *A thermosensitive chitosan-based hydrogel for the local delivery of paclitaxel* Eur. J. Pharm. Biopharm. 57 **2004** 53-63

24. M.M. Amiji, et al. *Intratumoral administration of paclitaxel in an in situ gelling poloxamer 407 formulation* Pharm. Dev. Technol. 7 **2002** 195-202

25. J.R. Tauro and R.A. Gemeinhart *Extracellular Protease Activation of Chemotherapeutics from Hydrogel Matrices: A New Paradigm for Local Chemotherapy* Molecular Pharmaceutics in press **2005**

26. B.W.J. Hellebrekers, et al. *Use of fibrinolytic agents in the prevention of postoperative adhesion formation* Fertility and Sterility 74 **2000** 203-212

27. W.W. Vrijland, et al. *Abdominal adhesions - Intestinal obstruction, pain and infertility* Surgical Endoscopy 17 **2003** 1017-1022

28. J.L. Hill-West, et al. *Local Release of Fibrinolytic Agents for Adhesion Prevention* J. Surg. Res. 59 **1995** 759-763

29. J.L. West and J.A. Hubbell *Comparison of covalently and physically cross-linked polyethylene glycol-based hydrogels for the prevention of postoperative adhesions in a rat model* Biomaterials 16 **1995** 1153-1156

30. S.H. Oh, et al. *Prevention of postsurgical tissue adhesion by anti-inflammatory drug-loaded Pluronic mixtures with sol-gel transition behavior* J. Biomed. Mater. Res. 72A **2005** 396-316

31.   S.M. Chowdhury and J.A. Hubbell *Adhesion Prevention with Ancrod Released via a Tissue-Adherent Hydrogel* J. Surg. Res. 61 **1996** 58-64

Acknowledgements

Working on my thesis involved much more than the results presented here; it has also been a learning and maturation process at many different levels, from working with other people to planning and conducting independent research.

Nicola Tirelli started everything by offering me this PhD position. His guidance and advice was invaluable during my first steps in the world of polymeric and colloidal chemistry and writing of scientific papers. I would like to sincerely thank him for setting the basis of my scientific development in the period we worked together in Zurich, before he moved on to the University of Manchester.

Jeff Hubbell has been my doctor father and gave me the opportunity to join his group... twice!! I have been amazed by his ability to remember the details of my project, to distinguish the critical issues, and to always come up with ideas and potential applications for my nanoparticles. I would particularly like to thank him for the freedom he allowed in my research.

I am grateful to Robert Gurny and Hans Peter Merkle who accepted to be my co-examiners. Working in this field, I came across their work constantly; it is an honor for me of having them in my defense committee.

I would like to thank all my colleagues (many of whom became also friends) from the Hubbell lab, both in Zurich and Lausanne, who have contributed, each in their own way, to my scientific work and to creating an agreeable and stimulating lab environment. I feel I have been lucky to join a lab with so many different project and interests.

I would like to express in particular my gratitude to a few people I worked with back in Zurich:

A special thanks goes to Annemie Rehor, with whom I believe I shared the same scientific loneliness in the beginning, in a lab without strong background on colloidal drug delivery, and with whom I had fruitful discussions concerning our projects as well as techniques and experiments.

Ronald Schoenmakers, who always took the time to listen and think over my questions and problems, and surprised me when he came up with answers or suggestions, long after I had forgotten my question.

Alessandro Napoli, with whom scientific discussions were always very stimulating (although lacking a little bit of the southern passion present in our political arguments).

Francesco Cellesi, who introduced me to polymer functionalization (I owe the whiteness of my polymers to him) and rheology.

Malou Gengler, who was always there to discuss our projects; a lot of interesting ideas and challenges arose from our conversations.

I would especially like to thank Simone Rizzi, Diana Trentin and George Raeber for 'mental' support and advice concerning intellectual, scientific and sentimental matters.

Moving to Lausanne I received valuable help and support from the 'snobby PostDos': Harry Bermudez, Tatiana Segura and Tom Barker. Tatiana was of great help with my cell culture experiments as well, both in practical and interpretation issues. André van der Vlies was kind and patient enough to perform my NMR measurements; I also thank him for his sincere interest in my chemical difficulties.

During my thesis I had the chance to supervise the work of two students: Ryuzo Kawamura contributed greatly on the study presented in chapter 3 during his stay in Zurich. Claudio Usai was very helpful in developing the in vitro cell studies during his semester thesis at EPFL.

I would also like to thank external support: Andrea Vaccaro and Peter Sandkuehler from Morbidelli group (ETHZ) for assistance with light scattering and Doris Sutter for NMR analysis (ETHZ).

I thank our secretaries for essential support and organization of all administrative issues: Esther Singer in Zurich and Melanie Colanero, Carol Bonzon and Christina Mattsson in Lausanne. My thanks also to all the people involved with computer support.

A special thanks to Federica Pinto and Alice Tomei for translating my summary in Italian, my favorite from the official languages of Switzerland.

Thinking about the people who contributed to the fullfillment of this thesis, I could not leave out all those who shared my life outside the lab over these last years. It has been a difficult yet rewarding period and I would like to thank all of my friends for the special moments we had together. Last but not least my thanks goes to my family for their unlimited support.

Curriculum Vitae

Personal Information

Name:	Dimitrios Missirlis
Date of Birth:	1 August 1978
Place of Birth:	Hamilton, Canada
Nationality:	Greek & Canadian
Marital status:	Single

Education-Academic Experience

2004-present	Ph.D, Biomedical Engineering
	Ecole Polytechnique Fédérale de Lausanne (EPFL)
	Integrative Biosciences Institute (IBI)
	Advisor : Jeffrey A. Hubbell
2001-2004	Ph.D, Biomedical Engineering
	Eidgenössische Technische Hochschule Zürich (ETHZ)
	Institute for Biomedical Engineering
	Advisors : Nicola Tirelli, Jeffrey A. Hubbell
1996-2001	Diploma, Chemical Engineering (8.3/10.0)
	University of Patras
	Department of Chemical Engineering
	Diploma thesis advisor : Petros Koutsoukos

Further Experience

07/2000-08/2000	Summer project at EPFL (Switzerland)
	Project: Arterial Wall Remodelling
	Advisor : N. Stergiopulos
07/1999-08/1999	Internship at Vanderstraaten Co. & K.U. Leuven (Belgium)
	Project: Transfer of technology for oral implant from lab to industry
	Advisor : J. Helsen

Publications

1. **Thermally-induced responses in PEG-Pluronic hydrogel nanoparticles: the formation of a colloidal glass and its possible applications**, <u>D. Missirlis</u>, N. Tirelli, J.A. Hubbell, submitted in Biomacromolecules

2. **Doxorubicin encapsulation and diffusional release from stable, polymeric, hydrogel nanoparticles**, <u>D. Missirlis</u>, R. Kawamura, N. Tirelli, J.A. Hubbell, submitted in Journal of Controlled Release

3. **Amphiphilic hydrogel nanoparticles. Preparation, characterization and preliminary assessment as new colloidal drug carriers**, <u>D. Missirlis</u>, N. Tirelli, J.A. Hubbell, 2005, Langmuir, 21, 2605-2613

4. **Seeded growth of hydroxyapatite in simulated body fluid**, N. Spanos, <u>D.Y. Missirlis</u>, D.G. Kanellopoulou, P.G. Koutsoukos, Journal of Materials Science, in press

Presentations

- **Hydrogel nanoparticles via inverse emulsion photopolymerization** , <u>D. Missirlis</u>, N. Tirelli, J.A. Hubbell, Controlled Release Society Meeting, Glasgow 2003, *poster*

- **Amphiphilic, PEG-based nanoparticles for the delivery of hydrophobic drugs**, <u>D. Missirlis</u>, N. Tirelli, J.A. Hubbell, 7th World Biomaterials Conference, Sydney 2004, *oral presentation*

- **Temperature-dependent 'gelation' of Pluronic-based nanoparticles in water**, <u>D. Missirlis</u>, N. Tirelli, J.A. Hubbell, European Polymer Conference, Gargnano (Italy) 2004, *oral presentation*

- **Thermally-induced, colloidal glass formation from amphiphilic, hydrogel nanoparticles: a novel drug delivery system**, <u>D. Missirlis</u>, N. Tirelli, J.A. Hubbell, 6th International Symposium on Frontiers in Biomedical Polymers, Granada 2005, *poster*

- **Thermally-induced responses in biocompatible, amphiphilic, hydrogel nanoparticles: the formation of a colloidal glass and possible biomaterial applications**, <u>D. Missirlis</u>, N. Tirelli, J.A. Hubbell, 19th European Conference of Biomaterials, Sorrento (Italy) 2005, *oral presentation*

Languages

English: *Fluent* (Cambridge Certificate of Proficiency, TOEFL: 277/300)
French: *Good Knowledge* (Diplome d'Etudes en Langue Francaise)
Spanish, Italian, German: *Basic knowledge*
Greek: *Mother tongue*